Scale Effects in Finite Elasticity and Thermoelasticity

Zemfira F. Khisaeva

Department of Mechanical Engineering
McGill University, Montreal
October 2006

Thesis submitted to McGill University in partial fulfillment of the requirements of the degree of Doctor of Philosophy
in Mechanical Engineering

Your file Votre référence
ISBN: 978-0-494-32198-0
Our file Notre référence
ISBN: 978-0-494-32198-0

Abstract

The main focus of this thesis is on investigating the minimum size of the Representative Volume Element (RVE) and finite-size scaling of properties of random linear and nonlinear elastic composites. The RVE is a material volume which accurately describes the overall behavior of a heterogeneous solid, and is the core assumption of continuum mechanics theory. If the composite microstructure admits the assumption of spatial homogeneity and ergodicity, the RVE can be attained within a specific accuracy on a finite length-scale. Determining this scale is the key objective of this thesis.

In order to theoretically analyze the scale-dependence of the apparent response of random microstructures, essential and natural boundary conditions which satisfy Hill's averaging theorem in finite deformation elasticity are first considered. It is shown that the application of the partitioning method and variational principles in nonlinear elasticity and thermoelasticity, under the two above-mentioned boundary conditions, leads to the hierarchy of mesoscale bounds on the effective strain- and free-energy functions, respectively. These theoretical derivations lay the ground for the quantitative estimation of the scale-dependence of nonlinear composite responses and their RVE size.

The hierarchies were computed for planar matrix-inclusion composites with the microstructure modeled by a homogeneous Poisson point field. Various nonlinear composites with Ogden-type strain-energy function are considered. The obtained results are compared with those where both matrix and inclusions are described by a neo-Hookean strain-energy function as well as with the results obtained from the linear elasticity theory. The trends toward the RVE are also computed for nonlinear elastic composites subjected to non-isothermal loading. The accuracy of the RVE size estimation is calculated in terms of the discrepancy between responses under essential and natural boundary conditions. Overall, the results show that the trends toward the RVE as well as its minimum size are functions of the deformation, deformation mode, temperature, and the mismatch between material properties of the phases.

The last part of the thesis presents an investigation of the size effect on thermoelastic damping of a micro-/nanobeam resonator. It does not follow the framework described above. The main concern here is the size and the vibration frequency, at which

the classical Fourier law of heat conduction is no longer valid, and the finite speed of heat propagation has to be taken into account.

Résumé

Le point principal de cette thèse est la recherche de la taille minimale de l'élément de volume représentatif (EVR) et de l'échelonnage à dimension finie des propriétés des composites élastiques aléatoires linéaires et non linéaires. L'EVR est un volume matériel, qui décrit le comportement global d'un solide hétérogène de manière précise, et est l'assomption principale dans la mécanique aux milieux continus. Si la microstructure du composite présente une homogénéité spatiale et une hypothèse d'ergodicité, l'EVR peut être décrit avec une grande exactitude sur une échelle de longueur finie. Déterminer cette échelle est l'objectif clé de cette thèse.

Afin d'analyser théoriquement la dépendance à l'échelle de la réponse apparente des microstructures aléatoires, les conditions limites naturelles et essentielles, satisfaisant le théorème de Hill sur l'élasticité à déformations finies, sont d'abord considérées. Il est montré que l'application de la méthode à partitionnement et les principes variationnels en élasticité non linéaire et en thermoélasticité, avec les deux conditions limites mentionnées ci-dessus, conduisent à la hiérarchisation des limites à échelle mésoscopique sur les fonctions d'énergie de déformation effective et d'énergie libre. Ces dérivations théoriques construisent la base de l'estimation quantitative de la dépendance à l'échelle des réponses des composites non linéaires.

Les hiérarchies ont été calculées en deux dimensions pour des matrices contenant des inclusions avec une microstructure modélisée par un champ homogène ponctuel de Poisson. Plusieurs composites non linéaires avec une fonction d'énergie de déformation de type Ogden ont été considérés. Les résultats obtenus sont comparés à ceux où la matrice et les inclusions sont décrits par une fonction d'énergie de déformation de type néo-Hookéenne ainsi qu'avec ceux obtenus à partir de la théorie d'élasticité linéaire. Les tendances de l'EVR sont également calculées pour les composites élastiques non-linéaires sujets à des contraintes non-isotherme. L'exactitude de l'estimation de la taille de l'EVR est calculée en termes de divergence entre les réponses sous conditions limites naturelles et essentielles. De façon générale, les résultats montrent que les tendances de l'EVR ainsi que sa taille minimale sont fonction de la déformation, du mode de déformation, de la température et de la variation entre les propriétés des matériaux des différentes phases.

La dernière partie de la thèse présente une recherche sur l'effet de taille sur l'atténuation thermoélasticitique d'un résonateur à micro/nanofaisceau. Celle-ci ne suit pas le schéma décrit ci-dessus. Dans ce cas, le problème principal est la taille et la fréquence de vibration, pour lesquelles la loi de Fourier classique sur la conduction de la chaleur n'est plus valide. La vitesse finie de la propagation de la chaleur doit également être prise en considération.

Acknowledgements

I would like to express my sincerest gratitude to my supervisor, Professor Martin Ostoja-Starzewski. I thank him for his guidance, encouragement and kindness throughout this work. He has provided me with excellent facilities for this study, and his experience has been crucial in selecting the original topic of my research. Without his supervision, this work would not have been possible.

I also would like to thank my colleagues from the Structures and Composites Laboratory, and, especially, my research mates Xiangdong Du, Shivakumar Iyer and Wei Li for friendly atmosphere, support and helpful discussions during the time of my PhD. I thank my friend and colleague Mohsen Shahi for his dedicated and patient help in proofreading my thesis.

Finally, I wish to thank my parents, Raisa Khisaeva and Fanil Khisaev, and, especially, my grandmother, Zaituna Tchanisheva, for constant support and love. Without their encouragement this work would have been hardly started.

The financial support from the Werner Graupe International Fellowship during the course of my PhD is gratefully appreciated.

Table of contents

Abstract i

Résumé iii

Acknowledgements v

List of symbols ix

List of figures xiii

List of tables xvi

1 Introduction 1

1.1 Motivation 1

1.2 Background and state of the art 4

1.3 Structure of the thesis 6

2 Mesoscale bounds in finite elasticity and thermoelasticity of random composites: theoretical considerations 8

2.1 Continuum mechanics preliminaries 8

2.2 Minimum theorems in finite elasticity and thermoelasticity 10

2.2.1 Variational principles in finite elastostatics 11

2.2.2 Variational principles in finite thermoelastostatics 12

2.3 Averaging theorems in finite deformation theory 14

2.3.1 Average deformation gradient theorem 15

2.3.2 Average stress theorem 15

2.3.3 Hill condition for finite deformations 16

2.4 Hierarchies of mesoscale bounds in finite elasticity and thermoelasticity of random composites 17

2.5 Classical bounds 22

2.6 Order relationships for mixed boundary conditions 23

2.7 Linear versus nonlinear bounding problems 26

2.8 Closure 28

3 The minimal size of the representative volume element for nonlinear elastic random composites: computational results 29

3.1 Material model 29

3.2 Discretization 32

3.3 Ensemble averaging 33

3.4 Numerical results 34

3.4.1 Bounds on effective properties 34

3.4.2 Statistical approach to the RVE size estimation 49

3.5 Closure 51

4 Scale effects in linear and finite thermoelasticity of nonlinear random composites 56

4.1 Constitutive relations in linear and nonlinear thermoelasticity 56

4.1.1 Thermodynamic potential for a linear thermoelastic composite 58

4.1.2 Thermodynamic potential for a nonlinear thermoelastic composite 61

4.2 Numerical experiments 63

4.3 Scaling trends of the free energy function 64

4.4 Scaling trends of the thermoelastic parameters 67

4.5 Closure 71

5 Scale effects on thermoelastic damping in nanomechanical resonators with finite wave speeds 72

5.1 Introduction 72

5.2 General theory 74

5.2.1 Classical thermoelasticity 74

5.2.2 Thermoelasticity with one relaxation time 76

5.3 Flexural vibrations of a Bernoulli-Euler beam 77

5.4 Numerical results and discussion 81

5.5 Closure 87

6 Summary and future work 92

6.1 Summary 92

6.2 Future work 93

Appendix A 96

Appendix B 100

References 103

List of symbols

Chapters 1-4:

L: mesoscale (window size, element size) of heterogeneous medium;

d: microscale (grain or inclusion size);

L_{macro}: macroscale (body size);

L_{RVE}: the size of the Representative Volume Element (RVE);

δ: nondimentional window size;

$B(\omega)$: random material realization;

Ω: sample space;

$\overline{F}$: volume average of quantity F;

$\langle F \rangle$: ensemble average of function F;

x_i or $\mathbf{x}$: the position vectors of a particle inside the body in current configuration;

X_i or $\mathbf{X}$: the position vectors of a particle inside the body in reference configuration;

u_i or $\mathbf{u}$: displacement vector;

U_i: admissible displacement field;

t_i: nominal traction;

δ_{ij}: Kronecker delta

F_{ij} or $\mathbf{F}$: deformation gradient tensor;

λ_a: principal values of the deformation gradient;

J: Jacobian;

P_{ij} or $\mathbf{P}$: first Piola-Kirchoff stress tensor;

ε_{ij} or $\boldsymbol{\varepsilon}$: small strain tensor;

e: volumetric part of the strain field;

ε'_{ij}: deviatoric part of the strain field;

σ_{ij} or $\boldsymbol{\sigma}$: Cauchy stress tensor;

p: mean pressure;

σ'_{ij}: deviatoric part of the stress field;

ψ: strain energy per unit reference volume;

ψ_{vol}: volumetric part of the strain energy;

ψ_{iso}: isochoric part of the strain energy;

Ψ: strain energy;

ψ_c: complementary energy per unit reference volume;

Ψ^*: complementary energy;

G: Gibbs thermodynamic potential;

V_0: material volume in the reference configuration;

S_0: boundary surface in the reference configuration;

S_U: the portion of the boundary where displacement is prescribed;

S_T: the portion of the boundary where traction is prescribed;

n_j: outward normal vector to the boundary surface in the reference configuration;

T: absolute temperature;

θ_0: prescribed temperature field;

T_0: temperature at reference state;

ΔT: temperature change;

ψ_0: free energy at reference temperature;

e_0: internal energy at reference temperature;

$\hat{T}$: purely thermal contribution to the free energy;

c_F: specific heat capacity at constant deformation;

C_{ijkl}: stiffness tensor;

S_{ijkl}: compliance tensor;

Γ_{ij}: thermal stress coefficient tensor;

α_{ij}: thermal strain coefficient tensor;

ν: Poisson's ratio;

E: Young's modulus;

κ: bulk modulus;

μ: shear modulus;

K: apparent bulk modulus;

M: apparent shear modulus;

κ_0: initial bulk modulus in the reference configuration;

μ_0: initial shear modulus in the reference configuration;

N, μ_i,

α_i, D_i: material parameters of Ogden model;

A, m, B,

n, C, k,

D, p: parameters of bounds on initial shear modulus;

f: prescribed volume fraction of inclusions;

α: mismatch between composite phases.

$N(A)$: number of successful trials;

Superscripts:

i: inclusion:

m: matrix;

*: effective properties.

Chapter 5:

ψ: thermoelastic damping;

ψ_L: local specific damping capacity;

ψ_0: characteristic Zener damping;

W: elastic energy density stored in the body;

ΔW: total work lost throughout the body;

q_i: heat flux;

t: time;

s: entropy production within a system per unit time per unit mass;

Δs: entropy production per unit mass per cycle period;

u: internal energy per unit mass;

ω: circular frequency;

κ_0: beam curvature;

ρ: mass density;

υ: phonon velocity;

k: thermal conductivity;

c: specific heat per unit mass;

t_0: relaxation time;

h: beam thickness;

τ characteristic time;

Y: nondimensional coordinate;

V^*: normalized temperature;

Ω: normalized frequency;

γ: normalized relaxation time;

A_R: real part of the normalized temperature;

A_I: imaginary part of the normalized temperature;

B_R: real part of $\frac{\partial V^*}{\partial Y}$;

B_I: imaginary part of $\frac{\partial V^*}{\partial Y}$;

C_1: integration constant.

List of figures

Figure 1.1. Representative volume element of a periodic composite.

Figure 1.2. Two-dimensional realization of a random composite.

Figure 2.1. A continuum body in the reference and current configuration.

Figure 2.2. (a) a disordered microstructure of a periodic composite with a periodic window of size L; (b) one realization of a random composite $B_\delta(\omega)$ of size L.

Figure 2.3. Partition of a window B_δ of scale δ into four square-shaped sub-windows B'_δ.

Figure 2.3. Partitioning of a window of scale δ into four squares of scale $\delta' < 1$.

Figure 3.1. The finite element mesh of a composite in (a) undeformed and (b) deformed (traction boundary conditions) configurations.

Figure 3.2. Dependence of the average strain energy of a composite on the number of degrees of freedom.

Figure 3.3. Probability densities for the stored strain energy density of the nonlinear composite No. 1 under (a) uniform displacement and (b) uniform traction boundary conditions.

Figure 3.4. Loading under orthogonal-mixed boundary condition, MIXED1.

Figure 3.5. Loading under uniform mixed boundary conditions, MIXED2.

Figure 3.6. Contour plots of logarithmic strain in the direction X_2 under different boundary conditions: (a) SUBC, (b) KUBC, (c) MIXED1, (d) MIXED2.

Figure 3.7. Stress-strain curves of the random composite No. 1 under uniaxial loading.

Figure 3.8. Stress-strain curves of the random composite No. 2 under uniaxial loading.

Figure 3.9. Stress-strain curves of the random composite No. 3 under uniaxial loading.

Figure 3.10. Stress-strain curves of the random composite No. 4 under uniaxial loading.

Figure 3.11. Stress-strain curves of the random composite No. 1 under uniaxial loading with the mixed boundary conditions of the second type.

Figure 3.12. Bounds on the initial shear modulus for different composites: (a) No. 1, (b) No. 2, (c) No. 3, (d) No. 4.

Figure 3.13. Energy bounds for the nonlinear random composite of Ogden - neo-Hookean type (No. 1 and No. 2) under (a, b) uniaxial tension, (c, d) biaxial tension, (e, f) pure shear.

Figure 3.14. Energy bounds for the nonlinear random composite of neo-Hookean – neo-Hookean type (No. 3 and No. 4) under uniaxial tension.

Figure 3.15. Bounds on the strain energy (a,b) and material properties (c,d) of the linear elastic composite (No. 5 and No. 6) under uniaxial tension.

Figure 3.16. Dependence of the strain energy on the stretch value for the composite No. 1.

Figure 3.17. Discrepancies in the energy density of the composite No. 1 between displacement and traction boundary conditions for uniaxial and biaxial tension for various mesoscales.

Figure 3.18. Dependence of the coefficient of variation of the strain energy (a) and complementary energy (b) on the mesoscale for different composite models.

Figure 4.1. Scale effects on the strain energy under constrained deformations (a,c) and stress-free boundary conditions (b,d).

Figure 4.2. Mesoscale bounds on the thermal expansion coefficient, α, and the thermal stress coefficient, Γ, for different nonlinear composites.

Figure 4.3. Dependence of the thermal stress coefficient Γ on the temperature change ΔT for the rubber-polystyrene composite.

Figure 5.1. Coordinate system and geometry of the beam.

Figure 5.2. Variation of the magnitude of the temperature change across the thickness of the beam for (a) classical theory and (b) ORT theory (Si).

Figure 5.3. Variation of the magnitude of the temperature change with the normalized frequency for (a) classical theory and (b) ORT theory (Si).

Figure 5.4. Dependence of the real part of the temperature variation on the normalized frequency for ORT theory (Si).

Figure 5.5. Variation of the phase of the temperature change across the thickness of the beam for (a) classical theory and (b) ORT theory (Si).

Figure 5.6. Variation of the phase of the temperature change with the normalized frequency for (a) classical theory and (b) ORT theory (Si).

Figure 5.7. A comparison of a classical solution for thermoelastic damping with one relaxation time solution for different γ.

Figure B.1. Material microstructure.

List of tables

Table 3.1. Material properties used in the computational examples.

Table 3.2. Boundary conditions used in the computational examples.

Table 3.3. Parameters in equations (3.6) and (3.7) for different composite models.

Table 4.1. Material properties of constituents for rubber–polystyrene composite.

Table 4.2. Material properties of constituents for sodium-chloride–rubber composite.

To my family

Chapter 1
Introduction

1.1 Motivation

Nearly any engineering material, conventionally considered homogeneous on a macroscale, displays heterogeneity on a microscale. Typical examples include metals, rocks, wood, biological tissues, foams, etc. In addition, man-made composites, which are more and more employed in various fields of engineering, form an important class of heterogeneous materials. High stiffness and strength or high flexibility, light weight, increased toughness, low thermal expansivity, high fatigue performance and durability is an incomplete list of attainable properties of modern composites.

There are two fundamental questions when dealing with heterogeneous media: (i) how to relate the macroscopic behavior of the composite body to the properties of its individual components, and (ii) what is the smallest material volume to represent the behavior of the composite microstructure. The existing theories are primarily focused on the first question, where high level of sophistication has been developed especially in the case of linear elastic materials (see, for example, Sanchez-Palencia and Zaoui, 1987; Nemat-Nasser and Hori, 1999; Suquet, 1997; Castañeda *et al.*, 2004); while the second question, dealing with the determination of the size of a Representative Volume Element (RVE), is often ignored.

The RVE replaces the true material microstructure with a continuum model, existence of which is the first assumption of any continuum field theory. Knowing the minimal size of RVE becomes important in a number of situations:

- when statistical fluctuations of the material microstructure exist on a scale conventionally considered as homogeneous, but in reality it is not. Such situation is encountered when, for example, the size of the finite element is smaller than the RVE, which might lead to inaccurate modeling of the engineering problem at hand;
- the size of a material specimen for testing is smaller than the RVE, which happens when there is a need to determine material properties of a structure several meters in size (Huet, 1999);

- a composite is so expensive that only small samples of it are available or manufacturing of the RVE size material is too time-consuming;
- the dimension of the structure is smaller than the RVE of the material. The examples of such structures include thin films, pavements, coatings, MEMS or NEMS (micro- or nano- electromechanical systems).

The RVE is clearly set up in two basic cases (Ostoja-Starzewski, 1999, 2001): (i) a unit cell in a periodic microstructure (Fig. 1.1), and (ii) a domain containing infinitely many microscale elements (e.g. crystals or inclusions) in a random medium (Fig. 1.2). A periodic microstructure is a good approximation of ordered composites, where the certain part of the microstructure repeats itself in space. In a random composite, the validity of the *separation of scales* of continuum mechanics should be considered:

$$d < L_{RVE} \leq L_{macro}, \tag{1.1}$$

where d is the heterogeneity size (e.g. dispersion, void or single grain), L_{RVE} is the size of the mesoscale or RVE, at which the composite appears to be a representative of the entire ensemble, L_{macro} is the macroscale (the size of the body). For large mismatches in properties, inequality $(1.1)_1$ can be replaced by a stronger statement $d << L_{RVE}$.

Equation (1.1) allows one to smooth the heterogeneous microstructure, characterized by the microscale d, and work with an effective continuum over the range of scales from L_{RVE} through L_{macro}. The mesoscale links microscopic properties with the macroscopic behavior and is a convenient intermediate scale to work with.

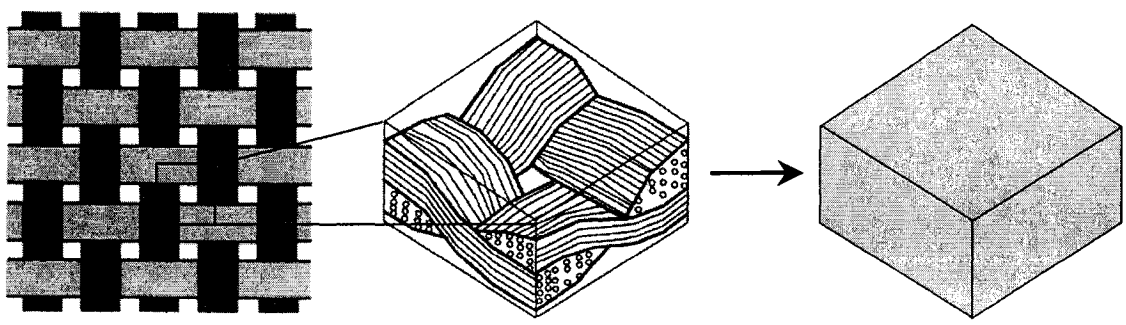

Figure 1.1. Representative volume element of a periodic composite (adapted from Tanov and Tabiei, 2001).

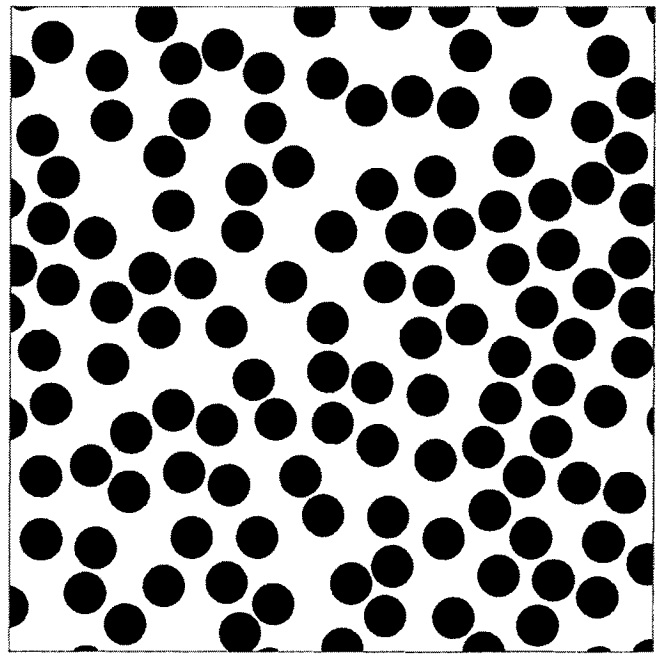

Figure 1.2. Two-dimensional realization of a random composite.

Overwhelmingly, in the case of random media, the prediction of effective properties of heterogeneous materials is usually based on *a priori* assumption of existence of the RVE, without clearly specifying its size relative to *d*. L_{RVE} is often taken to be 10 to 100 times bigger than the heterogeneity dimension without any clear reasoning. It is also very common to assume the microstructure to be periodic with random distribution of inclusions or grains inside the composite. In reality, however, responses of heterogeneous materials are not periodic and one cannot even produce a periodic material that would respond periodically (Ostoja-Starzewski, 2005).

In the absence of spatial periodicity in a random microstructure, the RVE is achieved exactly only in the limiting case of $\delta \to \infty$, where $\delta = L/d$ is a non-dimensional measure of the scale size. In many cases, however, one does not need to consider infinitely large domains for the determination of material properties, as these can be attained with a sufficient accuracy on a finite scale. The compelling questions become: what is the error in the material response as a result of assuming a specific RVE, and what is the effect of scale on the effective constitutive laws?

1.2 Background and state of the art

The standard way of estimating the minimum size of RVE of *random* materials is considering a relative error or deviation from the mean value of a specific property with increasing sample size. When deviations become negligibly small, the composite is assumed to converge toward the RVE. This representation of the RVE was adopted by many authors (Zohdi and Wriggers, 2000, 2001; Kanit *et al.*, 2003; Ren and Zheng, 2004; Lachihab and Sab, 2005; Sab and Nedjar, 2005). An alternative definition was proposed by Drugan and Willis (1996), who considered the RVE as the volume for which the overall effective constitutive model can be accurately characterized by the mean constitutive response obtained from the ensemble-averaged mean strain field. In other words, it requires not the scatter of results to be small but the average to be accurate. This leads to a relatively small RVE size estimation, as was shown by Gusev (1997), using Monte Carlo simulations, and by Drugan (2000), using a higher order analysis of overall constitutive equation. The numerical simulations, based on the approaches described above, can be found in Povirk (1994), Terada *et al.* (1998), Zeman and Sejnoha (2001), Roberts and Garboczi (2000, 2001), Meille and Garboczi (2000), Forest *et al.* (2000) and Segurado and Llorca (2002). Experimental investigation of the minimum size of RVE, using digital image correlation technique, was performed by Liu (2005).

The above-mentioned approaches do not consider the dependence of the RVE response on the type of boundary conditions applied, which, on the other hand, should be an inherent property of the RVE. Indeed, consider the response obtained on the composite samples satisfying two above definitions: if the composite is subjected to the traction boundary conditions, but the properties are determined under displacement boundary conditions, the response obtained can lead to an erroneous result. These considerations were taken into account by Hill (1963), who stated that the RVE must satisfy two requirements, namely, (i) it should be structurally typical to the whole microstructure and (ii) its properties should be the same under traction and displacement boundary conditions. This approach is called an asymptotic bound approach (Huet, 1990; Sab, 1992; Ostoja-Starzewski, 1998, 2006), which for linear elastic composites can be formulated as follows (Ostoja-Starzewski, 1998):

$$\left\langle \mathbf{S}_1^{\sigma} \right\rangle^{-1} \le \cdots \le \left\langle \mathbf{S}_{\delta'}^{\sigma} \right\rangle^{-1} \le \left\langle \mathbf{S}_{\delta}^{\sigma} \right\rangle^{-1} \le \cdots \le \mathbf{S}_{eff}^{-1} = \mathbf{C}_{eff} \le \cdots \le \left\langle \mathbf{C}_{\delta}^{\varepsilon} \right\rangle \le \left\langle \mathbf{C}_{\delta'}^{\varepsilon} \right\rangle \le \cdots \le \left\langle \mathbf{C}_1^{\varepsilon} \right\rangle,$$

for $1 < \delta' < \delta$. (1.2)

Here, $\left\langle \mathbf{S}^{\sigma} \right\rangle$ is an apparent compliance tensor obtained under uniform static boundary conditions and $\left\langle \mathbf{C}^{\varepsilon} \right\rangle$ is an apparent stiffness tensor obtained under uniform kinematic boundary conditions. Both $\left\langle \mathbf{S}^{\sigma} \right\rangle$ and $\left\langle \mathbf{C}^{\varepsilon} \right\rangle$ are sample size and shape dependant with $\left\langle \mathbf{S}^{\sigma} \right\rangle^{-1}$ approaching effective properties from below and $\left\langle \mathbf{C}^{\varepsilon} \right\rangle$ from above, thus, allowing to estimate the minimum RVE size within a specific relative error. Note, for any two fourth rank tensors $\mathbf{A}$ and $\mathbf{B}$, $\mathbf{A} \le \mathbf{B}$ means that $\mathbf{b} : \mathbf{A} : \mathbf{b} \le \mathbf{b} : \mathbf{B} : \mathbf{b}$ for any second rank tensor $\mathbf{b} \ne \mathbf{0}$.

The asymptotic bounds were theoretically derived and numerically estimated for many different physical problems, such as linear elasticity (Ostoja-Starzewski, 1998, 1999), heat transfer (thermal conductivity) (Ostoja-Starzewski and Schulte, 1996), plasticity (Jiang *et al.*, 2001; Ostoja-Starzewski, 2005; Li and Ostoja-Starzewski, 2006) and linear thermoelasticity (Du and Ostoja-Starzewski, 2006). It was shown (see the above-mentioned references) that as δ increases, the material properties approach effective values with a certain rate, either rapid, moderate or slow, depending on the composite microstructure, properties mismatch of the constituents and their interaction on a microscale, the physics of the problem (elastic, elastic-plastic, etc.) and the setting in 2-D or 3-D.

In this thesis the asymptotic bound approach is extended to nonlinear composites.

The examples of composites with nonlinear behavior include filled polymers and biological tissues. The addition of soft elastomers to hard brittle polymers improves fracture properties; a well-known example of such material is rubber-toughened epoxy resin. Other examples are neat plastics, which are often not strong enough to meet the requirements of some applications such as structural adhesives and high-performance composite materials. The addition of various fillers is a common way of improving their properties (Paul and Bucknall, 2000). Specific chemical treatment of polymers results in their embrittlement and loss of hyperelasticity. When such treatment is localized, which is often observed in polymeric membranes used in geo-environmental barrier systems

(Selvadurai and Yu, 2006), initially homogeneous membrane becomes a two-dimensional composite of stiff inclusions in soft hyperelastic matrix.

Various procedures have been developed to estimate the effective properties of nonlinear composites, especially for materials governed by power law constitutive response at small strains, see, for example the work by Talbot and Willis (1985), Willis (1989, 1991), Castañeda (1989, 1991), Suquet (1992), Moulinec and Suquet (1998, 2003), Michel *et al.* (1999), Hazanov (1999), Castaneda *et al.* (2004), Michel and Suquet (2004) and Lopez-Pamies and Castañeda (2006). The influence of the number of particles on the effective stress response of the composite subjected to *finite* deformations was studied numerically by Löhnert and Wriggers (2003) and Löhnert (2004). Hohe and Becker (2005) performed numerical homogenization of a periodic polymeric foams at finite strain. A second-order homogenization scheme was considered by Kouznetsova *et al.* (2004). However, no information has been obtained on the size of the RVE of nonlinear random composites in the framework of finite theory of elasticity, while nonlinear thermoelasticity to the author's best knowledge has not been considered at all. The objective of this work is to fill this gap and to develop scale-dependent homogenization technique which would allow estimation of bounds on the effective response of random composites and the size of the RVE for *physically nonlinear* materials subjected to *large isothermal* and *non-isothermal* deformations[1].

1.3 Structure of the thesis

In Chapter 2, some basics of continuum mechanics are briefly reviewed and the variational principles of finite elasticity are introduced. Details of the formulation of a boundary-value problem of the body, subjected to large deformations, are given. Through the application of variational principles, a scale-dependent hierarchy of strain-energy functions (i.e., mesoscale bounds) is derived for the effective strain-energy function. In order to account for the thermoelastic effects, the variational principles are first generalized, and then analogous bounds on the effective thermoelastic response are

[1]Chapter 5 does not follow the framework described above. It presents a study of the *size* effect on thermoelastic damping of nanomechanical resonators (see, Section 5.1).

derived. Different types of boundary conditions are considered and the relations between them are discussed. Finally, the difference between nonlinear and linear asymptotic bounding problems is considered.

In order to demonstrate the application of the developed scale-dependant homogenization, in Chapter 3, the procedure to quantitatively homogenize the heterogeneous medium and determine the RVE size is outlined. Mesoscale bounds defined under essential or natural boundary conditions are computed for several nonlinear elastic, planar composites, in which the matrix and inclusions differ not only in their material parameters but also in their strain-energy function representations. Various combinations of matrix and inclusion phases described by either neo-Hookean or Ogden function are then examined, and the results are compared to those of the linear elastic types.

Chapter 4 is focused on the application of the theory to the estimation and comparison of the trends toward the RVE of random non-periodic composites for two different theories of *thermoelasticity*: infinitesimal and finite. The free-energy function representation for a composite smaller than the RVE is considered for both theories. The scale-dependent bounds are computed for thermal strain and stress coefficients.

In Chapter 5 we study size effect on the vibration of a micro-/nanobeam resonator. The associated thermoelastic damping in such beams is considered from the standpoint of a generalized theory of thermoelasticity with one relaxation time. We study the size and vibration frequency at which the regular Fourier law of heat conduction is no longer valid and the finite speed of heat propagation has to be taken into account.

Finally, Chapter 6 gives a brief summary of the results obtained in this thesis and outlines perspectives for future work.

Chapter 2

Mesoscale bounds in finite elasticity and thermoelasticity of random composites: theoretical considerations [1]

In this chapter, we develop scale-dependent bounds on the effective response of random composites for *physically nonlinear* materials subjected to *large isothermal* and *non-isothermal* deformations. We follow the approach that originated in micromechanics some fifteen years ago (Huet, 1990; Sab, 1992; see also the review by Ostoja-Starzewski, 2001), driven by the need to derive continuum random field models from microstructures (Ostoja-Starzewski & Wang, 1989). We shall deal with "apparent" material properties at finite strain, that is, when the body is smaller than the RVE and when deformations are large. The idea is to consider properties of a composite material of the size smaller than the representative volume and apply variational principles along with different types of boundary conditions to investigate scale-dependence of material properties for various types of material microstructure. These results lay the ground for a quantitative estimation of the real size of the RVE presented in subsequent chapters.

2.1 Continuum mechanics preliminaries

There are three major differences, which distinguish the asymptotic bounding problem in finite elasticity from that of infinitesimal linear elasticity, namely, for the former:

1. The deformation can be described in different forms and in terms of different tensor quantities.
2. The complementary energy function is generally unknown, which results in problems in formulating the complementary energy principle and the minimum variational principles.
3. The constitutive equations are in general nonlinear and therefore a hierarchy of bounds for effective properties cannot be obtained in tensor form.

---

[1]Most of the material in this chapter has been published as an article in the *Proceedings of Royal Society, London A* (**85**, 153-173, 2006).

The present section deals with the first of these three aspects of the finite deformation theory. Consider a thermoelastic body undergoing equilibrium deformation in a three-dimensional Euclidian space. Let **x** and **X** denote the position vectors of a particle inside the body in the current and reference configurations, respectively; then the deformation of the body can be described as $\mathbf{x} = \chi(\mathbf{X})$ (Fig. 2.1). The deformation gradient tensor is given by

$$\mathbf{F} = \frac{\partial \chi(\mathbf{X})}{\partial \mathbf{X}} = \mathrm{Grad}\mathbf{x} = \mathrm{Grad}\mathbf{u} + \mathbf{I} \qquad \text{or} \qquad F_{ij} = \frac{\partial x_i}{\partial X_j} = \frac{\partial u_i}{\partial X_j} + \delta_{ij}, \tag{2.1}$$

where Grad**u** is the displacement gradient in material description, δ_{ij} is the Kronecker delta, and the indices i, j and k take on the values 1, 2, 3. Einstein summation convention is used. The equation of equilibrium in the absence of body forces has the form

$$\mathrm{Div}\mathbf{P} = \mathbf{0} \qquad \text{or} \qquad \frac{\partial P_{ij}}{\partial X_j} = 0. \tag{2.2}$$

Here **P** denotes the generally non-symmetric first Piola-Kirchhoff stress tensor and Div is the divergence calculated with respect to the reference configuration.

The key assumption of the finite hyperelasticity theory is the existence of a strain-energy function $\psi = \psi(F_{ij})$ per unit volume of the undeformed body, which depends on the deformation of the material and its properties. In the reference configuration, the equation of state of the material can be written as:

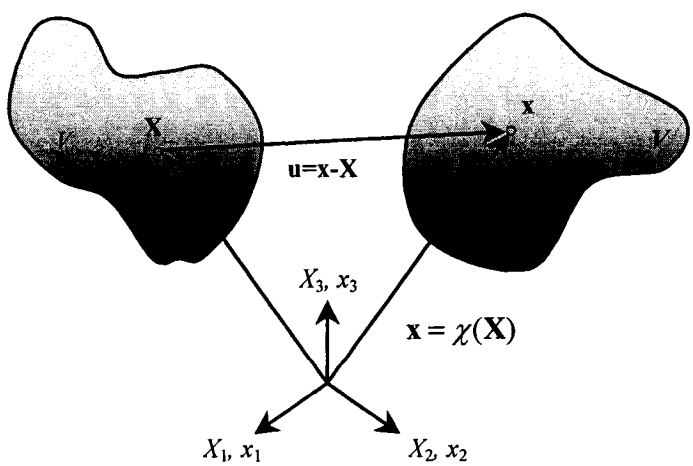

Figure 2.1. A continuum body in the reference and current configurations.

$$P_{ij} = \frac{\partial \psi}{\partial F_{ij}}, \tag{2.3}$$

If the temperature changes are to be considered, the strain-energy density should be replaced by the free energy as a function of both the deformation gradient and the temperature.

The constitutive relation (2.3) is given in the material description, because the first Piola-Kirchhoff stress tensor and the deformation gradient tensor are the only quantities, for which the averaging theorems and the Hill condition can be formulated in a way analogous to the infinitesimal deformation theory (for a discussion of these theorems the reader is referred to Section 2.4 of the thesis). Moreover, most of the strain-energy functions commonly employed in the literature are defined in the reference configuration. Using Eqs. (2.3) and (2.1), Eq. (2.2) can be rewritten as

$$\frac{\partial}{\partial X_j}\left(\frac{\partial \psi}{\partial u_{i,j}}\right) = 0, \tag{2.4}$$

2.2 Minimum theorems in finite elasticity and thermoelasticity

Variational principles for a material undergoing finite strains have been studied extensively by many researchers (e.g. Gao, 1999; Lee & Shield, 1980; Ogden, 1984; Koiter, 1976; de Veubeke, 1972; Zubov, 1971; Levinson, 1965). If the principle of stationary potential energy in finite elasticity can be formulated similar to that in infinitesimal-strain elasticity, the complementary energy principle cannot be established without certain restrictions, placed on the strain-energy function. In nonlinear elasticity, the strain-energy function may be nonconvex and therefore non-invertible; i.e., the deformation gradient cannot be expressed in terms of stress. Even the inversion of convex strain-energy functions is extremely difficult in general, which places a limitation on the use of the complementary energy theorem.

To overcome the difficulty of inversion, different "complementary-type" variational principles have been introduced in the literature. For the bounding problem considered here, we use the variational principles proposed by Lee & Shield (1980). In the following section, we outline this theory and extend it to the case of nonlinear thermoelastostatics.

2.2.1 Variational principles in finite elastostatics

Consider the functional

$$P\{U_i\} = \int_{V_0} \psi(U_{i,j})dV - \int_{S_T} t_i^0 U_i dS\,, \tag{2.5}$$

where V_0 is the material volume in the reference state, U_i is an admissible displacement field such that $U_i = u_i^0$ on the portion of the boundary where displacement is prescribed, S_U, and t_i^0 is the prescribed nominal traction on the remaining part of the boundary, S_T. Equation (2.5) represents the finite elasticity counterpart of the principle of stationary potential energy in linear elasticity theory. The functional $P\{U_i\}$ is stationary for the actual solution u_i, which satisfies the equilibrium equation (2.4) in V_0 and natural boundary conditions

$$\frac{\partial \psi}{\partial u_{i,j}} n_j = t_i^0 \text{ on } S_T. \tag{2.6}$$

Here n_j denotes an outward normal vector to the boundary surface in the reference configuration. Expanding the quantity $P\{u_i+\delta u_i,\ u_{i,j}+\delta u_{i,j}\}$ in Taylor series and ignoring terms of the third and higher order in δu_i, one can obtain the condition under which the functional $P\{U_i\}$ assumes a local minimum for the actual solution u_i for all non-zero values of δu_i such that $\delta u_i = 0$ on S_U (Lee & Shield, 1980):

$$\int_{V_0} \frac{\partial^2 \psi}{\partial u_{i,j} \partial u_{p,q}} \delta u_{i,j} \delta u_{p,q} dV > 0\,. \tag{2.7}$$

If the condition (2.7) holds, the principle of stationary potential energy becomes the minimum principle. Assuming interface continuity of the displacement and traction field inside the body, the above variational principle becomes valid for multiphase materials as well as for materials with continuously varying properties and can be used to estimate bounds on the effective material response.

We now turn to the investigation of the principle of minimum complementary energy. To overcome the difficulties of inversion in formulating the complementary energy functional, Lee & Shield (1980) proposed to consider the complementary strain-energy function ψ_c as a function of the deformation gradient rather than the stress:

$$\psi_c = \frac{\partial \psi}{\partial u_{i,j}} x_{i,j} - \psi\,. \tag{2.8}$$

Then, the complementary energy-type functional Q can be written as:

$$Q\{U_{ij}\} = \int_{V_0}\left\{\frac{\partial\psi}{\partial U_{ij}}U_{ij} - \psi\right\}dV - \int_{S_U}\frac{\partial\psi}{\partial U_{ij}}n_j u_i^0 dS\,, \tag{2.9}$$

where U_{ij} is an admissible deformation gradient tensor field satisfying

$$\frac{\partial}{\partial X_j}\left(\frac{\partial\psi}{\partial U_{ij}}\right) = 0 \text{ in } V_0 \text{ and } \frac{\partial\psi}{\partial U_{ij}}n_j = t_i^0 \text{ on } S_T. \tag{2.10}$$

Using the Lagrange multiplier method, it can be shown that the functional (2.9) is stationary for $U_{ij} = u_{i,j} + \delta_{ij}$, where u_i is the actual solution of a given elasticity problem. In order for Q to have a local minimum, the following condition should be fulfilled

$$\int_{V_0}\frac{\partial^2\psi}{\partial u_{i,j}\partial u_{p,q}}\delta u_{ij}\delta u_{pq}dV > 0 \tag{2.11}$$

for all nonzero δu_{ij} satisfying

$$\frac{\partial}{\partial X_j}\left(\frac{\partial^2\psi}{\partial u_{i,j}\partial u_{p,q}}\delta u_{pq}\right) = 0 \text{ in } V_0,\ \frac{\partial^2\psi}{\partial u_{i,j}\partial u_{p,q}}\delta u_{pq}n_j = 0 \text{ on } S_T. \tag{2.12}$$

Equation (2.11) is obtained by applying Taylor series expansion up to the second order in δu_{ij} to the quantity $Q\{u_{i,j}+\delta u_{ij}\}$, taking into account that Eqs. (2.12) need to be satisfied by both the actual and the admissible solution (see Apendix A).

Equations (2.5) through (2.12) define the variational principles in finite elastostatics for elastic bodies not subjected to constraints. For the case when internal constraints, such as incompressibility, are present, the components of the deformation gradient tensor are not arbitrary, and additional conditions need to be considered in formulating minimum potential and complementary energy-type theorems (Lee & Shield, 1980).

2.2.2 Variational principles in finite thermoelastostatics

Here we consider an uncoupled thermoelastic problem, in which the material is at rest and the heat flow is steady. In this case, the equation of heat conduction can be solved separately from the remaining field equations, and the temperature field T is determined uniquely by thermal boundary conditions. Minimum energy principles in this case can be derived using the Helmholtz free-energy function $\psi = \psi(\mathbf{F}, T)$ and the Gibbs

thermodynamic potential $g = g(\mathbf{P},T)$ in place of the isothermal strain energy and the complementary strain energy, respectively. g is associated with ψ by the transformation

$$g(\mathbf{P},T) = \psi - \mathbf{P}:\mathbf{F} \qquad \text{or} \qquad g\left(\frac{\partial \psi}{\partial u_{i,j}},T\right) = \psi - \frac{\partial \psi}{\partial u_{i,j}} x_{i,j}. \tag{2.13}$$

The potential energy functional (2.5) can be rewritten as

$$P\{U_i\} = \int_{V_0} \psi(U_{i,j},\theta_0)dV - \int_{S_T} t_i^0 U_i dS, \tag{2.14}$$

where θ_0 is the prescribed temperature field. For simplicity we will assume the temperature to be uniform throughout the volume. The Helmholtz free energy in nonlinear elasticity has the form (Holzapfel, 2000)

$$\psi(U_{i,j},T) = \psi_0(U_{i,j})\frac{T}{T_0} - e_0(U_{i,j})\frac{\Delta T}{T_0} + \hat{T}(T), \tag{2.15}$$

where T_0 is the temperature at reference state, $\Delta T = T - T_0$ is the temperature change, ψ_0 is the free energy at reference temperature, e_0 is the internal energy at reference temperature and $\hat{T}$ is a purely thermal contribution defined as

$$\hat{T} = -\int_{T=T_0}^{T=\theta_0} c_{\mathbf{F}}(T)(\theta_0 - T)\frac{dT}{T}. \tag{2.16}$$

Here $c_{\mathbf{F}}(T)$ is the specific heat capacity at constant deformations. For infinitesimal elastic deformations, Eq. (2.15) can be easily reduced to a well-known Helmholtz free-energy form by taking $\psi_0 = \frac{1}{2}C_{ijkl}\varepsilon_{ij}\varepsilon_{kl}$, $e_0 = \frac{1}{2}C_{ijkl}\varepsilon_{ij}\varepsilon_{kl} + C_{ijkl}\varepsilon_{ij}\alpha_{kl}T_0$, and assuming $c_{\mathbf{F}}$ to be a constant over a given small temperature change. In the above equations, ε_{ij} is the strain tensor, C_{ijkl} is the stiffness tensor and α_{ij} is the coefficient of thermal expansion.

Varying independently the quantities u_i and $u_{i,j}$, while keeping the temperature θ_0 constant, it can be proven by the same procedure as used in Section 2.3.1 that the functional (2.14) is stationary for the actual solution $U_i = u_i$ and provides a local minimum if

$$\int_{V_0}\left(T\frac{\partial^2 \psi_0}{\partial u_{i,j}\partial u_{p,q}} - \Delta T\frac{\partial^2 e_0}{\partial u_{i,j}\partial u_{p,q}}\right)\delta u_{i,j}\delta u_{p,q}dV > 0 \tag{2.17}$$

for all non-zero δu_i vanishing over the surface upon which the displacement is prescribed. Applying the transformation (2.13), the complementary functional becomes

$$Q\{U_{ij}\} = -\int_{V_0} g(U_{ij},\theta_0)dV - \int_{S_U} \frac{\partial \psi}{\partial U_{ij}} n_j u_i^0 dS, \tag{2.18}$$

where g can be written as

$$g = -\frac{\theta_0}{T_0}\left(\frac{\partial \psi_0}{\partial u_{i,j}} x_{i,j} - \psi_0\right) + \frac{\Delta T}{T_0}\left(\frac{\partial e_0}{\partial u_{i,j}} x_{i,j} - e_0\right) + \hat{T}(\theta_0) \tag{2.19}$$

The functional (2.19) assumes a local minimum provided

$$\int_{V_0}\left(T\frac{\partial^2 \psi_0}{\partial u_{i,j}\partial u_{p,q}} - \Delta T\frac{\partial^2 e_0}{\partial u_{i,j}\partial u_{p,q}}\right)\delta u_{ij}\delta u_{pq}dV > 0 \tag{2.20}$$

for all nonzero δu_{ij} satisfying Eq. (2.12), in which ψ is replaced by the free-energy function (2.15). The energetic contribution, e_0, to Eq. (2.15) appears only in the modified entropic theory of rubber thermoelasticity, and is equal to zero in the case of a purely entropic theory, for which conditions (2.17) and (2.20) simply reduce to the isothermal inequalities (2.7) and (2.11).

Note that inequalities (2.7) and (2.11) are the convexity conditions on ψ. They play an important role in hyperelasticity by ensuring the stability of the material; the strain-energy models fitted to available experimental data are commonly designed so as to avoid the lack of convexity (Holzapfel *et al.*, 2000). The discussion of the convexity condition on the strain-energy function can be found in the work of Ball (1977), Ogden (1984), Ciarlet (1988), Gao (1999) and Steigmann (2003).

2.3 Averaging theorems in finite deformation theory

Averaging theorems play a key role in the estimation of the overall properties of heterogeneous materials. It is known that, in the small deformation theory, volume averages of infinitesimal strain and stress fields can be fully determined from the surface data (e.g. Nemat-Nasser & Hori, 1999). In finite elasticity theory, the relation between strain and displacement gradient is nonlinear, which leads to difficulties in evaluation of the volume averages. Hence, different deformation measures should be considered when dealing with a problem involving finite strain. In this section we will formulate averaging

theorems along with the Hill condition for two conjugate quantities, namely, the deformation gradient tensor and the first Piola-Kirchhoff stress tensor. For the sake of completeness, the proofs of the given theorems are outlined in Appendix B.

2.3.1 Average deformation gradient theorem

Deformation gradient is one of the simplest kinematic variables and the only deformation measure for which the average theorem can be derived in finite elasticity theory. The average theorem for the deformation gradient can be formulated as follows: under uniform displacement boundary conditions the volume average of the deformation gradient is equal to the deformation gradient applied at the boundary:

$$\overline{F}_{ij} \equiv \frac{1}{V_0}\int_{V_0} F_{ij}(X_k)dV = F^0_{ij}, \tag{2.21}$$

where F^0_{ij} is the prescribed deformation gradient acting on the boundary, S_0, in the reference configuration. The superposed bar here and elsewhere denotes the volume average of the overall macroscopic quantity.

2.3.2 Average stress theorem

The average stress theorem states that under uniform traction boundary conditions the volume average of stress is equal to the stress applied at the boundary:

$$\overline{P}_{ij} \equiv \frac{1}{V_0}\int_{V_0} P_{ij}(X_k)dV = P^0_{ij}, \tag{2.22}$$

where P^0_{ij} is a nominal stress prescribed through the traction field $t^0_i = P^0_{ij}n_j$ acting on the boundary S_0 in the reference configuration.

Assuming no jump in displacement and traction across the boundary between different phases of the composite, theorems (2.21) and (2.22) can be proven by transforming the volume integral via the Green-Gauss theorem. One of the main consequences of these theorems is that they allow controlling the values of the effective deformation gradient tensor and the first Piola-Kirchhoff stress tensor of a heterogeneous material.

Theorems (2.21) and (2.22) were first considered by Hill (1972) and then re-examined by many authors (e.g. Nemat-Nasser, 1999; Löhnert & Wriggers, 2003;

Costanzo *et al.*, 2005). In fact, in finite elasticity, the average stress theorem holds for both spatial and material descriptions (Hill, 1972), i.e., for both the Cauchy and the first Piola-Kirchhoff stress tensors. This is not surprising since both tensors represent the same resultant force acting on a surface element of the deformed body.

It is worth mentioning, that theorem (2.22) holds only for a static process in the absence of body forces. If that assumption fails, one has to consider the effective value of a target quantity, not the "true" average over the volume (Costanzo *et al.*, 2005). Moreover, in nonlinear elasticity the relations

$$\overline{\sigma}_{ij} = \overline{J}^{-1}\overline{P}_{ik}\overline{F}_{jk}, \tag{2.23}$$

where σ_{ij} is the symmetric Cauchy stress tensor and $J = \det(F_{ij})$ is the Jacobian, are found to be true only under uniform displacement and periodic boundary conditions, and meaningful in the case of traction boundary condition (Costanzo *et al.*, 2005). In linear homogenization problems, this relation always holds, which is expected since the first Piola-Kirchoff and the Cauchy stresses for infinitesimal deformations coincide.

2.3.3 Hill condition for finite deformations

A well-known criterion in a homogenization problem is the so-called *Hill condition.* It represents a condition under which the mechanical and energetic definitions of the effective properties are compatible. For the deformation gradient tensor and the first Piola-Kirchhoff stress tensor, it can be stated as follows (Hill, 1972; Nemat-Nasser, 1999):

$$\overline{P_{ij}F_{ij}} = \overline{P}_{ij}\overline{F}_{ij}. \tag{2.24}$$

The Hill condition is trivially satisfied by a homogeneous body, but imposes certain restrictions on the boundary conditions, if the body is heterogeneous.

Applying the Green-Gauss theorem and noting that from the equilibrium equation in the absence of body forces $P_{ij,j} = 0$, we get

$$\overline{P_{ij}F_{ij}} - \overline{P}_{ij}\overline{F}_{ij} = \frac{1}{V_0}\int_{S_0}\left(t_i - \overline{P}_{ij}n_j\right)\left(u_i - (\overline{F}_{ij} - \delta_{ij})X_j\right)dV, \tag{2.25}$$

where S_0 is the boundary surface of the body in the reference configuration. When the boundary conditions are such that the right hand side integral vanishes, the average of the

product of the deformation gradient tensor and the stress tensor is equal to the product of their averages. This leads to three types of boundary conditions, which allow the use of the Hill condition when dealing with inhomogeneous bodies:

1. Kinematic uniform boundary condition (KUBC) (prescribing a volume average deformation gradient):

$$u_i = (F_{ij}^0 - \delta_{ij})X_j, \ \forall X_j \in S_0. \tag{2.26}$$

2. Static uniform boundary condition (SUBC) (prescribing a volume average nominal stress):

$$t_i = P_{ij}^0 n_j, \ \forall X_j \in S_0. \tag{2.27}$$

3. Uniform orthogonal-mixed boundary condition:

$$\left(t_i - P_{ij}^0 n_j\right)\left(u_i - (F_{ij}^0 - \delta_{ij})X_j\right) = 0, \ \forall X_j \in S_0, \tag{2.28}$$

where the averaging theorems (2.21) and (2.22) have been used.

In linear elasticity, the Hill condition is written in the following form

$$\overline{\sigma_{ij}\varepsilon_{ij}} = \bar{\sigma}_{ij}\bar{\varepsilon}_{ij} \Leftrightarrow \frac{1}{V_0}\int_{S_0}\left(t_i - \bar{\sigma}_{ij}n_j\right)\left(u_i - \bar{\varepsilon}_{ij}x_j\right)dV = 0, \tag{2.29}$$

and is satisfied by two boundary conditions analogous to the one considered above: KUBC $u_i^0 = \varepsilon_{ij}^0 x_j, \ \forall x_j \in \partial S$, and SUBC $t_i = \sigma_{ij}^0 n_j, \ \forall x_j \in \partial S$.

In the following, we shall use the boundary conditions (2.26) and (2.27) along with the variational principles introduced in Section 2.3 for the estimation of bounds on the effective response of nonlinear composites.

2.4 Hierarchies of mesoscale bounds in finite elasticity and thermoelasticity of random composites

Consider a random heterogeneous material, $\mathbf{B} = \{B(\omega); \omega \in \Omega\}$, where each point ω corresponds to a sample space Ω and $B(\omega)$ is a specific realization of some spatial (2-D or 3-D) random process. Here we distinguish only two phases: matrix $B_1(\omega)$ and inclusion $B_2(\omega)$ although the results presented in the chapter can be readily extended to multiphase materials. In general, the random medium is described by a distribution of phases, such that $B_1(\omega) \cup B_2(\omega) = B(\omega)$ and $B_1(\omega) \cap B_2(\omega) = \varnothing$ (Torquato, 2002), which can be set

up on the basis of point fields. While in the periodic homogenisation one is usually concerned with phase distribution within the periodic window directly taken as the RVE (Fig. 2.2), the homogenisation in random media can be carried out only if a statistical homogeneity assumption is imposed. This implies the invariance of probability distributions under arbitrary translations. In addition, we require the random medium to be ergodic, i.e., that any one realization of the composite is representative of the entire ensemble:

$$\langle F \rangle = \lim_{V_0 \to \infty} \frac{1}{V_0} \int_{V_0} F dV , \tag{2.30}$$

where $\langle \bullet \rangle$ denotes ensemble average.

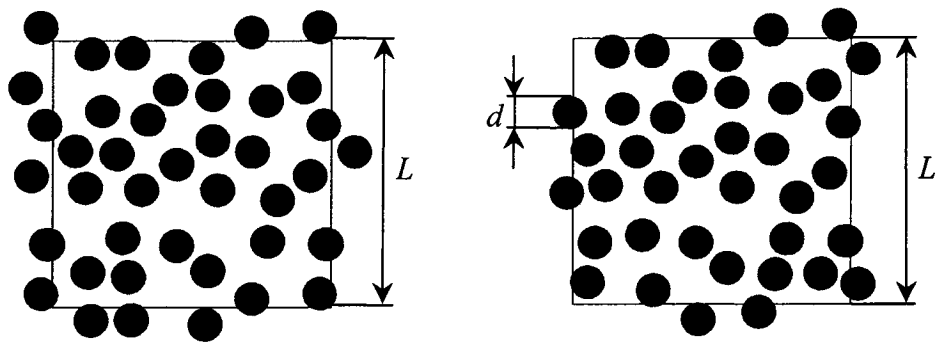

(a) (b)

Figure 2.2. (a) a disordered microstructure of a periodic composite with a periodic window of size L; (b) one realization of a random composite $B_\delta(\omega)$ of size L.

Next, we introduce a non-dimensional scale parameter, $\delta = L/d$, where d is the heterogeneity size (e.g. single grain) and L is the size of a *mesoscale* domain. Consider a partition of a body of size δ into n smaller square elements of size $\delta' = \frac{\delta}{n}$ ($n = 2$ in Fig. 2.3). Defining two types of boundary conditions (e.g. Ostoja-Starzewski, 2001) – *restricted* (the boundary condition specified on the boundary of each element) and *unrestricted* (the boundary condition specified on the boundary of the whole body) - one observes that the deformation of the material under the restricted boundary condition represents an admissible field for the unrestricted boundary condition, but not conversely.

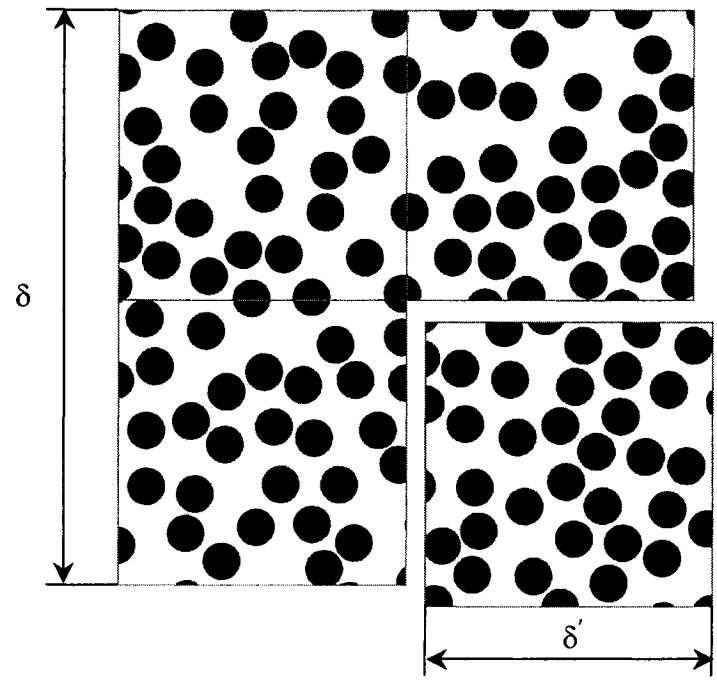

Figure 2.3. Partition of a window B_δ of scale δ into four square-shaped sub-windows B'_δ.

Consider now the uniform displacement boundary condition (2.26) when the volume average deformation gradient is prescribed. In this case, S_T is equal to zero and the functional (2.5) reduces to

$$P\{U_i\} = \int_{V_0} \psi(U_{i,k}, X_j)\, dV\,, \tag{2.31}$$

where the strain-energy function is now a function of both deformation gradient and coordinates. Under the assumption that the minimum theorem holds, the energy stored in the body under the restricted boundary conditions is related to the unrestricted one as

$$\Psi(\omega, \mathbf{F}^0) \leq \Psi^r(\omega, \mathbf{F}^0)\,, \tag{2.32}$$

where $\Psi(\omega, \mathbf{F}^0) = \int_{V_0} \psi(\omega, \mathbf{X}, \mathbf{F})\, dV$ is the elastic energy of any given realization B(ω) of the composite, and the superscript r denotes the effective properties obtained under restricted boundary conditions. Henceforth, in order to simplify the notation, we shall write ψ instead of $\psi(\omega, \mathbf{X}, \mathbf{F})$. With Δ and 1 denoting the RVE size and inhomogeneity size, respectively, upon ensemble averaging, we obtain for the upper bound

$$\left\langle \Psi(\mathbf{F}^0) \right\rangle_\Delta \leq \left\langle \Psi(\mathbf{F}^0) \right\rangle_\delta \leq \left\langle \Psi(\mathbf{F}^0) \right\rangle_{\delta'} \leq \left\langle \Psi(\mathbf{F}^0) \right\rangle_1, \text{ for } 1 < \delta' < \delta < \Delta\,. \tag{2.33}$$

The hierarchy (2.33) can be generalized for the case of thermoelastostatics to be

$$\left\langle \Psi(\mathbf{F}^0,\theta_0)\right\rangle_{\Delta} \le \left\langle \Psi(\mathbf{F}^0,\theta_0)\right\rangle_{\delta} \le \left\langle \Psi(\mathbf{F}^0,\theta_0)\right\rangle_{\delta'} \le \left\langle \Psi(\mathbf{F}^0,\theta_0)\right\rangle_{1}, \text{ for } 1<\delta'<\delta<\Delta. \quad (2.34)$$

We now turn to the investigation of an analogous reciprocal expression for the lower bounds. Under the uniform traction boundary condition (2.27), the functional Q reduces to

$$Q\{U_{ik}\} = \int_{V_0}\left\{\frac{\partial \psi}{\partial U_{ik}}U_{ik} - \psi\right\}dV. \quad (2.35)$$

Since we consider dead loading, the choice of a statically admissible stress does not depend on the kinematically admissible deformation, and, thus, the following inequality holds between responses under restricted and unrestricted boundary conditions

$$\Psi^*(\omega,\mathbf{P}^0) \le \Psi^{*r}(\omega,\mathbf{P}^0), \quad (2.36)$$

where $\Psi^*(\omega,\mathbf{P}^0) = \int_{V_0}\left\{\frac{\partial \psi}{\partial U_{ij}}U_{ij} - \psi\right\}dV$. From this, upon ensemble averaging, we can derive a scale-dependent hierarchy of the lower bound on the effective properties

$$\left\langle \Psi^*(\mathbf{P}^0)\right\rangle_{\Delta} \le \left\langle \Psi^*(\mathbf{P}^0)\right\rangle_{\delta} \le \left\langle \Psi^*(\mathbf{P}^0)\right\rangle_{\delta'} \le \left\langle \Psi^*(\mathbf{P}^0)\right\rangle_{1}, \text{ for } 1<\delta'<\delta<\Delta, \quad (2.37)$$

which in thermoelastostatics takes the form

$$\left\langle G(\mathbf{P}^0,\theta_0)\right\rangle_{\Delta} \ge \left\langle G(\mathbf{P}^0,\theta_0)\right\rangle_{\delta} \ge \left\langle G(\mathbf{P}^0,\theta_0)\right\rangle_{\delta'} \ge \left\langle G(\mathbf{P}^0,\theta_0)\right\rangle_{1}, \text{ for } 1<\delta'<\delta<\Delta, \quad (2.38)$$

where $G(\omega,\mathbf{P}^0,\theta_0) = \frac{1}{V_0}\int_{V_0} g(\omega,\mathbf{X},\mathbf{P},\theta_0)dV$.

Noting that $\frac{\partial \psi}{\partial U_{ik}}U_{ik}$ can be equivalently expressed as $\mathbf{P}:\mathbf{F}$ we can write

$$\Psi^*(\omega,\mathbf{P}^0) = V_0\left(\overline{\mathbf{P}:\mathbf{F}}\right) - \Psi(\omega,\mathbf{P}^0) = V_0\left(\mathbf{P}^0:\overline{\mathbf{F}}\right) - \Psi(\omega,\mathbf{P}^0), \quad (2.39)$$

where averaging theorems (2.22) and (2.24) have been employed. For the RVE size composite material, application of different types of boundary conditions leads to a similar response, and, therefore, $\Psi^*(\omega,\mathbf{P}_0) = \Psi^*(\omega,\mathbf{F}_0)$ and $\Psi(\omega,\mathbf{F}_0) = \Psi(\omega,\mathbf{P}_0)$. Then, the lower bound (2.37) can be rewritten as

$$\left\langle \Psi(\mathbf{P}^0)\right\rangle_{1} - V_0\left\langle \overline{\mathbf{P}:\mathbf{F}}\right\rangle_{1} + V_0\left\langle \overline{\mathbf{P}:\mathbf{F}}\right\rangle_{\Delta} \le \left\langle \Psi(\mathbf{P}^0)\right\rangle_{\delta'} - V_0\left\langle \overline{\mathbf{P}:\mathbf{F}}\right\rangle_{\delta'} + V_0\left\langle \overline{\mathbf{P}:\mathbf{F}}\right\rangle_{\Delta}$$

$$\le \left\langle \Psi(\mathbf{P}^0)\right\rangle_{\delta} - V_0\left\langle \overline{\mathbf{P}:\mathbf{F}}\right\rangle_{\delta} + V_0\left\langle \overline{\mathbf{P}:\mathbf{F}}\right\rangle_{\Delta} \le \left\langle \Psi(\mathbf{P}^0)\right\rangle_{\Delta}, \text{ for } 1<\delta'<\delta<\Delta. \quad (2.40)$$

Bounds (2.33) and (2.40) allow estimating the convergence rate and, consequently, the RVE size for any nonlinear composite satisfying convexity requirements (2.7) and (2.11) on their strain-energy function.

Note that, strictly speaking, Δ (denoting the RVE size L relative to the microheterogeneity, d) is infinite for a random medium lacking any spatial periodicity, but the convergence of upper and lower bounds may well be achieved within an accuracy of a few percent already at small scales (see e.g. Jiang *et al.*, 2001; Ostoja-Starzewski & Castro, 2003 for case studies of two physically nonlinear composites).

In the small deformation theory, the effective strain-energy function, $\Psi_{eff} = \frac{1}{2}\boldsymbol{\varepsilon} : \mathbf{C}_{eff} : \boldsymbol{\varepsilon}$, is equal to the complementary energy function, $\Psi^{*}_{eff} = \frac{1}{2}\boldsymbol{\sigma} : \mathbf{S}_{eff} : \boldsymbol{\sigma}$, and hierarchies (2.33) and (2.37) can be combined to give (Ostoja-Starzewski, 2006):

$$\left\langle \mathbf{S}_1^{\sigma} \right\rangle^{-1} \le \cdots \le \left\langle \mathbf{S}_{\delta'}^{\sigma} \right\rangle^{-1} \le \left\langle \mathbf{S}_{\delta}^{\sigma} \right\rangle^{-1} \le \cdots \le \mathbf{S}_{eff}^{-1} = \mathbf{C}_{eff} \le \cdots \le \left\langle \mathbf{C}_{\delta}^{\varepsilon} \right\rangle \le \left\langle \mathbf{C}_{\delta'}^{\varepsilon} \right\rangle \le \cdots \le \left\langle \mathbf{C}_1^{\varepsilon} \right\rangle . \quad (2.41)$$

Here $\mathbf{S}$ is the compliance tensor and the superscripts ε and σ define properties obtained under uniform kinematic and uniform static boundary conditions in linear elasticity, respectively.

Introducing a power-law type energy function into the inequalities (2.33) and (2.37), a hierarchy of bounds on elastic tensors can be obtained in the same manner as in the infinitesimal strain theory (Hazanov, 1999). In the case of more complex energy functions (such as those described by Ogden (1972)), it is more convenient to work directly with the energy functions.

It is worth mentioning that the main assumption involved in the derivation of Eqs. (2.33), (2.34), (2.37) and (2.38) is that the minimum principles described in Section 2.3 hold for any kinematically admissible displacement. In reality, these inequalities provide a *global* minimizer criterion only if the strain-energy function is convex, which is just a mathematical assumption. For materials described by nonconvex strain-energy functions, bounds (2.33) – (2.38) hold only locally in the range of validity of inequalities (2.7) – (2.20), which places a limitation on their use. If the inversion of the constitutive relation (2.3) is not unique, an alternative complementary variational principle, such as the one proposed by Gao (1999) can be used.

2.5 Classical bounds

Early theoretical studies on bounding of effective properties in linear elasticity were carried out by Voigt and Reuss, who proposed approximations for the effective material properties based on simplifying assumptions, respectively, of uniform strain and uniform stress fields inside a composite. A generalization of the above mentioned bounds in the context of finite elasticity was first carried out by Ogden (1978) for a convex strain-energy function. A more general assumption of polyconvexity of ψ was later considered by Castañeda (1989).

It follows from the minimum potential energy theorem that under kinematic uniform boundary conditions

$$\int_{V_0} \psi(u_{i,k}, X_j) dV \leq \int_{V_0} \psi(\bar{u}_{i,k}) dV \tag{2.42}$$

or

$$\langle \Psi \rangle_{\Delta} \leq \overline{\Psi}, \tag{2.43}$$

which provides a *strict* upper (Voigt) bound on material properties. Indeed, as δ approaches zero, the displacement gradient field within the composite becomes more and more uniform (Fig. 2.3), which finally results in the strain-energy function tending to a simple weighted average of the energy functions of both phases:

$$\left\langle \Psi(\mathbf{F}^0) \right\rangle_{\delta \to 0} = V_1 \psi_1(\mathbf{F}^0) + V_2 \psi_2(\mathbf{F}^0). \tag{2.44}$$

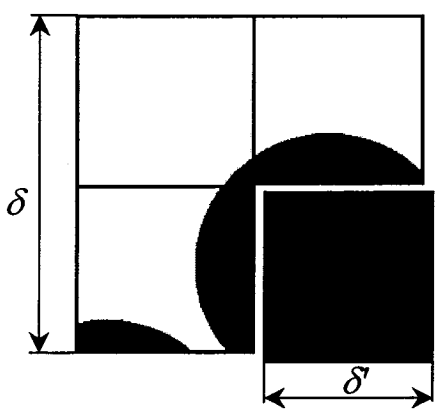

Figure 2.3. Partitioning of a window of scale δ into four squares of scale $\delta' < 1$.

The *strict lower* (Reuss) bound can be obtained in the same fashion from the complementary energy theorem:

$$\left\langle \Psi^* \right\rangle_{\Delta} \le \overline{\Psi^*} . \tag{2.45}$$

In practice, the bound (2.45) is of little use since the complementary energy function in nonlinear elasticity is generally unknown. We shall therefore investigate the strict lower bound in a different way. Consider the complementary energy-type functional in the form

$$Q\{U_{ij}\} = \int_{V_0} \left\{ \frac{\partial \psi}{\partial U_{ij}} U_{ij} - \psi \right\} dV - \int_{S_U} \frac{\partial \psi}{\partial U_{ij}} n_j x_i^0 dS , \tag{2.46}$$

where x_i^0 denotes the coordinates of a particle inside the body in the current configuration. Under the kinematic uniform boundary condition $S_U = S_0$ and upon application of the Green-Gauss theorem, the functional (2.46) reduces to

$$Q\{U_{ij}\} = -\int_{V_0} \psi dV . \tag{2.47}$$

At the same time, for an admissible stress field in the composite we have

$$Q\{P_{ij}\} \le Q\{\overline{P}_{ij}\} \tag{2.48}$$

or

$$\left\langle \Psi \right\rangle_{\Delta} \ge \overline{\Psi}(\overline{\mathbf{P}}) , \tag{2.49}$$

which provides a strict lower bound on the effective strain-energy function.

Note, that the Voigt and Reuss bounds do not give any information on the size of the RVE and, while rigorous, provide a very bad estimate of the effective material properties. As is well known, the Hashin-Shtrikman bounds (Hashin and Shtrikman, 1963; Castañeda, 1989) also provide bad estimates as the phases' mismatch in the microstructure grows. By contrast, the bounds investigated in Section 2.5 are progressively tight with the mesoscale growing.

2.6 Order relationships for mixed boundary conditions

In the above derivations, we used two boundary conditions (2.26) and (2.27), which provide upper and lower bounds on the effective response of random composites, respectively. These boundary conditions are easy to treat analytically and numerically, however, they are difficult to apply practically. On the other hand, an experimental setup

can be best represented by mixed boundary conditions. For example, in a simple tension test the displacement boundary conditions are applied on two parallel faces while the remaining four faces are traction-free.

The question of evaluating effective properties under mixed boundary condition (2.28) in linear elasticity was studied by Hazanov and Huet (1994), Hazanov and Amieur (1995) and Hazanov (1998). They considered a family of orthogonal mixed boundary-value problems, which satisfy the Hill condition and are defined in the following form:

$$u_i = \bar{\varepsilon}_{ij} x_j, \tag{2.50}$$

$$t_i = \bar{\sigma}_{ij} n_j. \tag{2.51}$$

It was shown that under this type of loading, the overall mixed stiffness tensor falls between the static and kinematic one:

$$\left\langle \mathbf{S}_\delta^\sigma \right\rangle^{-1} \le \left\langle \mathbf{C}_\delta^m \right\rangle \le \left\langle \mathbf{C}_\delta^\varepsilon \right\rangle. \tag{2.52}$$

Here superscript m denotes the solution field in the mixed boundary-value problem.

Other types of boundary conditions considered in the literature involve earlier discussed periodic boundary conditions (see Chapter 1) and the so-called minimal kinematic boundary conditions introduced by Mesarovic and Padbidri (2005). While the stiffness from the periodic boundary conditions levels off very rapidly, the computed response, under the minimal kinematic boundary conditions, approaches the effective properties from below and generally represents an alternative to the lower bound with an artificially imposed averaged strain field. None of these boundary conditions satisfies the Hill averaging theorem (2.24) and, in general, cannot be applied experimentally.

Let us now examine order relations for mixed boundary-value problems in nonlinear elasticity.

Following Hazanov and Huet (1994), due to no stress requirements on the boundary, $S_0 = S_U$, any divergence-free stress field is an admissible field for the kinematic boundary condition, defined below by a superscript **F**. From the minimum complementary energy-type theorem it follows

$$\left\langle \int_{V_0} \{P_{ij} : F_{ij}^0 - \psi\} dV - \int_{S_0} P_{ij} n_j x_i^0 dS \right\rangle^{\mathbf{F}} \le \left\langle \int_{V_0} \{P_{ij} : F_{ij} - \psi\} dV - \int_{S_U} P_{ij} n_j x_i^0 dS \right\rangle^{m}, \tag{2.53}$$

or, applying the divergence theorem to the left hand side,

$$\left\langle \int_{V_0} \psi dV \right\rangle^{\mathbf{F}} \geq \left\langle -\int_{V_0} \{P_{ij} : F_{ij} - \psi\} dV + \int_{S_U} P_{ij} n_j x_i^0 dS \right\rangle^{m}. \tag{2.54}$$

Proceeding in an analogous way, but using the minimum potential energy theorem, we find

$$\left\langle \int_{V_0} \psi dV - \int_{S} P_{ij}^0 n_j x_i dV \right\rangle^{\mathbf{P}} \leq \left\langle \int_{V_0} \psi dV - \int_{S_T} P_{ij}^0 n_j x_i dS \right\rangle^{m}, \tag{2.55}$$

since under the static boundary condition, defined above by a superscript **P**, an admissible displacement field is not subject to any requirements on the boundary.

With the use of the divergence theorem, it can be easily shown that the right hand side of Eq. (2.54) is equal to the right hand side of Eq. (2.55). Therefore, combining Eq. (2.54) with Eq. (2.55), we get

$$\left\langle \int_{V_0} \{\psi - P_{ij}^0 F_{ij}\} dV \right\rangle^{\mathbf{P}} \leq \left\langle \int_{V_0} \psi dV - \int_{S_T} P_{ij}^0 n_j x_i dS \right\rangle^{m} \leq \left\langle \int_{V_0} \psi dV \right\rangle^{\mathbf{F}}. \tag{2.56}$$

We cannot further simplify inequalities (2.56) unless additional information is known about the strain-energy function, although certain conclusions can be made at this stage. Let us consider a specific mixed boundary-value problem, where $P_{ij}^0 = 0, \forall X_i \in S_T$. This will simplify Eq. (2.56) to

$$\left\langle \int_{V_0} \{\psi - P_{ij}^0 F_{ij}\} dV \right\rangle^{\mathbf{P}} \leq \left\langle \int_{V_0} \psi dV \right\rangle^{m} \leq \left\langle \int_{V_0} \psi dV \right\rangle^{\mathbf{F}}, \tag{2.57}$$

which shows that the strain-energy function under mixed boundary conditions is bounded from above by the strain-energy function, obtained under kinematic uniform boundary conditions. In the following chapter, we will numerically estimate bounds on the strain-energy function, and investigate the convergence of the material response under different types of mixed boundary conditions in nonlinear elasticity.

2.7 Linear versus nonlinear bounding problems

Effective properties of a random composite in linear thermoelasticity were recently studied by Du & Ostoja-Starzewski (2005); a scale-dependent hierarchy of bounds on the thermal expansion coefficient was derived in a way analogous to the one considered in this work. Now, contrary to the linear elasticity case, the behavior of random *nonlinear* composites, subjected to temperature changes, is not governed by a thermal expansion coefficient α_{ij} alone, but by a number of temperature dependent constants. Moreover, the only materials, which respond elastically when subjected to finite strains and temperature changes, are biological soft tissues and rubber-like materials (Holzapfel, 2000), whose thermomechanical behavior is almost entirely based on the entropy concept. Total stress in these materials is caused by a change in entropy with deformation, while internal energy does not change with deformation at all. Therefore, the behavior of composites in finite thermoelasticity is expected to be very different from the one in linear elasticity. The focus of this section is comparing the above-derived hierarchies in nonlinear elasticity with the results in the linear elasticity theory.

Consider an isothermal elasticity problem. In linear elasticity, the volume average of strain energy of the body can be fully determined from surface data, if one of the "canonical" boundary conditions, Eqs. (2.26) or (2.27), is applied. One of the main consequences is that, for a macroscopically isotropic composite with isotropic phases, the hierarchy on effective infinitesimal strain-energy function can be separated into volumetric and deviatoric parts, which cannot be done in nonlinear elasticity. Indeed, the isotropic strain-energy function for infinitesimal-strain elasticity can be stated in the following form:

$$\psi = \frac{1}{2}\kappa e^2 + \mu \varepsilon'_{ij}\varepsilon'_{ij}, \tag{2.58}$$

where κ is the bulk modulus, μ is the shear modulus, $e = \varepsilon_{kk}$ is the volumetric strain and $\varepsilon'_{ij} = \varepsilon_{ij} - \frac{1}{3}\varepsilon_{kk}\delta_{ij}$ is the deviatoric part of the strain. The strain-energy form (2.58) plays an important role in proving the existence and uniqueness of solution in linear elastostatics. The first and second terms of Eq. (2.58) are independent variables and

represent volumetric and deviatoric parts of ψ, respectively. Eq. (2.58) can be rewritten as

$$\psi = -\frac{1}{2} pe + \frac{1}{2}\sigma'_{ij}\varepsilon'_{ij}. \tag{2.59}$$

Here $p = -\frac{1}{3}\sigma_{kk}$ is the mean pressure and $\sigma'_{ij} = \sigma_{ij} - \frac{1}{3}\sigma_{kk}\delta_{ij}$ is the deviatoric part of the stress. Since the deviatoric and volumetric stress and strain tensors are mutually orthogonal, it follows from the Hill condition that

$$\frac{1}{V}\int_V \psi dV = -\frac{1}{2}\overline{p}\,\overline{e} + \frac{1}{2}\overline{\sigma'_{ij}\varepsilon'_{ij}} = -\frac{1}{2}\overline{p}\,\overline{e} + \frac{1}{2}\overline{\sigma'}_{ij}\overline{\varepsilon'}_{ij}. \tag{2.60}$$

Hence, the average strain energy under uniform volumetric or isochoric boundary conditions is fully determined by the corresponding volumetric or isochoric stress and strain fields on the boundary. It is important to notice that, by defining an apparent bulk modulus as $K = -\frac{\overline{p}}{\overline{e}}$ and an apparent shear modulus as $M = \frac{1}{2}\overline{\sigma'_{ij}\varepsilon'_{ij}}^{-1}$, one can estimate bounds on the effective volumetric and isochoric responses. Thus, applying uniform volumetric strain on the boundary after ensemble averaging we get

$$\kappa = \left\langle K_\Delta^\varepsilon \right\rangle \le \left\langle K_\delta^\varepsilon \right\rangle \le \left\langle K_{\delta'}^\varepsilon \right\rangle \le \left\langle K_1^\varepsilon \right\rangle, \text{ for } 1 < \delta' < \delta < \Delta, \tag{2.61}$$

Whereas the uniform isochoric kinematic boundary condition leads to

$$\mu = \left\langle M_\Delta^\varepsilon \right\rangle \le \left\langle M_\delta^\varepsilon \right\rangle \le \left\langle M_{\delta'}^\varepsilon \right\rangle \le \left\langle M_1^\varepsilon \right\rangle, \text{ for } 1 < \delta' < \delta < \Delta. \tag{2.62}$$

The reciprocal expression for the lower bound on the effective response can be obtained from the complementary energy function, which gives

$$\kappa^{-1} = \left\langle K_\Delta^\sigma \right\rangle^{-1} \le \left\langle K_\delta^\sigma \right\rangle^{-1} \le \left\langle K_{\delta'}^\sigma \right\rangle^{-1} \le \left\langle K_1^\sigma \right\rangle^{-1}, \text{ for } 1 < \delta' < \delta < \Delta, \tag{2.63}$$

$$\mu^{-1} = \left\langle M_\Delta^\sigma \right\rangle^{-1} \le \left\langle M_\delta^\sigma \right\rangle^{-1} \le \left\langle M_{\delta'}^\sigma \right\rangle^{-1} \le \left\langle M_1^\sigma \right\rangle^{-1}, \text{ for } 1 < \delta' < \delta < \Delta. \tag{2.64}$$

In the nonlinear elasticity of compressible rubber-like materials, the strain-energy function, ψ, can be also split into a volumetric part, ψ_{vol}, and isochoric part, ψ_{iso}, (Holzapfel, 2000). However, the application of the purely volumetric boundary condition does not give a zero isochoric contribution to the average strain energy and *vice versa*. The reason for this is the complex nature of the strain-energy function, which, in general,

cannot be expressed as a product of the nominal stress and the deformation gradient just as it was done in Eq. (2.60).

In the potential (2.15), the only term, that is independent of deformation, is the purely thermal contribution, $\hat{T}(T)$. This term does not depend on the type of the mechanical loading and, therefore, is the same under restricted and unrestricted boundary conditions:

$$\hat{T}(\omega,\theta_0) = \hat{T}(\omega,\theta_0)^r . \tag{2.65}$$

Hence, the purely thermal contribution can be ignored in hierarchies (2.34) and (2.38).

As pointed out in Section 2.3.2, the energetic contribution, e_0, to the free-energy function (2.15) is equal to zero in the case of a purely entropic theory, in which the thermoelastic bounding problem becomes identical to the purely elastic one. In the most general situation, e_0 is assumed to be a function of the volume ratio, $e_0(u_{i,j}) = e_0(J)$ (Chadwick, 1984). Thus, in contrast to the linear elasticity theory (see, Du and Ostoja-Starzewski, 2005), the hierarchy (2.34) cannot be separated into purely mechanical and purely thermal parts, and one has to consider the first two terms of ψ in Eq. (2.15) jointly.

2.8 Closure

In this chapter, the variational principles of Lee & Shield (1980) have been extended to the case of finite thermoelastostatics. It was shown that the uniform displacement and traction boundary conditions can be used, respectively, to obtain the upper and lower bounds on the effective energy functions of a composite at finite deformations under isothermal and nonisothermal loading. Rigorous upper and lower bounds are considered and the order relations for mixed boundary-value problem are discussed. The approach developed in this chapter can be used to estimate the scale dependence (i.e., the mesoscale bounds) on the effective response of random microstructures in finite elasticity and thermoelasticity and, hence, the size of the RVE. Such results are reported in the subsequent chapters.

Chapter 3

The minimal size of the representative volume element for nonlinear-elastic random composites: computational results [1]

Investigation of the convergence trend (i.e., scale effects) in the stochastic constitutive law of random composites allows the estimation of the size of the RVE within certain accuracy, which should be defined depending on the specific engineering applications. This chapter presents the computation of the derived mesoscale upper and lower bounds (based on the uniform kinematic and static boundary conditions, respectively) for nonlinear elastic random composites at finite strains. We compute these bounds for different types of composites, comparing linear and nonlinear elasticity theories.

3.1 Material model

We consider a material made of an elastomeric matrix with randomly distributed nonlinear elastic inclusions. Such a composite is often employed in industry to enhance the mechanical properties of polymeric materials (Gatos *et al.*, 2004), to improve their toughness (Martin *et al.*, 2004; Wong and Mai, 1999) or their impact strength (Schneider *et al.*, 1997). It also models some biological tissues (Brain network laboratory, Texas A&M University).

Here, we study a two-dimensional nonlinear composite with the microstructure modeled by a planar homogeneous Poisson point process with a probability mass function defined as

$$P\{N(A)=k\}=e^{-\lambda(A)}\frac{\lambda(A)^k}{k!},\ A\subset\mathbf{R}^2, \tag{3.1}$$

where $N(A)$ is the number of successful trials and $\lambda(A)$ is a parameter defined as

[1]Most of the material in this chapter has been published as an article in the *Journal of Elasticity* (**462**, 1167-1180, 2006).

$$\lambda(A) = f\frac{Area(B(\omega))}{Area(A)}, \tag{3.2}$$

where f is the prescribed volume fraction of inclusions. Poisson points are generated in such a way that no two points may be closer than a certain distance $D = 1.1d$, where d is the diameter of the inclusions. Imposing this non-overlap condition allows us to avoid numerical difficulties associated with narrow necks between inclusions, which can be crucial in simulations involving finite deformations.

For numerical simulations we consider a compressible isotropic hyperelastic material of Ogden type (Ogden, 1984) with the strain-energy function given by

$$\psi = \sum_{i=1}^{N}\frac{2\mu_i}{\alpha_i^2}(\tilde{\lambda}_1^{\alpha_i} + \tilde{\lambda}_2^{\alpha_i} + \tilde{\lambda}_3^{\alpha_i} - 3) + \sum_{i=1}^{N}\frac{1}{D_i}(J-1)^{2i}, \tag{3.3}$$

$$\tilde{\lambda}_a = J^{-\frac{1}{3}}\lambda_a,$$

where λ_a are the principal values of the deformation gradient, $J = \lambda_1\lambda_2\lambda_3$ is the Jacobian and N, μ_i, α_i, D_i are the material parameters.

When perturbed around the undeformed configuration, the material constants of any hyperelastic material are adjusted to give a response with known Lame constants, μ_0 and $\lambda_0 = \kappa_0 - \frac{2}{3}\mu_0$, (Ciarlet, 1988). For the Ogden form, these initial moduli are related to the material parameters by the expressions

$$\mu_0 = \sum_{i=1}^{N}\mu_i, \tag{3.4}$$

$$\kappa_0 = \frac{2}{D_i}, \tag{3.5}$$

where μ_0 is the initial shear modulus and κ_0 is the initial bulk modulus.

When dealing with a nonlinear composite, it is unclear how to define the mismatch between the phases, especially when they are described by two different forms of the strain-energy function. While most engineering materials for which the linear elasticity theory is applicable are compressible, the hyperelastic response is characterized by near incompressibility. For a typical elastomer, the initial bulk modulus exceeds the shear modulus by 1,000 to 10,000 times, and, therefore, a mismatch (or contrast) between two

phases α in the hyperelastic composite would be more logically defined in terms of the initial shear modulus rather than in terms of the bulk modulus or other material parameters in general.

The physical properties of the materials used in the illustrative examples are listed in Table 3.1. Material 1 defines a typical rubber (Ogden, 1984), and materials 2 and 3 are of neo-Hookean type (Rivlin, 1948), which, as can be seen from the table, can be obtained as a special case of the general Ogden strain-energy potential (3.3). The neo-Hookean type strain-energy function is the simplest form of ψ and a generalization of the linear stress-strain relation in finite elasticity. It yields results which are in a good agreement with experiments within the small strain domain, and, therefore, is preferable to be employed when deformations are relatively small.

Table 3.1. Material properties used in the computational examples.

Material	Material parameters	Initial shear modulus
1	$N=3,\ \mu_1=4.095\cdot10^5\,\mathrm{N/m^2},\ \alpha_1=1.3$ $\mu_2=0.03\cdot10^5\,\mathrm{N/m^2},\ \alpha_2=5.0$ $\mu_3=0.1\cdot10^5\,\mathrm{N/m^2},\ \alpha_3=-2.0$ $D_1=4.733\cdot10^{-8}\,\mathrm{N/m^2},\ D_2=0,\ D_3=0$	$\mu_0=4.225\cdot10^5\,\mathrm{N/m^2}$
2	$N=1,\ \mu_1=42.25\cdot10^5\,\mathrm{N/m^2},\ \alpha_1=2.0$ $D_1=4.733\cdot10^{-8}\,\mathrm{N/m^2}$	$\mu_0=42.25\cdot10^5\,\mathrm{N/m^2}$
3	$N=1,\ \mu_1=4.225\cdot10^5\,\mathrm{N/m^2},\ \alpha_1=2.0$ $D_1=4.733\cdot10^{-8}\,\mathrm{N/m^2}$	$\mu_0=4.225\cdot10^5\,\mathrm{N/m^2}$

It is worth mentioning that the strain-energy potential (3.3) together with the parameters defined in Table 3.1 satisfies inequalities (2.7) and (2.11), and, therefore, the bounds (2.33) and (2.37) hold over all admissible deformations.

To illustrate and compare the convergence of bounds (2.33) and (2.37), we investigate four nonlinear elastic composites of the following types:

No. 1: neo-Hookean inclusions in Ogden matrix with $\frac{\mu_0^{(i)}}{\mu_0^{(m)}} = 10$,

No. 2: Ogden inclusions in neo-Hookean matrix with $\frac{\mu_0^{(i)}}{\mu_0^{(m)}} = 0.1$,

No. 3: neo-Hookean inclusions in neo-Hookean matrix with $\frac{\mu_0^{(i)}}{\mu_0^{(m)}} = 10$,

No. 4: neo-Hookean inclusions in neo-Hookean matrix with $\frac{\mu_0^{(i)}}{\mu_0^{(m)}} = 0.1$,

as well as two linear elastic composites:

No. 5: $\frac{\mu^{(i)}}{\mu^{(m)}} = 10$, $\frac{\kappa^{(i)}}{\kappa^{(m)}} = 10$,

No. 6: $\frac{\mu^{(i)}}{\mu^{(m)}} = 0.1$, $\frac{\kappa^{(i)}}{\kappa^{(m)}} = 0.1$,

where μ is the shear modulus and κ is the bulk modulus. The volume percentage of inclusions is chosen to be 35%, which corresponds approximately to 18% in three dimensions (Zohdi and Wriggers, 2001). Perfect bounding between a matrix and inclusions is assumed.

3.2 Discretization

The finite element analysis is carried out using the commercial software ABAQUS 6.5. The discretization is performed with a non-uniform mesh (Fig. 3.1), generated automatically with the use of the scripting interface. This mesh shows a significantly better convergence to the true solution with a smaller number of degrees of freedom (DOF) compared to a mesh with square-shaped uniform elements. Over a series of repetitive refinements, an average element size of 0.75 for $d = 10$ (approximately 450 DOF for $\delta = 1$ and 70500 DOF for $\delta = 16$) was found to produce mesh-independent results (Fig. 3.2). Four-node bilinear elements with full integration are used in the analysis.

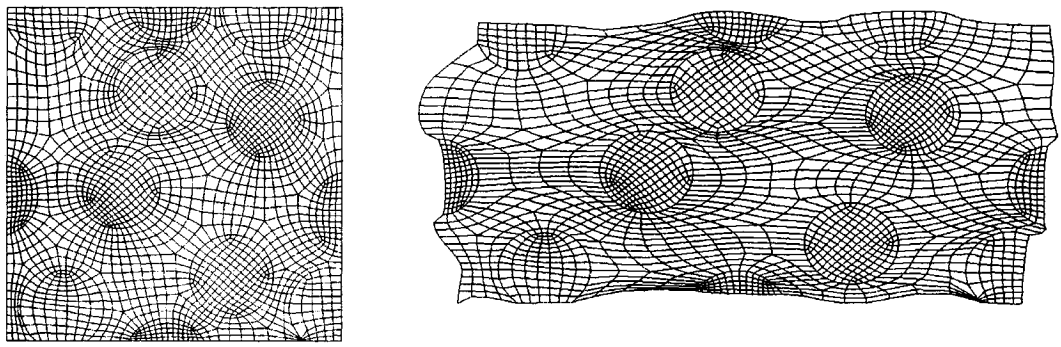

(a) (b)

Figure 3.1. The finite element mesh of a composite in (a) undeformed and (b) deformed (traction boundary conditions) configurations.

3.3 Ensemble averaging

Before proceeding with numerical experiments, the number of microstructural assemblies for each window size δ must be investigated. As the window size is increasing, the probability of occurrence of extremely large or small values of the stored strain energy becomes smaller. As a result, the standard deviation, σ, approaches zero as $\delta \to \infty$ (for the discussion of the dependence of the standard deviation on δ, see Section 3.4.2). Thus, the larger the window size, the lower the number of numerical experiments required to obtain statistically representative result. The following numbers of realizations of a random composite were generated: 512 for $\delta = 1$; 384 for $\delta = 2$; 160 for $\delta = 4$; 40 for $\delta = 8$ and 10 for $\delta = 16$.

It is also interesting to determine a probability density function that best describes the energy density distribution of the composite at different scales. Such an analysis was carried out for the nonlinear composite No. 1. It was found that the distribution function does depend on the scale. However, averaging over all the scales showed that, for both displacement and traction boundary conditions, the Beta and Chi distributions give the best fit among all the classical distributions with a 0.8% difference in the Kolmogorov-Smirnov test statistic. The plot of the corresponding Beta functions for each scale is given in Fig. 3.3.

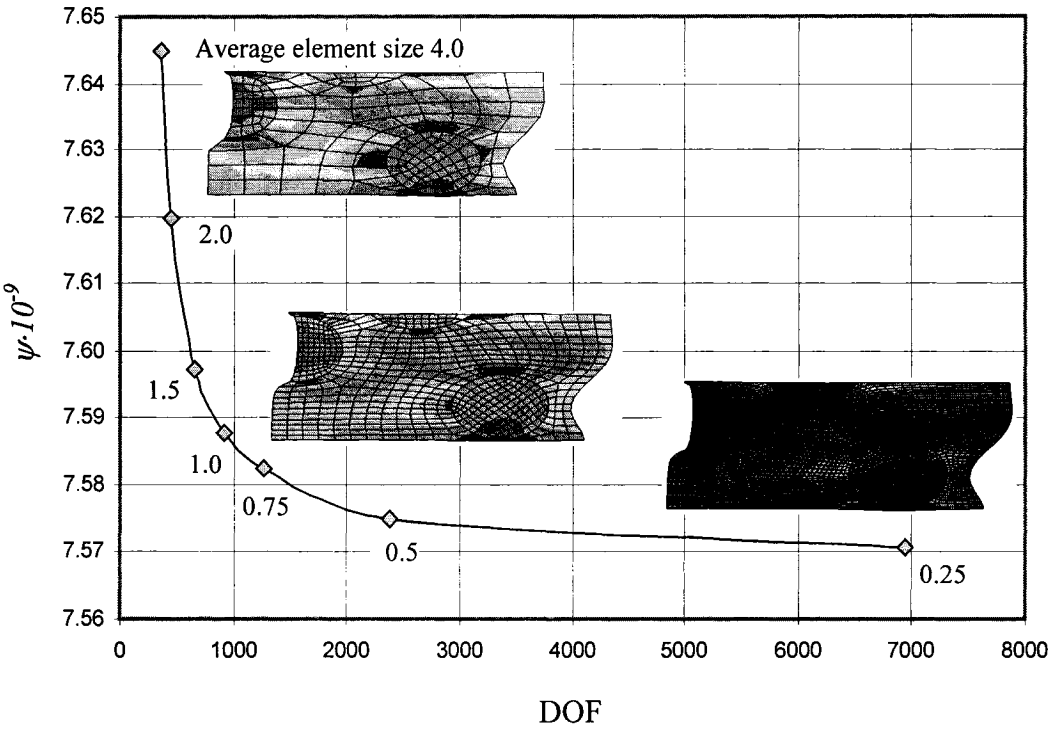

Figure 3.2. Dependence of the average strain energy of a composite on the number of degrees of freedom.

With the window size increasing, the probability density function flows away from the end points, converging to the Dirac delta as $\delta \to \infty$. Moreover, depending on the boundary conditions, the mean value shifts to the right or to the left. The negative sign of the strain energy in Fig. 3.3 (b) is a result of the way we calculate the energy density under traction boundary condition (2.39), and this is described in more detail in the next section.

3.4 Numerical results

3.4.1 Bounds on effective properties

If the microstructure statistics admits isotropy, then, upon ensemble averaging (which involves integration over all the realizations of the random microstructure), the microstructure response is isotropic – no material direction has any preference. This reasoning is implicitly involved in the development of the constitutive laws of materials in deterministic continuum mechanics. If sufficiently many realizations of a composite

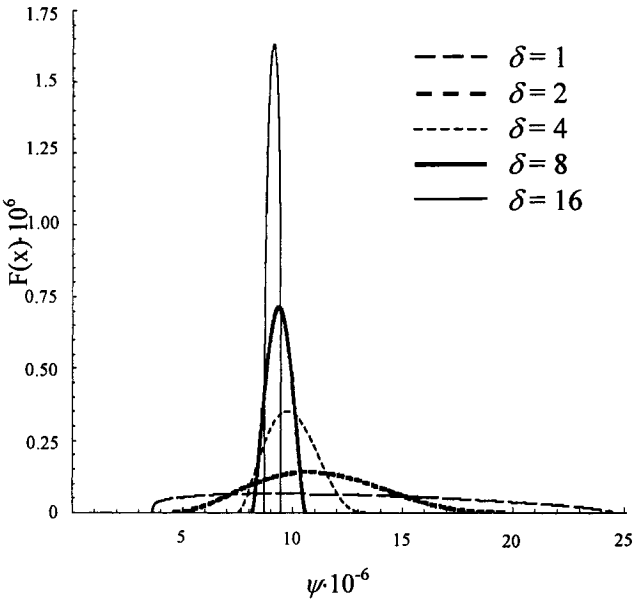

(a)

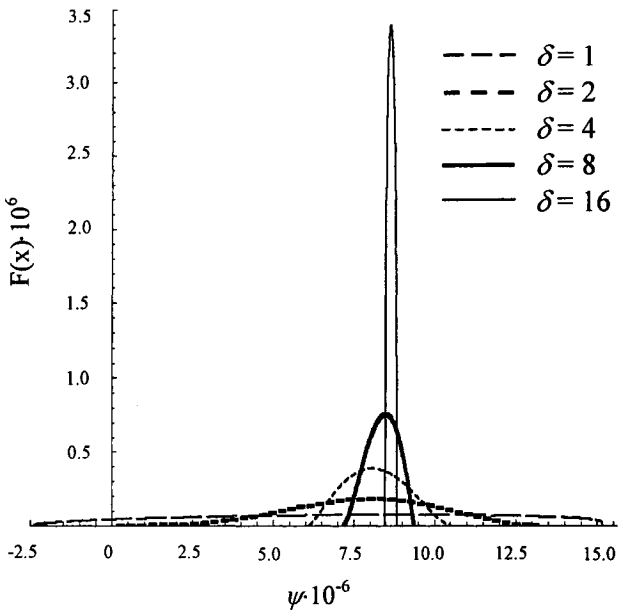

(b)

Figure 3.3. Probability densities for the stored strain-energy density of the nonlinear composite No. 1 under (a) uniform displacement and (b) uniform traction boundary conditions.

are taken to remove the directional dependence, then isotropy of the ensemble-averaged response is also very well supported by numerical simulations. For example, in linear elasticity, computational results show that $\langle \mathbf{C}_\delta \rangle$ is an isotropic forth-rank tensor (Lachihab and Sab, 2005), whereas in nonlinear elasticity the ensemble averaged stress under KUBC has zero shear components, which can be expected only for an isotropic response. Analogous results are obtained under static uniform boundary conditions for the ensemble averaged deformation gradient tensor.

In the following, we take $\langle \psi_\delta \rangle$ to be an isotropic scalar valued function of **F**, and we treat the ensemble averaged material response of the nonlinear composite as generally isotropic. Consequently, the stored energy function $\langle \psi_\delta \rangle$ may be regarded as a symmetric function of the three extension ratios λ_a.

For a good description of hyperelastic materials, more than one type of test is required. In case of only one test, the non-uniqueness of material parameters fitted to the experimental data may occur (Ogden *et al.*, 2004). This is particularly important when the material is defined by a complex strain-energy function, such as the one given by equation (3.3). Generally, any deformation mode can be investigated. However, from the experimental standpoint, the most common deformation modes are considered to be sufficient to determine material coefficients (Ogden, 1984). We assume plane-stress deformations and consider three different deformation modes: uniaxial tension, equibiaxial tension and pure shear; along with three types of boundary conditions, summarized in Table 3.2.

It is very difficult to obtain pure shear response in the nonlinear composite under SUBC specified in the reference configuration (see Eq. (2.27)), unless deformations of the material are known *a priori*. Moreover, since the surface traction applied on the boundary of the sample is a dead load, numerical difficulties associated with the excessive finite element distortions in shear and boundary contact make determination of the stress-strain curve almost impossible. Note that the dead load assumption allows us to use variational principles in the derivation of the mesoscale bounds without placing any limitation on the choice of the statically admissible stress.

Table 3.2. Boundary conditions used in the computational examples.

Deformation modes	Uniaxial tension	Equibiaxial tension	Pure shear
Static uniform b.c. (SUBC)	$P_{11}^0 = P$, $P_{22}^0 = P_{12}^0 = P_{21}^0 = 0$	$P_{11}^0 = P_{22}^0 = P$, $P_{12}^0 = P_{21}^0 = 0$	–
Kinematic uniform b.c. (KUBC)	$F_{11}^0 = \langle\overline{\lambda_1}\rangle^{\mathbf{P}}$, $F_{22}^0 = \langle\overline{\lambda_2}\rangle^{\mathbf{P}}$, $F_{12}^0 = F_{21}^0 = 0$	$F_{11}^0 = F_{22}^0 = \lambda$, $F_{12}^0 = F_{21}^0 = 0$	$F_{11}^0 = \lambda$, $F_{22}^0 = \frac{1}{\lambda}$, $F_{12}^0 = F_{21}^0 = 0$
Orthogonal-mixed b.c. (MIXED1)	$F_{11}^0 = \langle\overline{\lambda_1}\rangle^{\mathbf{P}}$, $F_{22}^0 = \langle\overline{\lambda_2}\rangle^{\mathbf{P}}$, $P_{12}^0 = P_{21}^0 = 0$	$F_{11}^0 = F_{22}^0 = \lambda$, $P_{12}^0 = P_{21}^0 = 0$	$F_{11}^0 = \lambda$, $F_{22}^0 = \frac{1}{\lambda}$, $P_{12}^0 = P_{21}^0 = 0$

Orthogonal-mixed boundary conditions specified in Table 3.2 reproduce a possible experimental setup, when displacements are applied without friction on all sides of the specimen (Fig. 3.4). These boundary conditions are important from the practical viewpoint as they allow one to compare numerical simulations with the experimental results.

For the sake of comparison, we also investigate a uniform mixed boundary condition (MIXED2), proposed by Hazanov and Amieur (1995), see Eqs. (2.50 - 2.51). In this boundary condition, the uniform displacement component is applied without friction in the direction X_1 at the upper and lower ends of the specimen (Fig. 3.5), on the lateral sides, $u_1 = (F_{11}^0 - 1)X_1$ and $t_2 = 0$ are applied. In Fig. 3.6, sample deformations of a rather large mesoscale under different boundary conditions are given.

Figures 3.7–3.10 present a nonlinear composite response under uniaxial loading. From the stress-strain curves, we observe that the effective response for all the composites is bounded from above by the response under displacement boundary conditions and from below by the response under traction boundary conditions. Orthogonal mixed boundary conditions, MIXED1, give an intermediate result for $\delta > 2$ and tend to overestimate the effective response for smaller window sizes. The curves obtained under uniform mixed loading, MIXED2, almost overlap the results under KUBC

(Fig. 3.11). It is interesting to note that, while in the first composite (where matrix is represented by a soft Ogden type material), the curves change their shape gradually from the neo-Hookean to Ogden type response, in the second composite the curves are more shifted toward the hard phase. Analogous results were obtained for all deformation modes considered, which are not shown here for the sake of brevity.

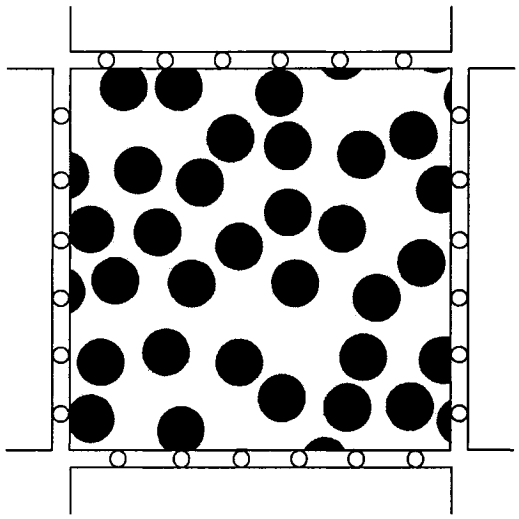

Figure 3.4. Loading under orthogonal-mixed boundary condition, MIXED1.

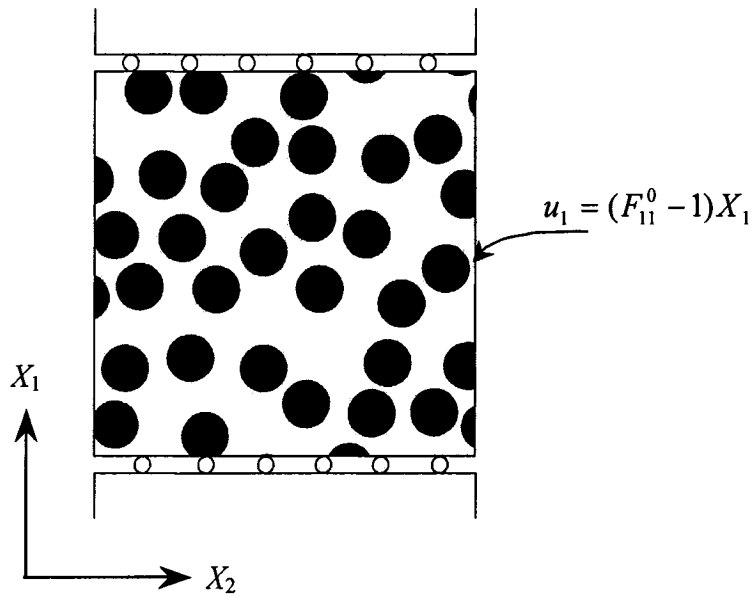

Figure 3.5. Loading under uniform mixed boundary conditions, MIXED2.

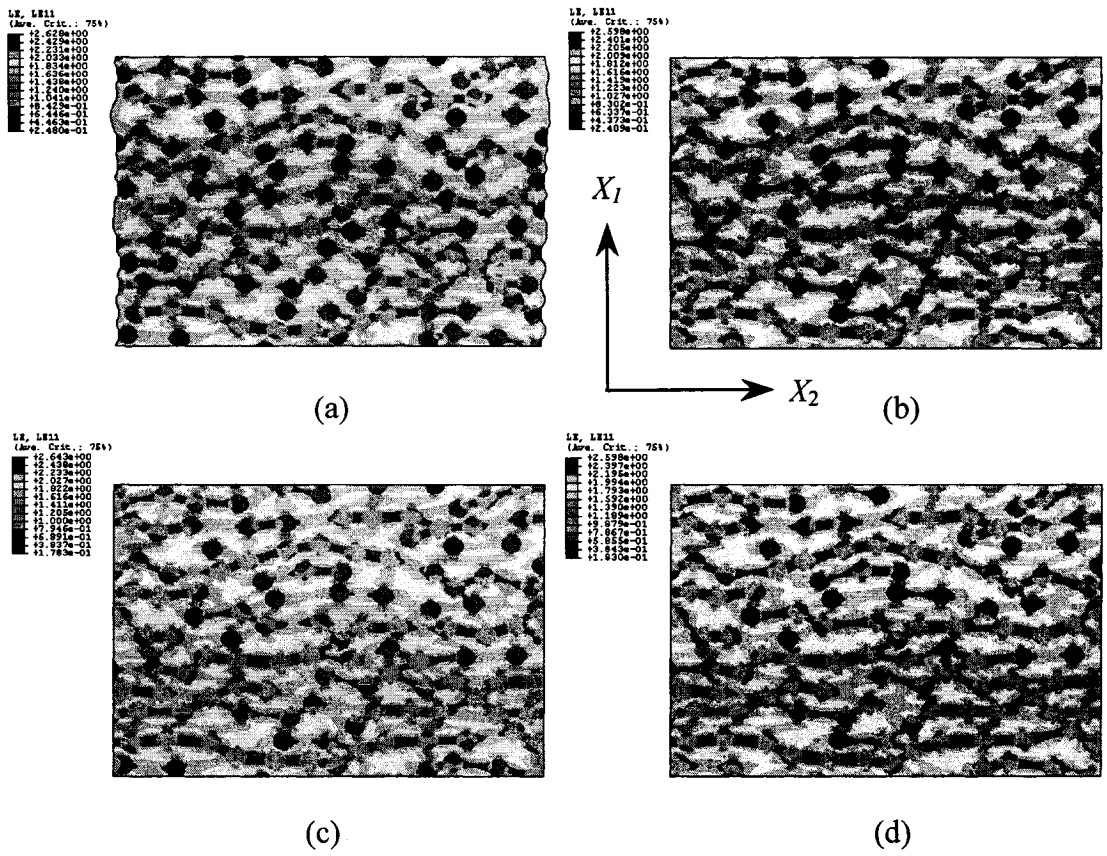

Figure 3.6. Contour plots of logarithmic strain in the direction X_2 under different boundary conditions: (a) SUBC, (b) KUBC, (c) MIXED1, (d) MIXED2.

The material coefficients were computed for each stress-strain data set using the standard fitting procedure and the Ogden model with $N = 1$, $N = 2$, $N = 3$ (Ogden *et al.*, 2004). It was found that for composite No. 1, the strain-energy function with three terms provides the best fit up to $\delta = 2$ under KUBC, whereas the one-term strain-energy function and the neo-Hookean model give better results for $\delta = 1$ under KUBC, and for the Voigt bound, respectively. An opposite situation is encountered for the composite No. 2, where the three-term Ogden function is slowly changing to a two-term function at $\delta = 2$ under SUBC, and to a neo-Hookean model at $\delta = 16$ under KUBC. Unfortunately, we cannot mathematically describe the transition of each material parameter from the lower to the upper bound. The reason for this is that even a slight change in the material response produces a completely different set of fitted material parameters, and, therefore, there is no continuous transition for individual coefficient from one scale to another.

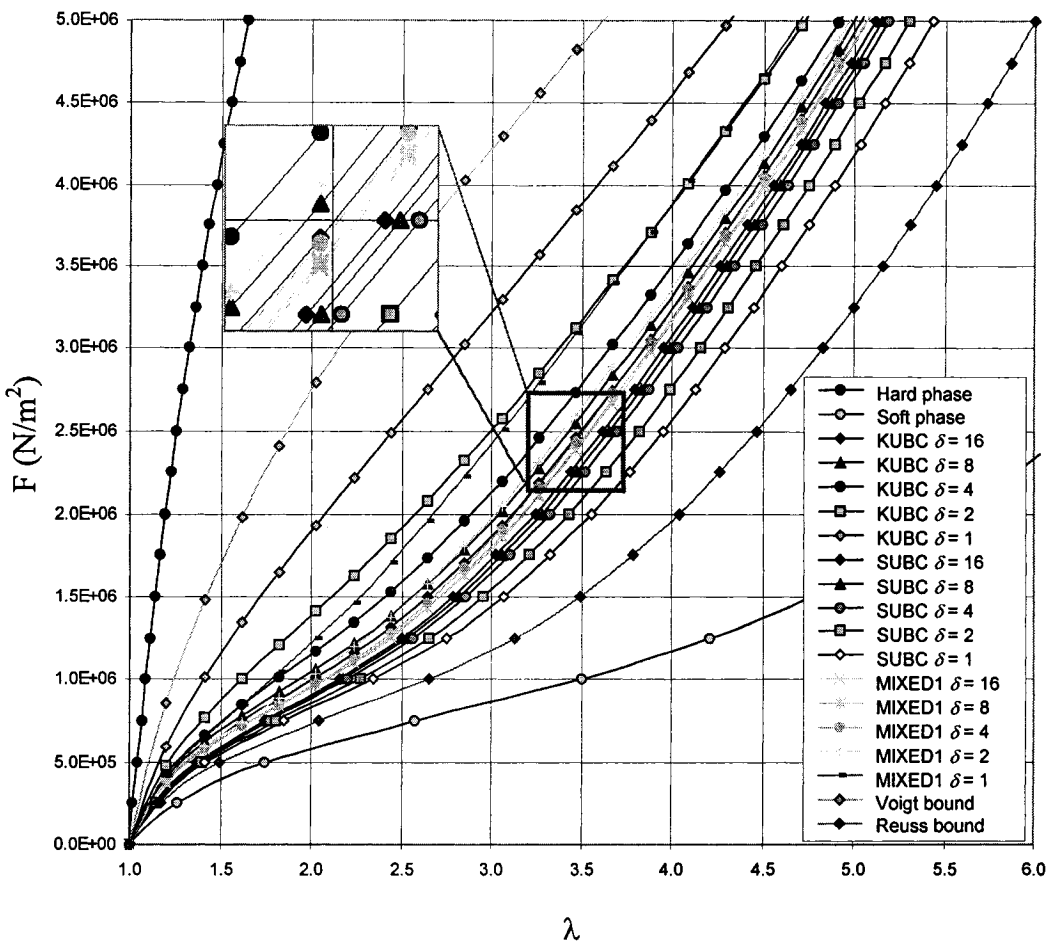

Figure 3.7. Stress-strain curves of the random composite No. 1 under uniaxial loading.

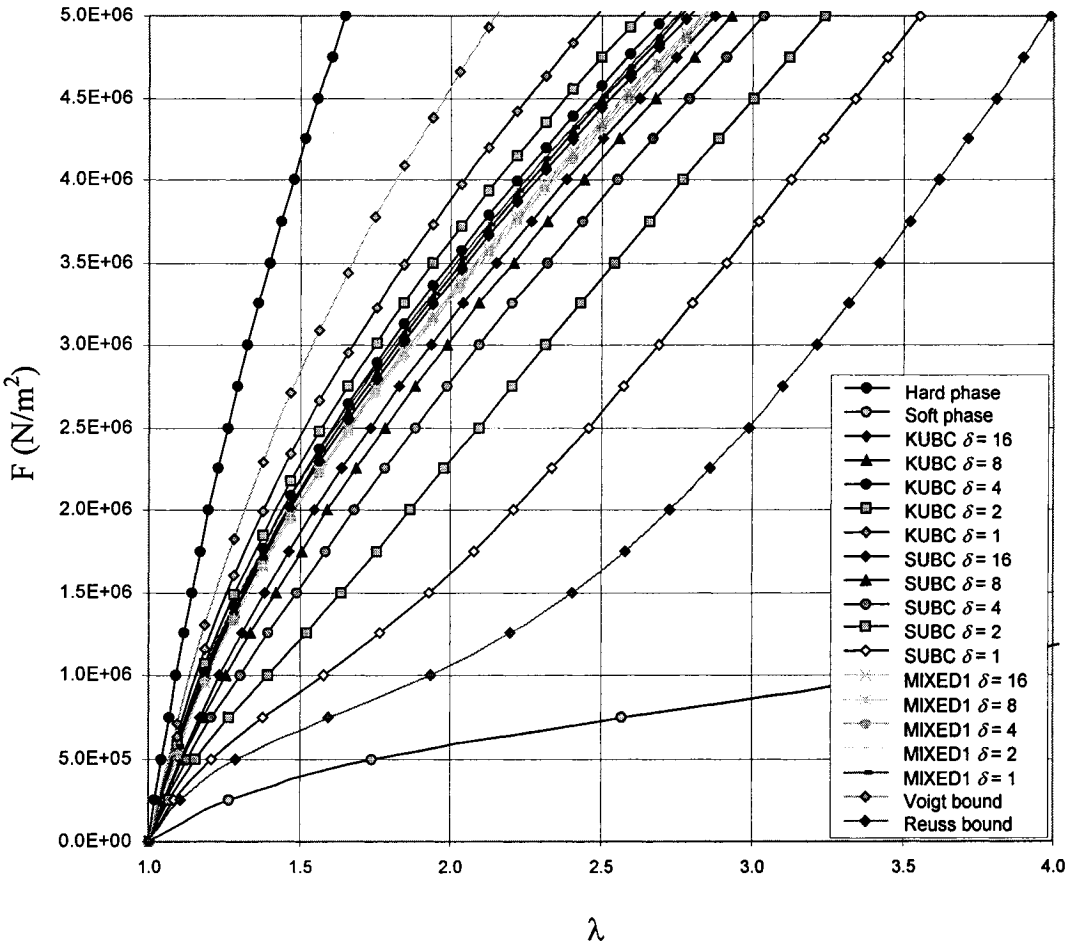

Figure 3.8. Stress-strain curves of the random composite No. 2 under uniaxial loading.

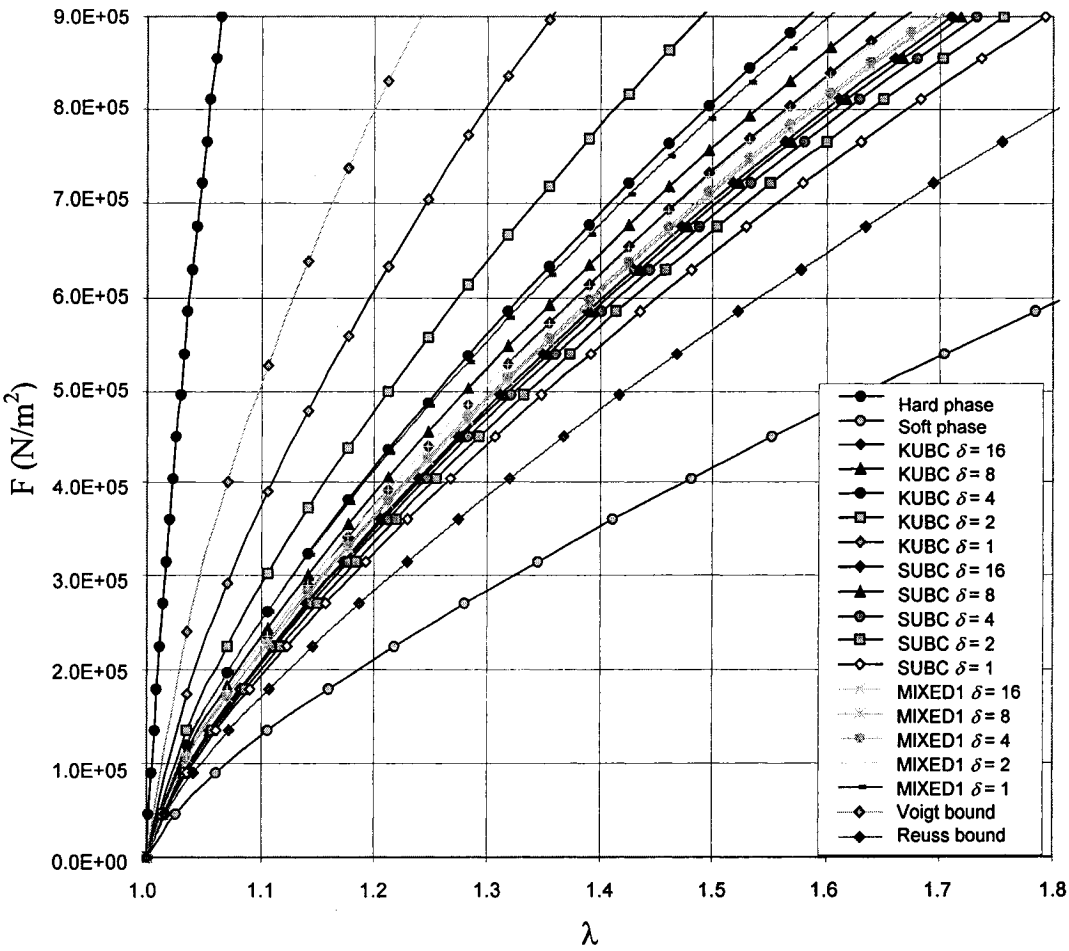

Figure 3.9. Stress-strain curves of the random composite No. 3 under uniaxial loading.

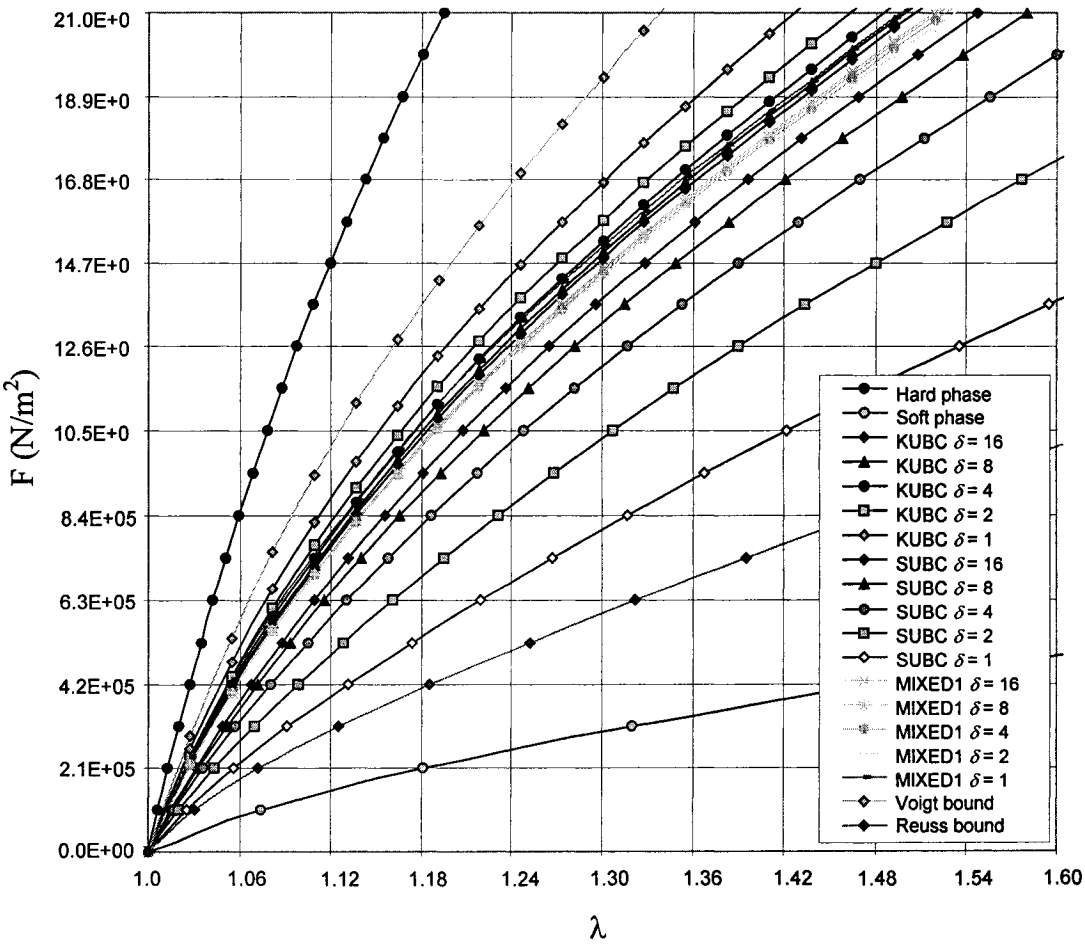

Figure 3.10. Stress-strain curves of the random composite No. 4 under uniaxial loading.

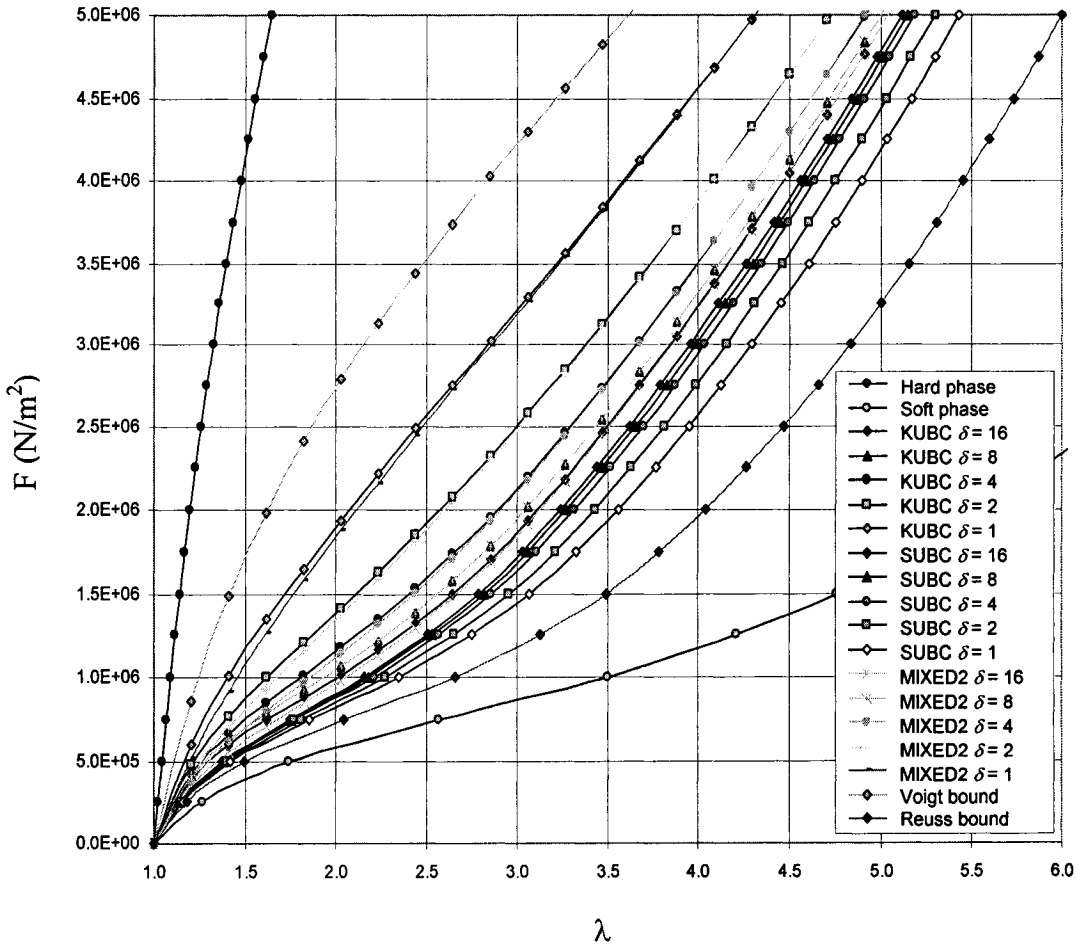

Figure 3.11. Stress-strain curves of the random composite No. 1 under uniaxial loading with the mixed boundary conditions of the second type.

The only material parameter for which the scale-dependence can be defined mathematically is the initial shear modulus (Fig. 3.12). Indeed, it was found that

$$\mu_0^{\mathrm{P}} = A\exp[m\delta] - B\exp[-n\delta], \tag{3.6}$$

$$\mu_0^{\mathrm{F}} = C\exp[-k\delta] + D\exp[-p\delta], \tag{3.7}$$

where A, m, B, n, C, k, D and p are parameters obtained through a nonlinear least-square fitting procedure (Table 3.3).

Table 3.3. Parameters in equations (3.6) and (3.7) for different composite models.

Composite	$A\cdot10^{-5}$	m	$B\cdot10^{-5}$	n	$C\cdot10^{-5}$	k	$D\cdot10^{-5}$	p
1	5.5	0.0004	0.3	0.766	6.2	0.0076	11.9	1.172
2	14.6	0.0065	10.3	0.472	18.7	0.0017	4.7	0.656
3	6.5	0.0010	0.8	0.635	7.6	0.0058	8.9	1.001
4	16.8	0.0054	10.7	0.587	20.6	0.0017	5.2	0.858

For the composite No.1 under KUBC, a difference of approximately 30% occurs between the initial shear modulus of samples that were 2 times and 16 times bigger than the heterogeneity size, whereas under SUBC, the difference is only 2%. The opposite result is encountered for the composite with soft inclusions (No. 2): 9% difference under KUBC and 33% under SUBC. It noteworthy that the studies of a linear microstructure with random distribution of pores, modeled as soft inclusions (Zohdi and Wriggers, 2000), revealed the difference of 2.6% for the effective shear response under KUBC. Our study shows that results obtained under only KUBC might lead to a wrong estimation of the RVE, and for a reliable estimate, one has to consider the convergence of both bounds.

The curve fitting for neo-Hookean type composites showed that all the ensemble-averaged responses are best represented by the neo-Hookean form. The slight deviations from the neo-Hookean model are small compared to the other forms. Analogous observations were made for the effective material response by Löhnert (2004).

A strain-energy density is a function of the three principal stretches, and, therefore, has different values for different boundary conditions. To demonstrate the convergent trends of bounds (2.33) and (2.37), we will consider each deformation mode given in Table 3.2 and proceed with the following steps:

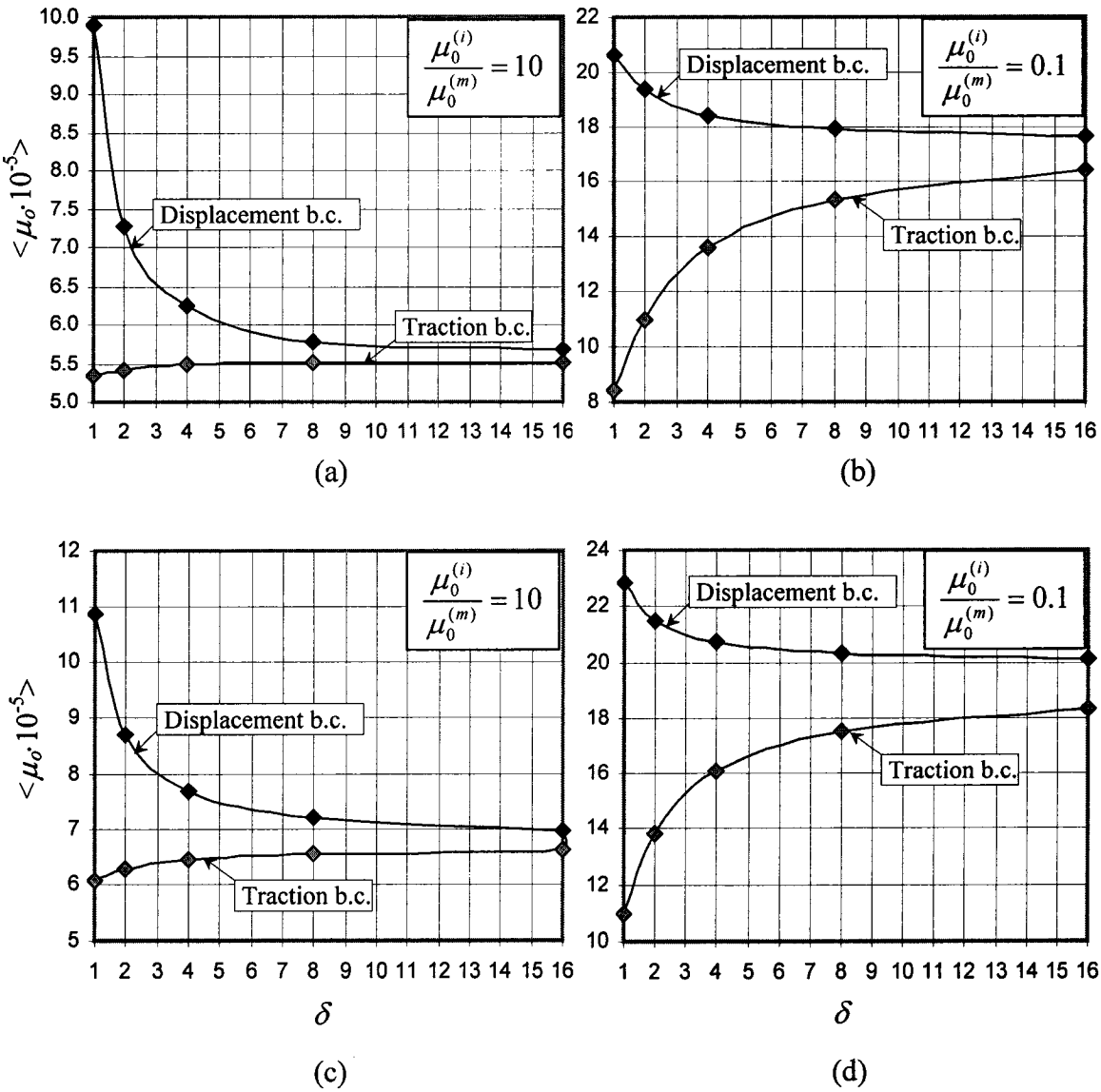

Figure 3.12. Bounds on the initial shear modulus for different composites: (a) No. 1, (b) No. 2, (c) No. 3, (d) No. 4.

1) Compute response under SUBC and obtain $\left\langle \Psi^*(\mathbf{P}^0) \right\rangle_\delta$.

2) Apply KUBC through $\lambda_i^0 = \left\langle \overline{\lambda_i} \right\rangle^{\mathbf{P}}_{\delta=\delta_{\max}}$ and obtain $\left\langle \Psi(\mathbf{F}^0) \right\rangle_\delta$.

3) Compute lower bound on the strain-energy function using the following relation:

$$\left\langle \Psi(\mathbf{P}^0) \right\rangle_\delta = \mathbf{P}_{\delta=\delta_{\max}} : \mathbf{F}_{\delta=\delta_{\max}} - \left\langle \Psi^*(\mathbf{P}^0) \right\rangle_\delta . \tag{3.8}$$

When δ increases, the gap between $\langle \Psi(\mathbf{F}^0) \rangle_\delta$ and $\langle \Psi(\mathbf{P}^0) \rangle_\delta$ becomes smaller, and this can then be used to estimate the size of the RVE with a certain accuracy. In our numerical analysis, we choose $\delta_{\max} = 16$, given the limitation of our computer (11GB of random access memory).

The results for two nonlinear composites are shown in Fig. 3.13. The values of the strain energy are normalized with respect to the Voigt bound. The numerical simulations support theoretically derived results (2.33) and (2.37): the natural boundary condition provides the upper bound, while the essential boundary condition provides the lower bound. The comparison shows that for all the deformation modes the hierarchical trends are similar. However, when the matrix is soft, the lower bound converges faster, whereas for a composite with the hard matrix the lower bound approaches the effective value slower than the upper one. An analogous conclusion can be made for all the composites studied (see Figs. 3.14 – 3.15). Surprisingly, a well-known fact in linear elasticity that the situation of soft inclusions in a stiff matrix converges slower toward the RVE than the situation of stiff inclusions in a soft matrix (Ostoja-Starzewski, 1998, 1999) (Fig. 3.15) does not hold in finite elasticity (Fig. 3.13 –3.14).

For illustration purposes the results under uniform mixed loading, MIXED2, are presented only for composite No. 1 (Fig. 3.13,a), as similar trends were observed for all the materials studied. As expected from the stress-strain response (Fig. 3.11), the strain-energy trend under this boundary condition almost overlaps the response under KUBC. This suggests that this type of loading cannot be used for a quick characterization of effective properties. On the other hand, the mixed-orthogonal boundary condition, MIXED1, yields an intermediate result, which asymptotes rapidly. This implies that the effective properties under this boundary condition can be obtained for a composite with relatively small number of heterogeneities.

When $\delta \to 0$, mesoscale samples can be considered to be homogeneous with the material corresponding to either matrix or inclusions; and mixed boundary conditions become identical to displacement-controlled boundary conditions. This explains why the response under the mixed-orthogonal boundary condition converges from above. It is

observed that for the composites with $\frac{\mu_0^{(i)}}{\mu_0^{(m)}} = 0.1$, the response under the mixed boundary condition does not decay monotonically: it shifts in the range of $1 < \delta < 4$ for all nonlinear materials under uniaxial and biaxial tension.

In Figure 3.15, we compare the mesoscale bounds on the strain-energy function with the bounds on the effective stiffness tensor in linear elasticity. These bounds represent different quantities and are computed under different boundary conditions. To estimate the convergence of the *strain energy*, we first compute the response under SUBC and then apply the resulting ensemble-averaged strain in KUBC using only *one* set of the boundary conditions defined above. In order to estimate apparent *moduli* in linear in-plane elasticity one needs, at least, *three* tests to determine six unknowns: C_{1111}, C_{2222}, C_{1212} C_{1122}, C_{2211}, C_{1211} under KUBC and S_{1111}, S_{2222}, S_{1212} S_{1122}, S_{2211}, S_{1211} under SUBC (Ostoja-Starzewski, 2006). Therefore, it is interesting to find that the convergence rates in both cases are similar, which means that both methods can be alternatively used in the estimation of the RVE.

Another distinct feature of nonlinear elasticity is the dependence of the convergence rate on the deformation. We investigate such dependence for the nonlinear composite No. 1 (Fig. 3.16, 3.17). We define a *discrepancy* as

$$D = \frac{R_\delta^e - R_\delta^n}{\left(R_\delta^e + R_\delta^n\right)/2} \cdot 100\%, \tag{3.9}$$

where $R_\delta^e = \left\langle \Psi^e \right\rangle_\delta$ is the response under essential boundary conditions (KUBC), and $R_\delta^n = \left\langle \mathbf{P}^n_{\delta=\delta_{\max}} : \mathbf{F}^n_{\delta=\delta_{\max}} - \Psi^{*n} \right\rangle_\delta$ is the response under natural boundary conditions (SUBC). Due to the high scatter of numerical results for $\lambda \leq 1.25$, the discrepancy curve in this range is replaced by a dashed line, approaching $D = \frac{\mu_0^e - \mu_0^n}{(\mu_0^e + \mu_0^n)/2}$ as $\lambda \to 1$. The graph shows that the dependence of the convergence rate on the stretch value is highly nonlinear, with a large difference between uniaxial and biaxial results for small λ. Moreover, the normalized *effective* response changes with the stretch ratio.

Even for the neo-Hookean type composites, there is a dependence of the convergence rate on the deformation. Comparing different composites at $\delta = 16$, the

discrepancy is increasing in the following order: linear elastic composite, neo-Hookean composite and Ogden-neo-Hookean composite for the mismatch ratio $\alpha = 10$, and in the inverse order for the mismatch ratio $\alpha = 0.1$. The comparative study of some other cases can be found in Ostoja-Starzewski *et al.* (2006).

In conclusion, the RVE size will change depending on the quantity of interest: the maximum stretch ratio, the deformation mode and the mismatch of properties of constituents. Based on the energy bounds for composite No.1, an approximate estimation of the RVE (under uniaxial tension, for stretch ratio $\lambda = 5$) is as follows: $\delta = 16$ corresponds to 6.4%, $\delta = 8$ to 11%, and $\delta = 4$ to 18.8% error/discrepancy in overall effective properties. Hence, if results with 6.4% accuracy are considered to be acceptable for a particular test or analysis, $\delta = 16$ can be chosen as the RVE.

3.4.2 Statistical approach to the RVE size estimation

One of the methods for determination of the RVE, often considered in the literature (see, for example Gusev, 1997; Zohdi and Wriggers, 2000; Zohdi and Wriggers, 2001; Löhnert and Wriggers, 2003; Löhnert, 2004; Hohe and Becker, 2005) is the investigation of a property or stress/strain field fluctuation when the sample size is increased. The RVE size is then taken to be the size at which the increase in the number of composite realizations does not improve the estimation of some particular property.

For the completeness of presentation, we consider such an approach and investigate the influence of the composite type and the boundary conditions on the coefficient of variation C_v of the corresponding strain energy and complementary energy (Fig. 3.18). As can be seen from the graphs, the coefficient of variation strongly depends on the boundary conditions, and, with a few exceptions, is almost identical for different composites for $\delta > 8$.

For the RVE size 16 times bigger than the heterogeneity size ($\delta = 16$), the normalized standard deviation of the random fluctuations of the effective strain energy is less than 2%, whereas the discrepancy in strain energy, as it is calculated in the previous section, can be estimated to be over 6%. Thus, the statistical approach generally underestimates the size of the RVE.

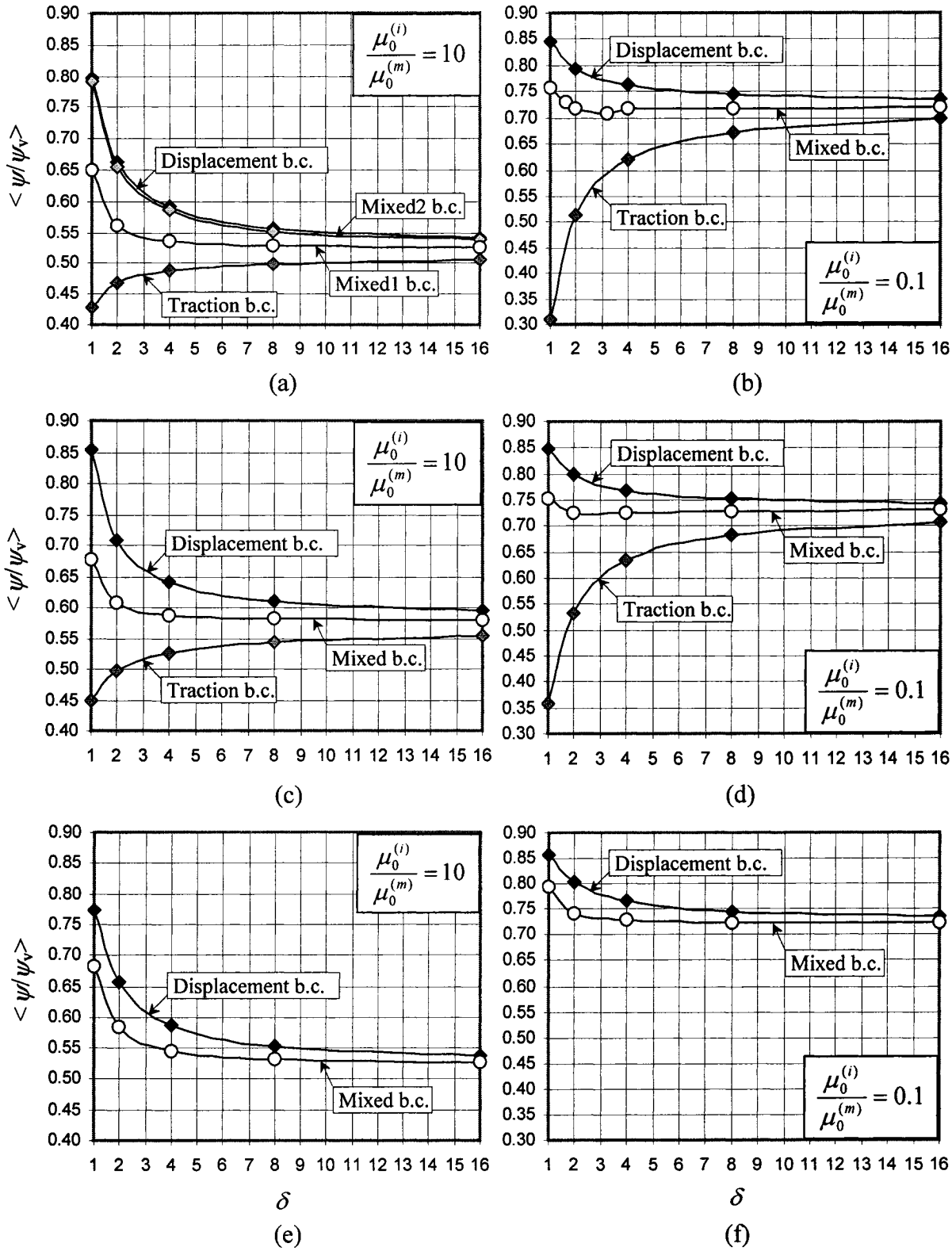

Figure 3.13. Energy bounds for the nonlinear random composite of Ogden - neo-Hookean type (No. 1 and No. 2) under (a, b) uniaxial tension, (c, d) biaxial tension, (e, f) pure shear.

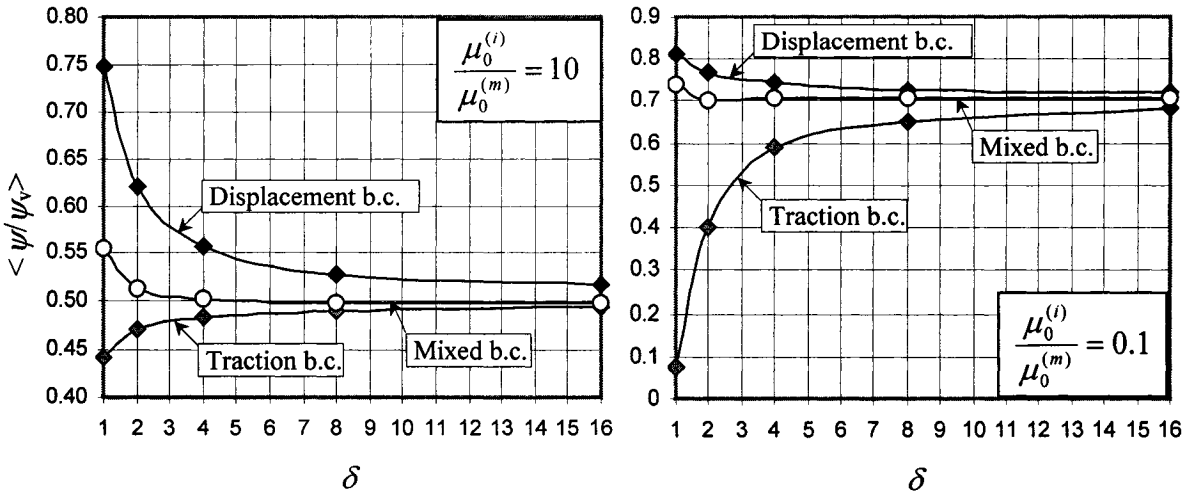

Figure 3.14. Energy bounds for the nonlinear random composite of neo-Hookean – neo-Hookean type (No. 3 and No. 4) under uniaxial tension.

3.5 Closure

In this chapter we presented and applied the homogenization procedure developed in Chapter 2 to quantitatively estimate the scale-dependence of the apparent responses of random composites for which material properties of the matrix and inclusions differ not only in material parameters but also in strain-energy function representations. The results obtained are compared with those where both matrix and inclusion are described by a neo-Hookean strain-energy function as well as with the results obtained from linear elasticity theory. The main findings and conclusions are summarized below:

(i) It is shown that the uniform displacement and traction boundary conditions provide, respectively, the upper and lower bounds on the stress-strain response and on the effective strain-energy function for all the nonlinear elastic and linear elastic composites considered. Thus, the proposed scale-dependent homogenization allows one to estimate the RVE properties on the finite scales within any desired precision.

(ii) Convergence of bounds towards the RVE depends on the mismatch α defined as the ratio between initial shear modulus of inclusions and matrix, the deformation and the deformation mode. For the mismatch ratio $\alpha = 10$ (stiff inclusions in a soft matrix), the lower bound converges faster, whereas the mismatch ratio $\alpha = 0.1$ (soft inclusions in a stiff matrix) provides faster convergence of the upper bound.

(iii) The orthogonal-mixed boundary conditions produce an intermediate response for all the considered composites, while the convergence trend under uniform mixed boundary conditions is similar to the kinematic one.

(iv) The homogenization technique, based on the investigation of the properties fluctuations with the sample scale, provides a smaller RVE size than the technique developed in the present study.

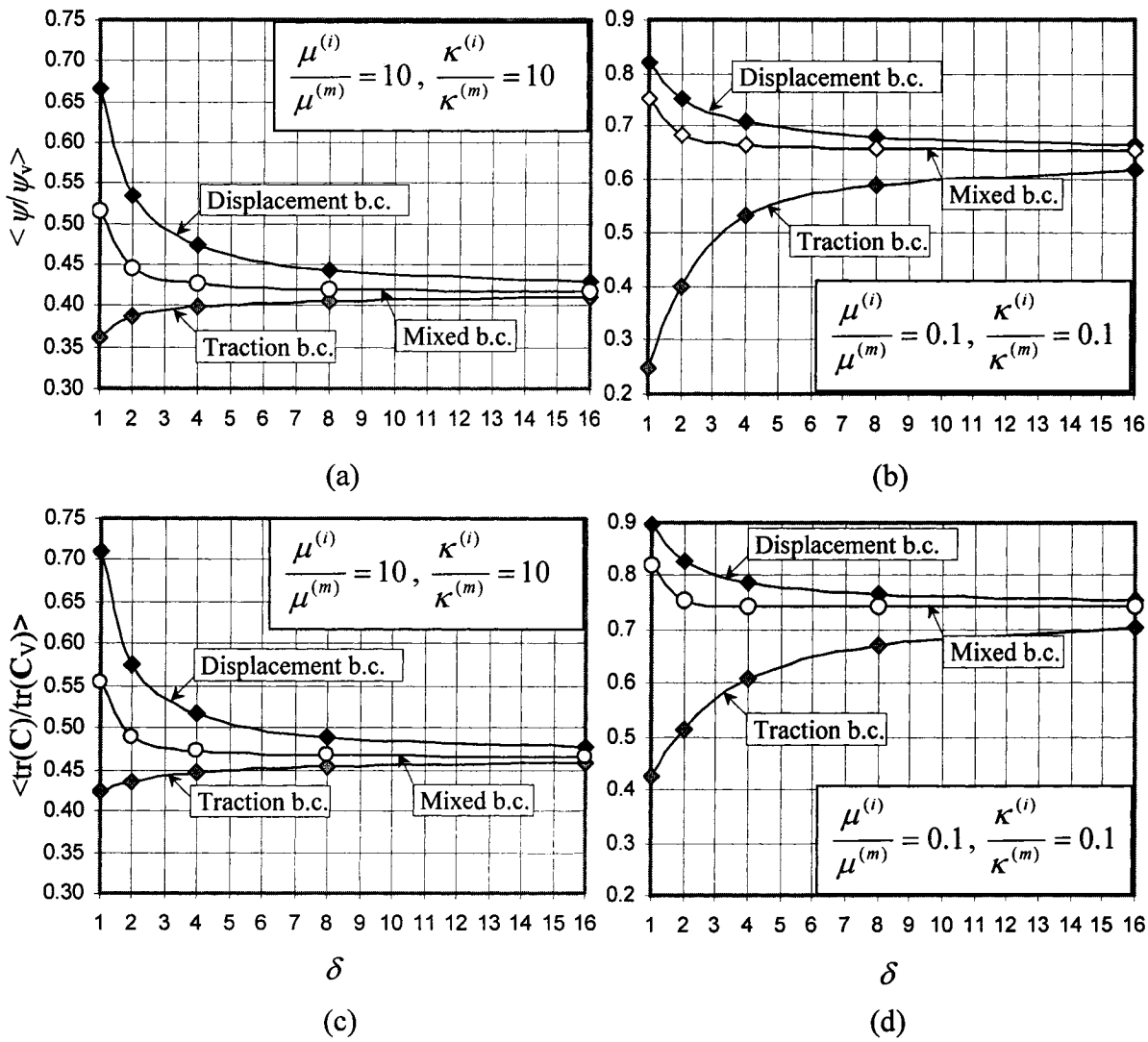

Figure 3.15. Bounds on the strain energy (a,b) and material properties (c,d) of the linear elastic composite (No. 5 and No. 6) under uniaxial tension.

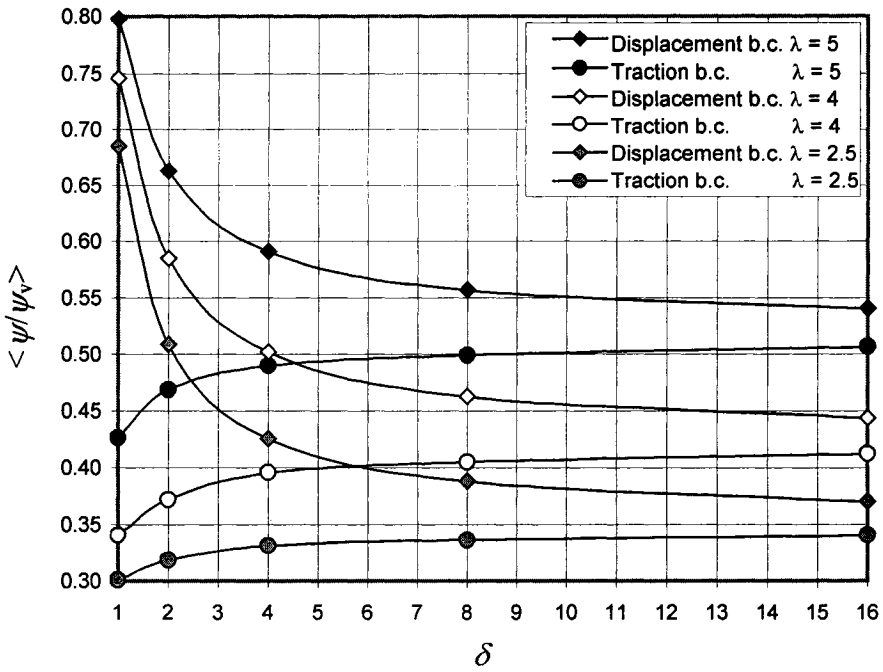

Figure 3.16. Dependence of the strain energy on the stretch value for the composite No. 1.

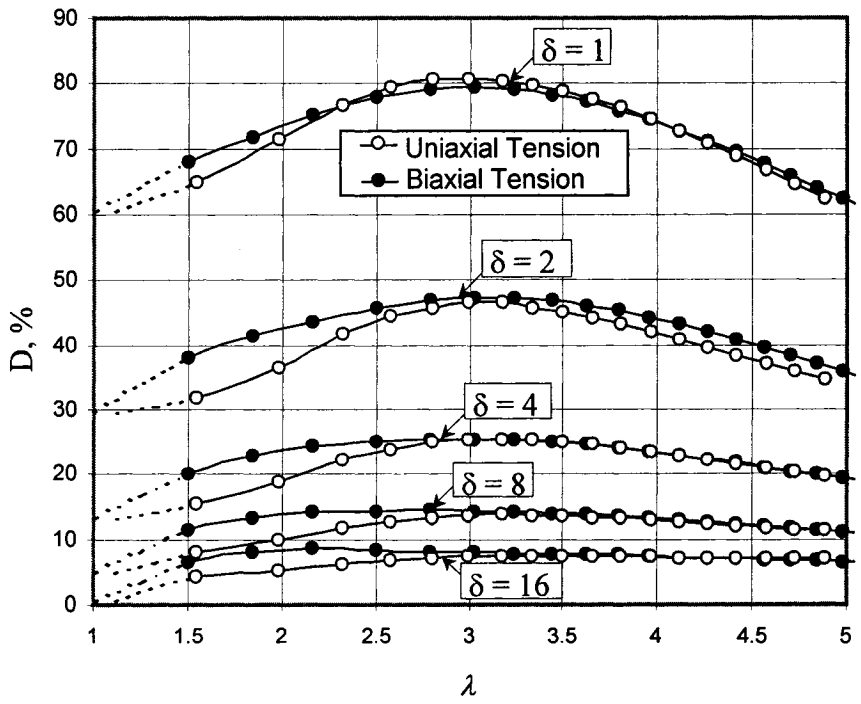

Figure 3.17. Discrepancies in the energy density of the composite No. 1 between displacement and traction boundary conditions for uniaxial and biaxial tension for various mesoscales.

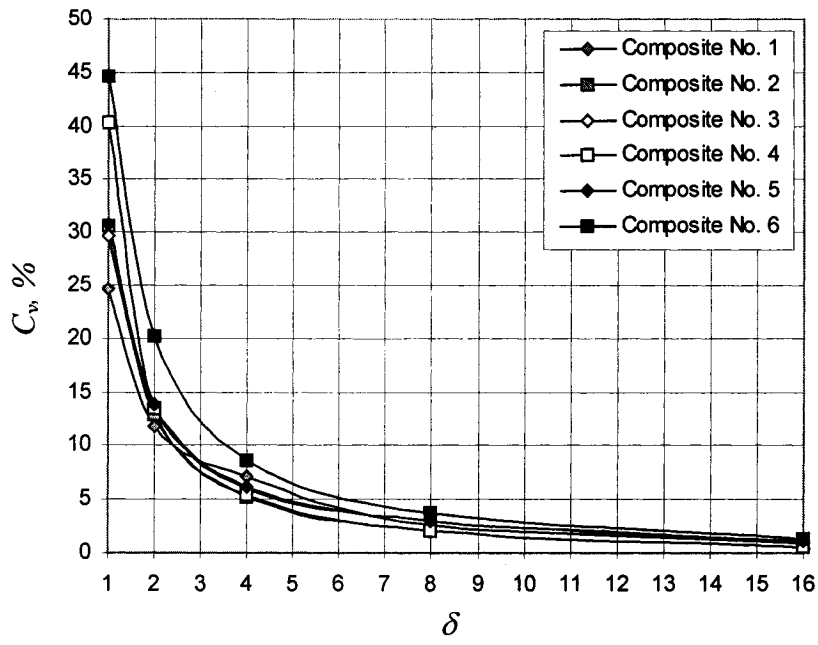

(a)

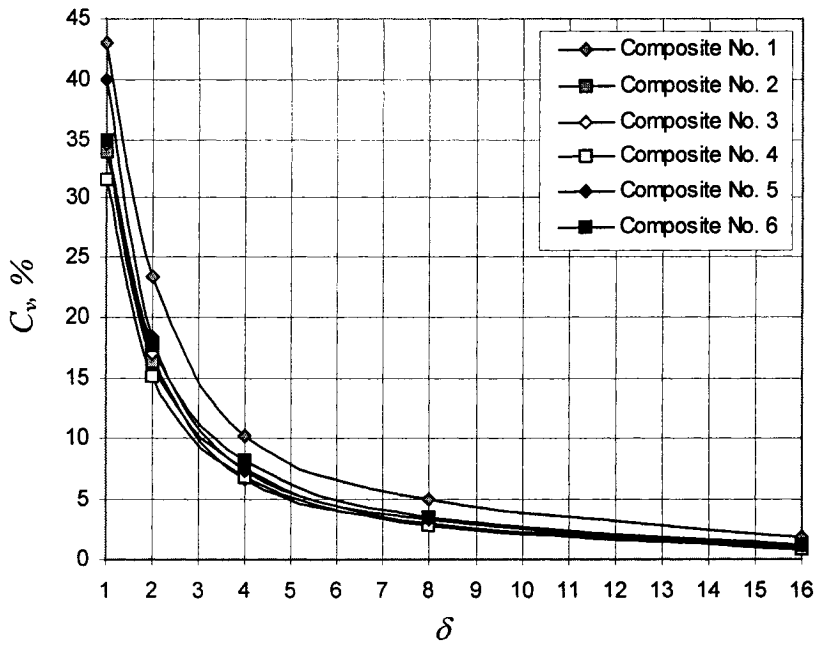

(b)

Figure 3.18. Dependence of the coefficient of variation of the strain energy (a) and complementary energy (b) on the mesoscale for different composite models.

Chapter 4

Scale effects in infinitesimal and finite thermoelasticity of random composites

Thermoelastic properties determine many important characteristics of composite materials. One of the examples is in polymer composites, where the incorporation of rubbery particles into glassy polymers increases both the toughness and the Coefficient of Thermal Expansion (CTE) of the material (Boyce *et al.,* 1987; Paul and Bucknall, 2000). Another example is the addition of a material with a low CTE to improve thermal properties of a material with high CTE (Yu *et al.,* 2000).

The effective (or overall) thermoelastic properties of linear elastic composites have been considered by Kerner (1956), Schapery (1968), Balch (1996), Rosen (1970), Rosen and Hashin (1970), McGee and McCullough (1981), Theocaris and Varias (1985) and Paul and Bucknall (2000). The scaling trend toward the RVE in linear thermoelasticity of random composites was theoretically and computationally investigated by Du and Ostoja-Starzewski (2006). In contradistinction to the linear theory of thermoelasticity, the nonlinear theory of thermoelasticity at finite strains has received little attention in the literature. This is despite the fact that rubber-like materials are very often used as composite constituents in various structural applications. In the present chapter, some aspects of the behavior of nonlinear thermoelastic composites at finite strains are investigated, using the methodology introduced in Chapter 2 as the foundation for the analysis. The primary goal is to apply the developed asymptotic homogenization framework to *quantitatively* estimate the trends toward the RVE of non-periodic *random* composites using nonlinear theory of thermoelasticity.

4.1 Constitutive relations in linear and nonlinear thermoelasticity

The general form of the constitutive equations for strain and stress in the presence of temperature effects has the form

$$\mathbf{P} = \frac{\partial \psi(\mathbf{F},T)}{\partial \mathbf{F}}, \qquad \mathbf{F} = \frac{\partial g(\mathbf{P},T)}{\partial \mathbf{P}}. \tag{4.1}$$

Supplemented by the suitable equations for enthalpy, temperature, and heat conduction, Eqs. (4.1) can be used to fully characterize the properties of a thermoelastic material. To obtain relations for infinitesimal elasticity, one has to replace **F** and **P** in Eqs. (4.1) by an infinitesimal strain tensor, **ε**, and a Cauchy stress tensor, **σ**, respectively.

While the deformations in linear elastic materials are fully internal energy driven, nonlinear elasticity of elastomers and biological tissues is almost entirely based on the entropy concept (Holzapfel, 2000). The reason for this is that the molecular chains inside the polymer change their conformation while they deform. Thus, nonlinear and linear thermoelasticity differ not only in their strain-energy representation but also in the nature of deformation. In the modified entropic theory of rubber thermoelasticity, the Helmholtz free-energy function can be written as (Holzapfel, 2000):

$$\psi(\mathbf{F},T) = \psi_0(\mathbf{F})\frac{T}{T_0} - e_0(\mathbf{F})\frac{\Delta T}{T_0} + \hat{T}(T). \tag{4.2}$$

The detailed explanation of the variables in Eq. (4.2) can be found in Section 2.3.2. Substituting for linear elastic relations and assuming specific heat at constant deformation to be constant over a small temperature change, Eq. (4.2) can be readily reduced to a Helmholtz free energy in linear elasticity:

$$\psi(\varepsilon_{ij},T) = \frac{1}{2}C_{ijkl}\varepsilon_{ij}\varepsilon_{kl} + \Gamma_{ij}\varepsilon_{ij}\Delta T - \frac{1}{2}c_{\upsilon}\frac{\Delta T^2}{T_0}. \tag{4.3}$$

The reciprocal expression for the Gibbs free energy in liner elasticity has the form

$$g(\sigma_{ij},T) = -\frac{1}{2}S_{ijkl}\sigma_{ij}\sigma_{kl} - \alpha_{ij}\sigma_{ij}\Delta T - \frac{1}{2}c_p\frac{\Delta T^2}{T_0}. \tag{4.4}$$

In the above equations, $\Gamma_{ij} = -C_{ijkl}\alpha_{kl}$ is the thermal stress coefficient, c_{υ} and c_p are specific heat at constant volume and constant stress, respectively. c_p is related to c_{υ} through an expression:

$$c_p - c_{\upsilon} = T_0 C_{ijkl}\alpha_{ij}\alpha_{kl}. \tag{4.5}$$

In nonlinear thermoelasticity, the Gibbs free-energy function as well as the complementary energy function are generally unknown. Moreover, it is often impossible to construct such functions due to the non-convexity of the energy density potential (Lee and Shield, 1980; Ogden, 1984; Gao, 1999). If unique inversion of Eq. (4.2) is assumed,

the Legenre transformation (2.13) offers a convenient way of estimation of the Gibbs free energy without unwieldy inversion of the constitutive relations:

$$g = -\frac{\theta_0}{T_0}\left(\frac{\partial \psi_0}{\partial u_{i,j}} x_{i,j} - \psi_0\right) + \frac{\Delta T}{T_0}\left(\frac{\partial e_0}{\partial u_{i,j}} x_{i,j} - e_0\right) + \hat{T}(\theta_0). \tag{4.6}$$

Note, Eqs. (4.2) and (4.6) have already been given in Chapter 2, and are repeated here for the convenience of the reader.

Equations (4.1-4.6) characterize the material locally, describing the behavior of a particular phase of a composite. It is not clear *a priori* whether the same constitutive equations hold for a mesoscale or not; or how the free energy and the constitutive parameters change while approaching the effective values. Later, we will try to address these questions and to show that the form of free energy changes with scale in nonlinear thermoelasticity, and is scale independent in linear thermoelasticity.

4.1.1 Thermodynamic potential for a linear thermoelastic composite

Asymptotic homogenization of a linear thermoelastic composite has been studied by Du and Ostoja-Starzewski (2005, 2006) and Du (2006). We will show some of their derivations leading to hierarchies on the effective specific heat. This will allow us to compare linear and nonlinear asymptotic homogenization problems.

Following Du (2006), upon the substitution of the Hooke's law, $\sigma_{ij} = C_{ijkl}\varepsilon_{kl} + \Gamma_{ij}\Delta T$, into Eq. (4.3), the free energy in linear elasticity can be written as

$$\Psi = \frac{1}{2V}\int_V \left(\sigma_{ij}\varepsilon_{ij} + \Gamma_{ij}\varepsilon_{ij}\Delta T - c_v\frac{\Delta T^2}{T_0}\right) dV. \tag{4.7}$$

Taking Γ_{ij} at every point to be a sum of the volume average and the local fluctuation, $\Gamma_{ij} = \overline{\Gamma}_{ij} + \Gamma'_{ij}$, and decomposing the strain, $\varepsilon_{ij} = \overline{\varepsilon}_{ij} + \varepsilon'_{ij}$, gives

$$\Psi = \frac{1}{2}\overline{\sigma}_{ij}\overline{\varepsilon}_{ij} + \frac{1}{2}\overline{\Gamma}_{ij}\overline{\varepsilon}_{ij}\Delta T + \frac{1}{2V}\int_V (\Gamma'_{ij}\varepsilon'_{ij}\Delta T)\, dV + \frac{1}{2}\overline{c}_v\frac{\Delta T^2}{T_0}. \tag{4.8}$$

In equation (4.8), we used the fact that the Hill condition (2.29) holds under KUBC, and the temperature change, ΔT, is spatially uniform. Following the usual assumption of

linear thermoelasticity, the total strain ε_{ij} can be considered as a superposition of two independent quantities

$$\varepsilon_{ij} = e_{ij} + \varepsilon_{ij}^{th}, \tag{4.9}$$

where e_{ij} is the elastic strain and $\varepsilon_{ij}^{th} = \alpha_{ij}\Delta T$ is the thermal (inelastic) strain. We can also decompose the fluctuations of strain $\varepsilon_{ij}^{'}$ into two parts

$$\varepsilon_{ij}^{'} = e_{ij}^{'} + \varepsilon_{ij}^{th'}, \tag{4.10}$$

where $e_{ij}^{'}$ is a function of the displacement boundary condition (i.e., the applied strain, ε_{kl}^{0}) and $\varepsilon_{ij}^{th'}$ is a function of the temperature:

$$e_{ij}^{'}(x_m) = D_{ijkl}(x_m)\varepsilon_{kl}^{0}, \tag{4.11}$$

$$\varepsilon_{ij}^{th'}(x_m) = E_{ij}(x_m)\Delta T. \tag{4.12}$$

In the above equations two tensors are introduced: the tensor $D_{ijkl}(x_m)$, that relates the applied strain, ε_{kl}^{0}, to the elastic strain fluctuation, $e_{ij}^{'}$, and the tensor $E_{ij}(x_m)$, that relates the temperature change to the thermal strain fluctuation. Substituting (4.10 - 4.12) into (4.8), results in

$$\Psi = \frac{1}{2}\overline{\sigma}_{ij}\varepsilon_{ij}^{0} + \frac{1}{2}(\overline{\Gamma}_{ij} + \frac{1}{V}\int_{V} D_{ijkl}\Gamma_{kl}^{'}dV)\varepsilon_{ij}^{0}\Delta T - \frac{1}{2}(\overline{c}_{v} - \frac{T_0}{V}\int_{V}\Gamma_{ij}^{'}E_{ij}dV)\frac{\Delta T^2}{T_0}. \tag{4.13}$$

Thus, Ψ is a functional of the applied strain, ε_{ij}^{0}, the temperature increment, ΔT, the actual realization of the microstructure, $B(\omega)$, and the mesoscale, δ. The foregoing derivation indicates that, for linear heterogeneous materials, the free energy has the same bilinear form as that for the homogeneous material (4.3):

$$\Psi = \frac{1}{2}C_{ijkl}(\omega)\varepsilon_{ij}^{0}\varepsilon_{kl}^{0} + \Gamma_{ij}(\omega)\varepsilon_{ij}^{0}\Delta T - \frac{1}{2}c_{v}(\omega)\frac{\Delta T^2}{T_0}, \tag{4.14}$$

where the mesoscale properties are identified as follows

$$\Gamma_{ij}(\omega) = \overline{\Gamma}_{ij} + \frac{1}{V}\int_V D_{ijkl}\Gamma'_{kl}dV\,, \qquad c_v(\omega) = \overline{c}_v - \frac{T_0}{V}\int_V E_{ij}\Gamma'_{ij}dV\,. \tag{4.15}$$

Proceeding in a similar fashion the Gibbs free energy can be shown to be:

$$G = \frac{1}{2}S_{ijkl}(\omega)\sigma^0_{ij}\sigma^0_{kl} + \alpha_{ij}(\omega)\sigma^0_{ij}\Delta T + \frac{1}{2}c_p(\omega)\frac{\Delta T^2}{T_0}, \tag{4.16}$$

with

$$\alpha_{ij}(\omega) = \overline{\alpha}_{ij} + \frac{1}{V}\int_V F_{ijkl}\alpha'_{kl}dV\,, \qquad c_p(\omega) = \overline{c}_p + \frac{T_0}{V}\int_V H_{ij}\alpha'_{ij}dV\,, \tag{4.17}$$

where F_{ijkl} and H_{ij} are tensors which relate the stress fluctuation to the traction prescribed on the boundary, σ^0_{ij}, and the temperature change, accordingly.

Setting $\varepsilon^0_{ij} = 0$ or $\sigma^0_{ij} = 0$ provides hierarchies of mesoscale bounds on effective specific heat (Du and Ostoja-Starzewski, 2006):

$$\langle c_v\rangle_\Delta \le \langle c_v\rangle_\delta \le \langle c_v\rangle_{\delta'} \le \langle c_v\rangle_1, \text{ for } 1 < \delta' < \delta < \Delta\,, \tag{4.18}$$

$$\langle c_p\rangle_\Delta \le \langle c_p\rangle_\delta \le \langle c_p\rangle_{\delta'} \le \langle c_p\rangle_1, \text{ for } 1 < \delta' < \delta < \Delta\,, \tag{4.19}$$

where c_p and c_v are obtained from the Eqs. (4.15) and (4.17).

Scale-dependent hierarchies on CTE cannot be obtained in a way similar to above, due to the presence of a non-quadratic term in both Eqs. (4.14) and (4.16), and, therefore, a different approach has to be used. Du and Ostoja-Starzewski (2006) proposed considering the equations for the effective CTE obtained by Levin (1967). They showed that scale-dependence of the elastic constants leads to the scale-dependence of both thermal strain and stress coefficients. We will show general results, referring to the original article for more details.

Depending on the relations between the material constants of composite constituents, two hierarchies are possible for the thermal expansion coefficient

(i) $\alpha_1 > \alpha_2 \ge 0$ and $k_1 > k_2$:

$$\langle\alpha\rangle_\Delta \ge \langle\alpha\rangle_\delta \ge \langle\alpha\rangle_{\delta'} \ge \langle\alpha\rangle_1 \text{ for } 1 < \delta' < \delta < \Delta\,, \tag{4.20}$$

(ii) $\alpha_1 > \alpha_2 \ge 0$ and $k_1 < k_2$:

$$\langle\alpha\rangle_{\Delta} \le \langle\alpha\rangle_{\delta} \le \langle\alpha\rangle_{\delta'} \le \langle\alpha\rangle_{1} \text{ for } 1 < \delta' < \delta < \Delta. \tag{4.21}$$

Similarly, there are two hierarchies for the thermal stress coefficients

(i) $0 \ge \Gamma_1 > \Gamma_2$ and $k_1 > k_2$:

$$\langle\Gamma\rangle_{\Delta} \le \langle\Gamma\rangle_{\delta} \le \langle\Gamma\rangle_{\delta'} \le \langle\Gamma\rangle_{1} \text{ for } 1 < \delta' < \delta < \Delta, \tag{4.22}$$

(ii) $0 \ge \Gamma_1 > \Gamma_2$ and $k_1 < k_2$:

$$\langle\Gamma\rangle_{\Delta} \ge \langle\Gamma\rangle_{\delta} \ge \langle\Gamma\rangle_{\delta'} \ge \langle\Gamma\rangle_{1} \text{ for } 1 < \delta' < \delta < \Delta. \tag{4.23}$$

In the above equations subscript 1 denotes properties of the phase 1, and subscript 2 denotes properties of the phase 2. Note that there is no distinction between the matrix and the inclusion materials.

4.1.2 Thermodynamic potential for a nonlinear thermoelastic composite

One of the most commonly used forms of Helmholtz strain-energy function in nonlinear elasticity is based on the hypothesis of additive decomposition of energy into its distortional and dilatational parts (Ogden, 1992; Holzapfel and Simo, 1996):

$$\psi = \psi_{iso}(\tilde{\lambda}_a, T) + \psi_{vol}(J, T),\ \tilde{\lambda}_a = J^{-\frac{1}{3}}\lambda_a,\ a = 1,2,3. \tag{4.24}$$

An always positive volume ratio J - a requirement placed by material impenetrability - is associated with the deformation gradient by the expression: $J = \det(\mathbf{F}) = \lambda_1\lambda_2\lambda_3$, where λ_a are principal stretches. If a body undergoes thermoelastic deformations, it is convenient to decompose J into purely mechanical (J_M) and purely thermal (J_T) parts, such that $J = J_M J_T$. For illustrative purposes, in the following, we will consider the simplest form of the strain-energy potential given by a neo-Hookean strain-energy function (Guido, 2004):

$$\psi = \frac{1}{2}\left[\mu(T)(\tilde{\lambda}_1^2 + \tilde{\lambda}_2^2 + \tilde{\lambda}_3^2 - 3) + \kappa(T)(J_M - 1)^2\right] + \tilde{T}(T),\ \tilde{\lambda}_a = J^{-\frac{1}{3}}\lambda_a \tag{4.25}$$

$\mu(T)$ and $\kappa(T)$ are temperature-dependent initial shear modulus and initial bulk modulus. $\tilde{T}(T)$ is the purely thermal contribution to the free energy. As it was pointed out in Chapter 2, $\tilde{T}(T)$ does not change with the scale and therefore can be ignored in hierarchies (2.34) and (2.38). The purely thermal volume ratio in Eq. (4.25) is defined as

$$J_T = (1+\alpha\Delta T)^3. \tag{4.26}$$

As it was mentioned in the previous chapter (see Section 3.4.1), the ensemble-averaged response of a random composite can be considered to be isotropic if a sufficient number of numerical realizations of the composite is considered. Thus, if all the phases of the composite were described by the strain energy specified by Eq. (4.24), one would expect to have the same form of the constitutive equation on a mesoscale. This holds in linear thermoelasticity (see Eqs. (4.14) and (4.16)), but not in nonlinear elasticity. Even examination of the simplest case of KUBC, $\mathbf{F}^0 = \mathbf{1}$, leads to the nonzero contribution of the distortional part to the free energy since $\overline{\tilde{\lambda}_a^2} \neq \tilde{\lambda}_a^{0\,2}$. Note that, in the absence of temperature effects, the aforementioned boundary condition will give $\Psi = 0$. Hence, the free energy of the composite can be written as

$$\Psi(\omega,\mathbf{F}^0,\theta_0) = \frac{1}{V_0}\int_{V_0}\left[\psi_\Delta(\omega,\mathbf{F}^0,\theta_0) + \psi'(\omega,\mathbf{X},\mathbf{F},\theta_0)\right]dV, \tag{4.27}$$

where

$$\psi_\Delta(\omega,\mathbf{F}^0,\theta_0) = \frac{1}{2}\left[\mu_\Delta(T)(\tilde{\lambda}_1^{0\,2}+\tilde{\lambda}_2^{0\,2}+\tilde{\lambda}_3^{0\,2}-3) + \kappa_\Delta(T)\left(\frac{J^0}{(1+\alpha_\Delta\Delta T)^3}-1\right)^2\right] + \tilde{T}(T), \tag{4.28}$$

and $\psi'(\omega,\mathbf{X},\mathbf{F},\theta_0)$ is a local fluctuation of the free energy.

Utilizing Eq. (2.13) and applying stress-free boundary conditions (free expansion) $\mathbf{P}^0 = \mathbf{0}$, hierarchy (2.38) transforms to

$$\left\langle\Psi(\mathbf{P}^0,\theta_0)\right\rangle_\Delta \geq \left\langle\Psi(\mathbf{P}^0,\theta_0)\right\rangle_\delta \geq \left\langle\Psi(\mathbf{P}^0,\theta_0)\right\rangle_{\delta'} \geq \left\langle\Psi(\mathbf{P}^0,\theta_0)\right\rangle_1, \text{ for } 1<\delta'<\delta<\Delta, \tag{4.29}$$

which provides a lower bound on the effective Helmholtz free energy. Note, under stress-free boundary conditions, the elastic part of Ψ is equal to zero for a homogeneous body. In contrast, for a heterogeneous material, the elastic contribution increases with the sample size (see Section 4.3).

In the following sections, we will examine the hierarchies (2.34), (4.29), and (4.20)-(4.23), and compare the results for linear and nonlinear thermoelastic composites.

4.2 Numerical experiments

To model a random microstructure, we consider a matrix with randomly distributed circular non-overlapping inclusions similar to the ones generated in the previous chapter. The various physical properties of two materials, used as illustrative examples, are shown in Tables 4.1 and 4.2, and correspond to commonly employed industrial composites: rubber-toughened polystyrene (Tables 4.1) is an example of a material where the incorporation of rubbery particles into a brittle polymer is used to improve the fracture properties (Boyce *et. al.*, 1987), and polyurethane rubber filled with sodium chloride (Table 4.2) is an example of highly filled elastomers, which are used as materials for solid propellants in rocketry (van der Wal *et al.*, 1965).

We will employ finite-strain elasticity and the neo-Hookean strain-energy function specified in Eq. (4.25). It is well known, that the neo-Hookean type material corresponds to the class of convex strain-energy functions, and, therefore, satisfies the convexity conditions (2.17) and (2.20) for any value of the material parameter $\mu(T)$.

The random distribution of inclusions was modeled by the planar homogeneous Poisson point process (see Eq. (3.1)). The finite element method with a non-uniform mesh (see Fig. 3.1) was used to simulate the response of the microstructure. The mesh was repeatedly refined until no significant changes in the response occurred, which, similar to the nonlinear elasticity problem (Chapter 3), was found to hold for an average element size of 0.75 for $d = 10$. Again, we assume perfect interfaces between different phases and perform calculations for the volume ratio of inclusions 35%. All tests were run in the commercial finite element software ABAQUS 6.5. Four-node bilinear coupled temperature-displacement plane stress elements were used in the analysis. The number of realizations for specific window size of a random composite was chosen to be the same as that for nonlinear elastic materials studied in Chapter 3 (see Section 3.3): 512 for $\delta = 1$; 384 for $\delta = 2$; 160 for $\delta = 4$; 40 for $\delta = 8$ and 10 for $\delta = 16$.

Table 4.1. Material properties of constituents for rubber–polystyrene composite.

Material	μ_0, MPa	κ_0, MPa	$\alpha \cdot 10^4$, °C^{-1}	c_υ, $\frac{J}{gK}$
Polystyrene	1200	4000	0.5	1.2
Rubber (polybutadiene)	0.62	2000	2.5	1.8
Mismatch	$\frac{\mu_0^{(i)}}{\mu_0^{(m)}} = 0.5 \cdot 10^{-3}$	$\frac{\kappa_0^{(i)}}{\kappa_0^{(m)}} = 0.5$	$\frac{\alpha^{(i)}}{\alpha^{(m)}} = 5$	$\frac{c_p^{(i)}}{c_p^{(m)}} = 1.5$

Table 4.2. Material properties of constituents for sodium-chloride–rubber composite.

Material	μ_0, MPa	κ_0, MPa	$\alpha \cdot 10^4$, °C^{-1}	c_υ, $\frac{J}{gK}$
Sodium-Chloride	12800	25300	0.4	0.85
Rubber (polyurethane)	1.32	1970	2.4	1.67
Mismatch	$\frac{\mu_0^{(i)}}{\mu_0^{(m)}} = 3.2 \cdot 10^3$	$\frac{\kappa_0^{(i)}}{\kappa_0^{(m)}} = 12.8$	$\frac{\alpha^{(i)}}{\alpha^{(m)}} = 0.17$	$\frac{c_p^{(i)}}{c_p^{(m)}} = 0.5$

4.3 Scaling trends of the free-energy function

The ensemble-averaged free energy under different boundary conditions is plotted in Fig. 4.1 as a function of scale for two considered composites (see Tables 4.1 and 4.2). The purely thermal contribution was ignored in the calculations due to its scale independence.

Graphs in Fig. 4.1 (a) and (c) present results under the constrained boundary condition, when $\mathbf{F}^0 = \mathbf{1}$ and the applied temperature change[1] is $\Delta T = 300\ ^\circ C$. In Fig. 4.1 (b) and (d) we show the lower bound (4.29) obtained under the stress-free boundary condition, $\mathbf{P}^0 = \mathbf{0}$, and $\Delta T = 300\ ^\circ C$. In agreement with theoretical predictions, the free energy, obtained under these two loadings, approaches the effective values from above and from below with an increasing sample size.

The two loadings considered above, although commonly employed in the experimental investigations, are not equivalent and cannot be used to calculate the

discrepancy, from which the minimal RVE size can be estimated. Indeed, the average stress field in a fully constrained composite is not equal to zero if $\Delta T \neq 0$, as it is for a fully unconstrained body. Similarly, the averaged deformation gradient in the unconstrained body cannot be equal to one if $\alpha \neq 0$ and $\Delta T \neq 0$. In order to estimate the size of the RVE, we will adopt the approach introduced in the previous chapter:

1) Compute response under SUBC $\mathbf{P}^0 = \mathbf{0}$ and obtain $\langle \Psi(\mathbf{P}^0) \rangle_\delta$.

2) Apply KUBC through $\lambda_i^0 = \langle \overline{\lambda_i} \rangle_{\delta=\delta_{\max}}^{\mathbf{P}=0}$ and obtain $\langle \Psi(\mathbf{F}^0) \rangle_\delta$.

The closer the composite size to the RVE, the smaller is the difference between the responses obtained under these two boundary conditions. For $\delta \to \infty$, the energy values calculated using the above methodology should coincide.

Note that, due to the scatter of the values of $\langle \Psi(F_{ij}^0) \rangle_\delta$ with small changes in $\lambda_i^0 = \langle \overline{\lambda_i} \rangle_{\delta=\delta_{\max}}^{P_{ij}=0}$, this methodology gives an approximate estimate of the minimum size of the RVE, which, however is sufficient for the comparison of different composites.

In Figs. 4.1 (b) and (d) the upper bound on the free energy corresponds to the values obtained with $\lambda_i^0 = \langle \overline{\lambda_i} \rangle_{\delta=\delta_{\max}}^{\mathbf{P}=0}$. In agreement with the results in isothermal elasticity (see Figs. 3.13), for a matrix with a CTE value smaller than that for inclusions (soft matrix in isothermal elasticity) the lower bound converges faster, whereas for a composite with the matrix having higher, compared to the inclusions, value of CTE (soft matrix in isothermal elasticity) the lower bound approaches the effective value slower than the upper one.

The differences between discrepancy values, D, obtained for $\delta = 16$ and $\delta = 8$ are 7% for a rubber-polystyrene composite and 20% for a sodium-chloride–rubber composite. This shows that the second composite converges to the RVE faster than the first one, although the discrepancy itself is larger for sodium-chloride–rubber composite (85% versus 56%, respectively). Moreover, it can be concluded that the non-isothermal

[1]The large temperature changes considered here are adopted for illustrative purposes only.

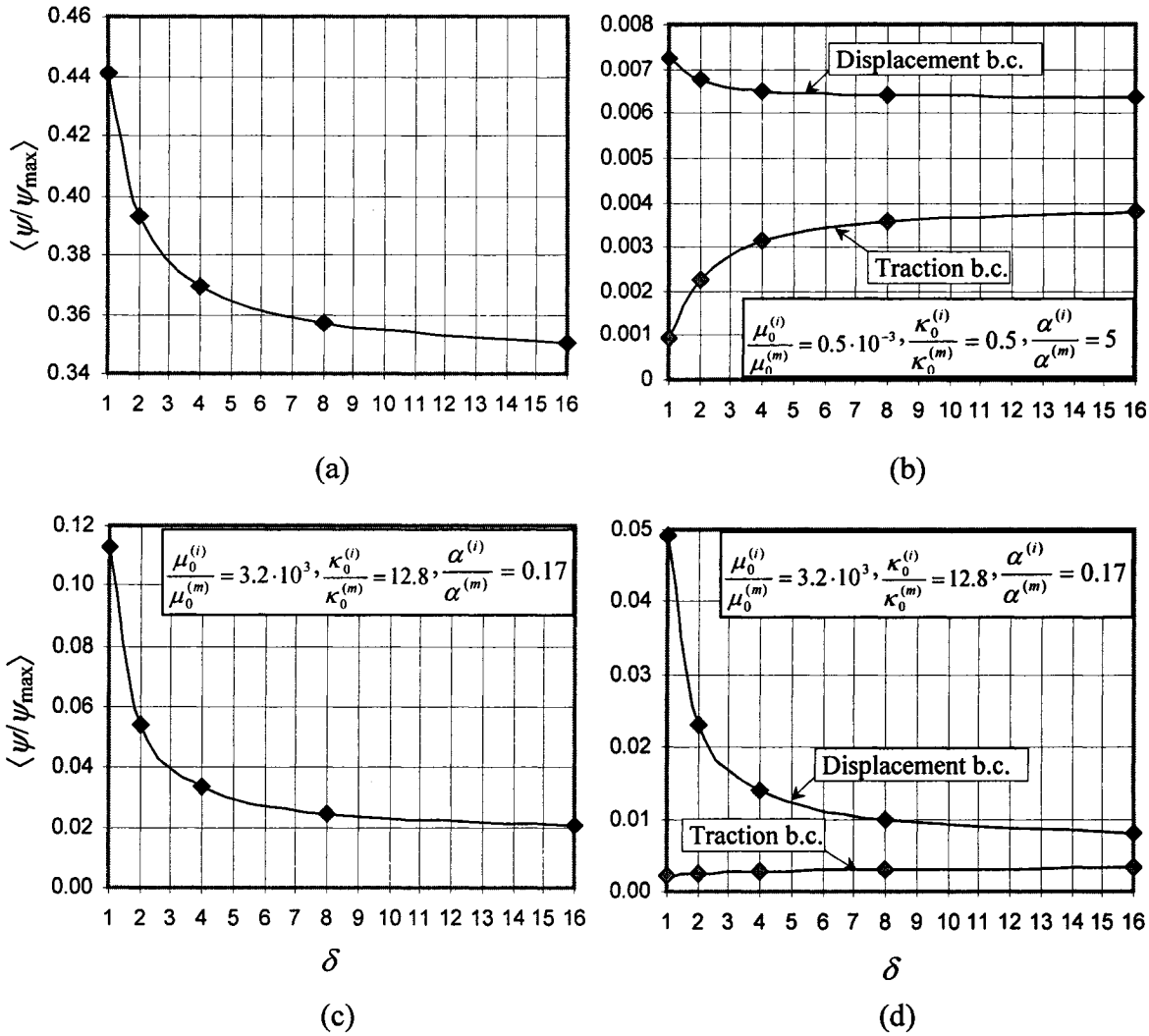

Figure 4.1. Scale effects on the strain energy under constrained deformations (a,c) and stress-free boundary conditions (b,d).

elasticity converges to the RVE slower than the isothermal one. This was also observed in the comparative study of mesoscale bounds in linear elasticity and thermoelasticity (Ostoja-Starzewski *et al.*, 2006).

Note that, for a homogeneous body, both the elastic part of $\Psi(\mathbf{P}^0 = \mathbf{0})$ and $\psi'(\mathbf{F}^0 = \mathbf{1})$ are equal to zero. According to Eq. (4.29) and Fig. 4.1, however, the elastic part of the free energy, $\langle \Psi(\mathbf{P}^0 = \mathbf{0}) \rangle_\delta$, increases when $\delta \to \infty$. This implies that energy

fluctuations, $\left\langle \overline{\psi'(\mathbf{F}^0 = \mathbf{1})} \right\rangle_\delta$, although decreasing with the growing scale, do not vanish as they do for a homogeneous material, when $\delta \to \infty$. This is an interesting observation and is a specific feature of a coupled field theory.

4.4 Scaling trends of the thermoelastic parameters

It is evident that the minimal RVE size is different for different quantities. For example, in linear thermoelasticity, the trend toward the RVE of thermal expansion coefficient is different from that of the bulk modulus or the specific heat capacity (Du and Ostoja-Starzewski, 2006). The mesoscale bounds on the free energy, investigated in the previous section, are the most general bounds, because they incorporate scale-dependence of all material parameters. For a specific application, however, one might be interested in one material parameter and not in the overall response of the material. In this section, we will study the trends and the speed of convergence of thermal expansion and thermal stress coefficients and compare the results obtained using the linear and nonlinear theories of thermoelasticity.

In order to calculate the convergence trend of the thermal expansion coefficient, α, we will adopt the following methodology:

(i) apply stress-free boundary conditions $\mathbf{P}^0 = \mathbf{0}$ with a temperature change[2] $\Delta T = 300\ ^\circ C$;

(ii) calculate $\left\langle \overline{F}_{ij} \right\rangle_\delta$;

(iii) calculate $\left\langle \alpha_{ij} \right\rangle_\delta = \dfrac{\left\langle \overline{F}_{ij} \right\rangle_\delta - \delta_{ij}}{\Delta T}$.

The thermal stress coefficient in the small deformation theory is defined as $\Gamma_{ij} = -C_{ijkl}\alpha_{kl}$, and relates the amount of stress generated in a constrained body to the applied temperature change. In finite-strain thermoelasticity, the relation between nominal stress and the temperature is nonlinear (see Eq. (4.25)), and the thermal stress coefficient cannot be expressed in terms of the material parameters only. For the sake of comparison, we will estimate Γ in a way analogous to the infinitesimal thermoelasticity:

(i) apply UKBC $\mathbf{F}^0 = \mathbf{1}$ and the temperature change $\Delta T = 300\ ^\circ C$;

(ii) calculate $\left\langle \overline{P}_{ij} \right\rangle_{\delta}$;

(iii) calculate $\left\langle \Gamma_{ij} \right\rangle_{\delta} = \dfrac{\left\langle \overline{P}_{ij} \right\rangle_{\delta}}{\Delta T}$.

This will allow us to study the difference in predictions of infinitesimal and finite theory of thermoelasticity and find whether finite deformations have significant effect on the asymptotic bounds of thermoelastic parameters or not.

The results of the numerical computation of thermal strain and stress coefficients for two composites described above are brought out in Fig. 4.2 (a) -(d). Since both considered composites fall into the category with material properties described by inequalities (4.21), on graphs in Fig. 4.2 (e) and (d) we study a hypothetical example of the composite which has a reverse relationship between its phases (Eq. (4.20)), i.e., $\alpha_1 > \alpha_2 \geq 0$ and $k_1 > k_2$. α and Γ in Fig. 4.2 define isotropic thermal strain and stress coefficients, respectively. This is due to the fact that ensemble averaging of a statistically isotropic microstructure leads to an isotropic response, as it was pointed out in Chapter 3, and, hence, the resulting thermal stress and strain coefficients are isotropic tensors of the second order: $\left\langle \alpha_{ij} \right\rangle_{\delta} = \alpha \delta_{ij}$ and $\left\langle \Gamma_{ij} \right\rangle_{\delta} = \Gamma \delta_{ij}$.

The asymptotic bounds on the thermal expansion coefficient demonstrate very little difference between values obtained using infinitesimal and finite theory of thermoelasticity, and, therefore, are presented for the latter case only. This is expected, since we assume linear relationship between the thermal strain, ε_{ij}^{th}, and the temperature change, ΔT, in both theories (see Eq. (4.26)). A different situation is encountered for the thermal stress coefficient: the asymptotic bounds, while converging in a similar way, have a considerable variation in values depending on the properties of the composite and the theory employed (see, Fig. 4.2 b, d and f).

---

[2]The temperature difference 5 $^{\circ}C$ was applied to study the response of the materials using the linear theory of thermoelasticity (Eq. 4.3).

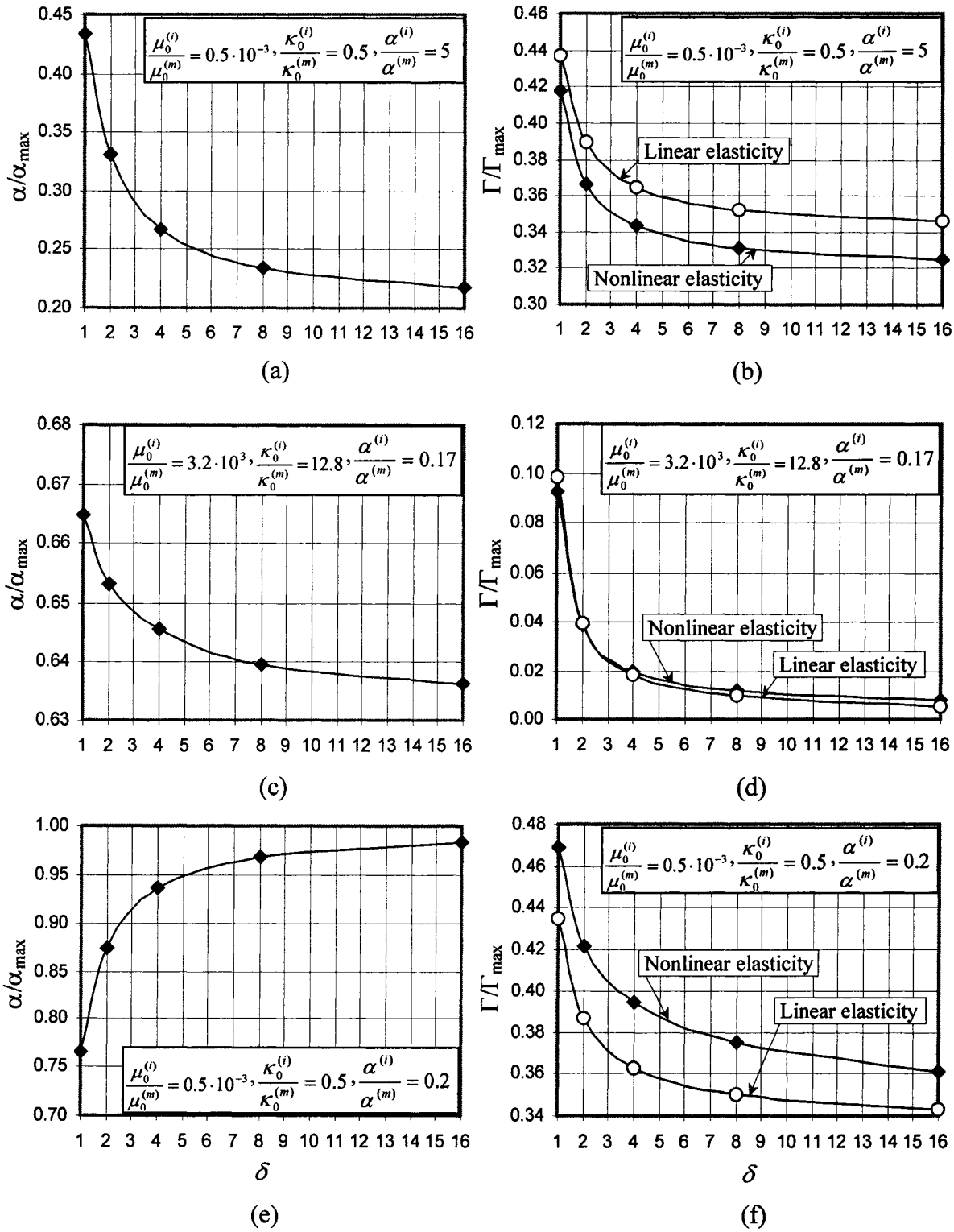

Figure 4.2. Mesoscale bounds on the thermal expansion coefficient, α, and the thermal stress coefficient, Γ, for different nonlinear composites.

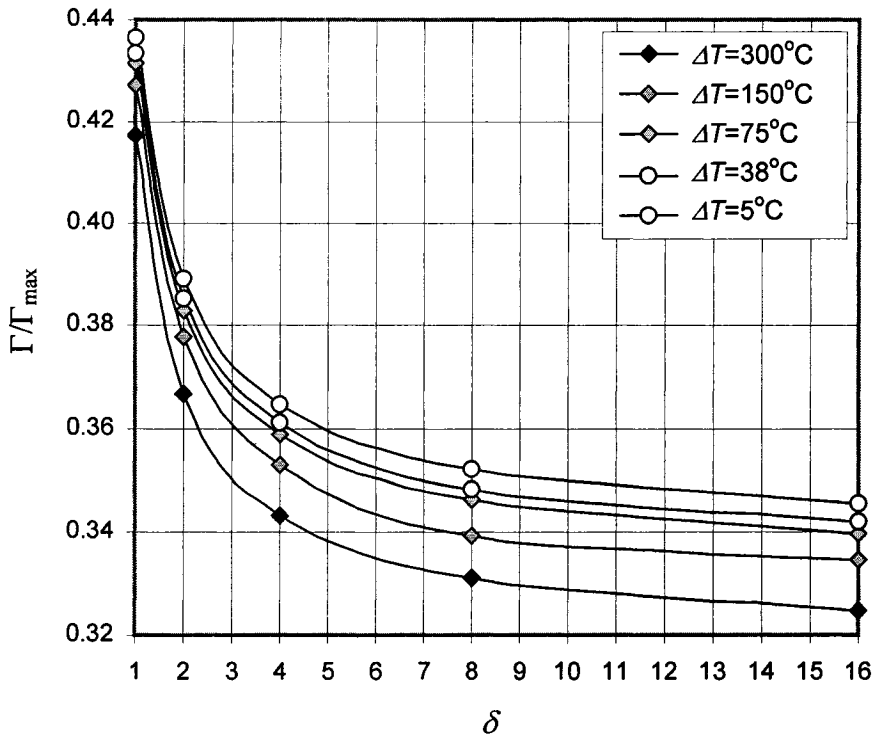

Figure 4.3. Dependence of the thermal stress coefficient Γ on the temperature change ΔT for the rubber-polystyrene composite.

The graphs in Figs. 4.2 and 4.3. are normalized with respect to the maximum value of the studied parameter, which can be the value for either a matrix or inclusions. This provides a reverse trend of the thermal stress coefficient due to its negative value, i.e., $\langle \Gamma_{ij} \rangle_\delta < 0$, but $\left\langle \frac{\Gamma_{ij}}{\Gamma_{\max}} \right\rangle_\delta > 0$.

In the work of Du and Ostoja-Starzewski (2006), the equation $\langle \Gamma_{ij} \rangle_\delta^\sigma = -\langle C_{ijkl} \rangle_\delta^\sigma \langle \alpha_{kl} \rangle_\delta^\sigma$ was applied to obtain the second bound and to estimate the minimal size of the RVE. In nonlinear elasticity, this transformation is not valid, and the thermal stress coefficient depends on both the deformation and the temperature change. The energy bounds, considered in the previous section, offer a way to estimate the gap between the responses under different boundary conditions and, correspondingly, the RVE size in nonlinear thermoelasticity.

From the above graphs it can be concluded that, regardless of the theory employed for mesoscale bound calculations, the convergence for all considered material parameters follows hierarchies (4.20) - (4.23). This suggests that the linear theory of thermoelasticity can be used as a first approximation in calculating the minimal size of the RVE. If, however, α_{ij} is a nonlinear function of temperature, the above conclusion may not be valid and further study is necessary.

4.5 Closure

The main conclusions of this chapter can be summarized as follows:

(i) In contrast to the linear theory of thermoelasticity, where the effective and the local forms of the free energy of a composite material coincide, the effective form of the free energy in nonlinear elasticity is different from the local one, even if all the phases of the composite follow the same constitutive law.

(ii) Scale-dependent homogenization can be used to estimate the size of the RVE in nonlinear thermoelasticity. It is shown that the free energy approaches the effective value from above and from below under KUBC and SUBC, respectively.

(iii) In nonlinear elasticity the asymptotic bounds on the thermal stress coefficient depend on the temperature difference and the property mismatches.

(iv) The convergence of both thermal strain and stress coefficient follows the same hierarchies independent of the theory used for the mesoscale bound calculations.

Chapter 5

Size effects on thermoelastic damping in nanomechanical resonators with finite wave speeds [1]

5.1 Introduction

The size affects not only the mechanical properties of heterogeneous materials and structures, as it is shown in the previous chapters, but also the behavior of structures made of materials conventionally considered homogeneous. Nanoelectromechanical systems, or NEMS, whose size can be as small as 10 nm, are one of the examples (Srikar and Senturia, 2002). When the dimensions of a body approach submicron scale, the continuum theory of elasticity becomes dubious and one has to take into account the size effect on the material behavior. In this chapter, we will demonstrate such effect, taking a completely different approach and thermoelastic problem physically different from the one considered before. We will study the change of the thermoelastic damping of a nanoresonator, when the scale changes from the micro to the nanolevel and the new laws of heat conduction should be taken into account.

NEMS attain extremely high fundamental frequencies of operation as a result of their reduced size and small force constants (Roukes, 2000). Such high-frequency mechanical devices have many important applications; among them are ultrasensitive mass detection, mechanical signal processing, scanning probe microscopes, etc.

An important attribute of any NEMS device is its quality or Q factor of resonance. The larger the quality factor, the smaller the energy dissipated during vibrations, and the higher the resonator sensitivity (Yasumura *et al.*, 2000). There are many mechanisms which contribute to energy dissipation in beam resonators. If the elimination of external damping mechanisms is the question of design and operation conditions, the removal of intrinsic damping sources is almost impossible. It is therefore important to investigate and

---

[1]Most of the material in this chapter has been published as an article in the *Journal of Thermal Stresses* (**29**, 201-216, 2006).

find a way to reduce intrinsic material losses such as thermoelastic damping, as much as possible.

Classical theory of thermoelastic damping was first presented by Zener (1948). He considered vibrations of a homogeneous, isotropic, thermoelastic beam, in which damping occurs due to heat transfer from a hotter (compressed) to a colder (stretched) side of the beam. Thermoelastic losses, calculated using Zener's viscoelastic model of the solid, were experimentally verified for many materials (Crowley & van Schoor, 1987; Bishop & Kinra, 1992; Bishop & Kinra, 1997). The subsequent analysis of thermoelastic vibrations of a beam includes the work of Jones (1966), where the effect of damping is calculated taking into account axial deformations of a beam of arbitrary cross section, and the later work of Lifshitz and Roukes (2000), who examined thermoelastic damping in micro- and nanomechanical resonators. Recently, based on the second law of thermodynamics, a fundamentally different approach to analyzing thermoelastic damping in a vibrating beam was introduced by Kinra and Milligan (1992, 1994).

In all the works mentioned above, thermoelastic damping is calculated using the classical theory of thermoelasticity, in which the equation governing the temperature distribution is of a parabolic type and therefore predicts infinite speed of propagation of thermal disturbances. However, in systems operating on a short-time scale, such as high-frequency nanoresonators, heat generated by the nonuniform stress distribution might not have enough time to propagate from one side of the device to another, and, therefore, properties of the system can differ significantly from the case of regular time operation. To eliminate the paradox of infinite propagation speeds, generalized theories have been formulated in the literature. These nonclassical theories admit finite speed of "wave-type" heat propagation - referred to as a "second sound" - either by adding a first time derivative of the heat flux into Fourier's law of heat conduction (Lord & Shulman, 1967) (thermoelasticity with one relaxation time) or by including the temperature rate among the constitutive variables (Chandrasekharaiah, 1986).

The aim of the present work is to determine the frequency of vibration and, thus, the size of the resonator, at which the effect of finite speed of heat conduction on thermoelastic damping becomes significant. The question is whether the classical theory

is still valid for the length scales of nanomechanical resonators or the second sound effect has to be taken into account. In this chapter, we follow the approach introduced by Kinra and Milligan (1994) using a hyperbolic heat conduction equation proposed by Lord and Shulman (1967).

5.2 General theory

5.2.1 Classical thermoelasticity

We will use the classical linear thermoelasticity theory as a starting point before the description of damping of a thermoelastic medium with finite wave speeds. The classical thermoelasticity theory for a linear isotropic homogeneous thermoelastic medium is described by the following system of field equations:

1. Equilibrium equations (in the absence of body forces)

$$\sigma_{ji,j} = \rho \ddot{u}_i . \tag{5.1}$$

2. Strain-displacement relations

$$\varepsilon_{ij} = \frac{1}{2}(u_{i,j} + u_{j,i}) . \tag{5.2}$$

3. Thermoelastic Hooke's law

$$\sigma_{ij} = \frac{E}{1+\nu}\left(\varepsilon_{ij} + \frac{\nu}{1-2\nu}\varepsilon_{kk}\delta_{ij}\right) - \frac{E}{1-2\nu}\alpha\delta_{ij}(T - T_0) . \tag{5.3}$$

4. Fourier's law of heat conduction

$$q_i = -kT_{,i} . \tag{5.4}$$

5. The law of conservation of energy

$$\rho\dot{u} = \sigma_{ij}\dot{u}_{i,j} - q_{i,i} . \tag{5.5}$$

Here a dot denotes differentiation with respect to time, σ_{ij} is the stress tensor, ε_{ij} is the linear strain tensor, u_i is the displacement vector, ρ is the mass density, t is time, E is Young's modulus of the material, ν is Poisson's ratio, α is the linear thermal expansion coefficient, T is the absolute temperature, T_0 is the absolute equilibrium temperature, q_i is the heat flux vector, k is the isotropic thermal conductivity, u is the internal energy per unit mass, δ_{ij} is the Kronecker delta, and the indices, i, j and k, take on the values 1, 2, 3.

Assuming small deviations of temperature from the equilibrium value, the coupled heat conduction equation for a classical thermoelastic body is given by (Nowacki, 1986)

$$T_{,ii} = \frac{\rho c}{k}\dot{T} + \frac{E\alpha}{k(1-2\nu)}T_0\dot{u}_{k,k}, \tag{5.6}$$

where c is the specific heat per unit mass and the dot denotes derivative with respect to time. The entropy production within a system per unit time per unit mass, s, in which a heat flow takes place, can be calculated from the entropy balance equation (Yourgrau, 1966)

$$\dot{s} = -\frac{1}{\rho T^2} q_i T_{,i}, \tag{5.7}$$

where in the approximation considered here T can be replaced by its reference value T_0. Eliminating q_i from Eq. (5.7) yields

$$\dot{s} = \frac{k}{\rho T_0^{\,2}} T_{,i} T_{,i}. \tag{5.8}$$

Thermoelastic damping, ψ, is defined as the ratio of the energy dissipated to the energy stored in the body over the same period of time, and can be expressed as (Kinra & Milligan, 1994)

$$\psi = \int_V \psi_L dV = \frac{\int_V \Delta W dV}{\int_V W dV} = \frac{\int_V \psi_L W dV}{\int_V W dV}, \tag{5.9}$$

where $\psi_L = \Delta W / W$ is the local specific damping capacity. Here W is the elastic energy density stored in the body, given by

$$W = \frac{1}{2}\sigma_{ij}\varepsilon_{ij}, \tag{5.10}$$

and ΔW is the total work lost throughout the body, which can be related to the entropy generation by the following equation (Bejan, 1988)

$$\Delta W = \rho T_o s. \tag{5.11}$$

Equations (5.1) through (5.11) define the classical theory of thermoelastic damping first presented by Kinra & Milligan (1994). In what follows, we consider a modification of this theory by taking into account the finite speed of thermal wave propagation.

5.2.2 Thermoelasticity with one relaxation time

The one relaxation time (ORT) theory proposed by Lord and Shulman (1967), and dating back to Maxwell and Cattaneo, eliminates the paradox of an infinite velocity peculiar to the classical theory by extension of Fourier's law of heat conduction to the most general case involving heat flux and its first time derivative

$$q_i + t_0 \dot{q}_i = -kT_{,i}, \tag{5.12}$$

where t_0 is the relaxation time. Proceeding in a way similar to that of the classical theory, it can be shown (Ignaczak, 1989) that a thermoelastic process in the ORT theory satisfies the same equilibrium equations, strain-displacement relations, constitutive equations and the law of conservation of energy as the classical process.

The coupled heat conduction equation (5.6) for an isotropic thermoelastic ORT body becomes (Chandrasekharaiah, 1986)

$$T_{,ii} = \frac{\rho c}{k}\left(\dot{T} + t_0 \ddot{T}\right) + \frac{E\alpha}{k(1-2\nu)} T_0 \left(\dot{u}_{k,k} + t_0 \ddot{u}_{k,k}\right). \tag{5.13}$$

Unlike the classical theory, this equation is of hyperbolic type and predicts a finite speed for heat propagation, provided $t_0 > 0$, and $u_{k,k}$ is a prescribed field. The constant t_0 has a clear physical interpretation: it is the time required to establish the steady state of heat conduction in a volume element suddenly subjected to a temperature gradient. Chester (1963) quantitatively estimated t_0 in terms of measurable macroscopic parameters to be

$$t_0 = \frac{3k}{\upsilon^2 \rho c}, \tag{5.14}$$

where υ is the phonon velocity. It is important to mention that Eq. (5.14) can only be used for a medium where the transport of heat occurs via the phonon gas, which is usually the case for MEMS/NEMS materials. To the first approximation, υ can be replaced by the elastic wave velocity (Francis, 1972).

The entropy production within a region of an ORT body can be obtained by substituting the solution of Eq. (5.12) for heat flux into Eq. (5.7). For the one-dimensional case, in which $T = T(y,t)$ and the temperature gradient is not equal to zero, the entropy production equation can be written as

$$t_0\ddot{s}+\dot{s}\left(1+t_0\frac{2\dot{T}}{T_0}-t_0\frac{\dot{T}'}{T'}\right)=\frac{k}{\rho T_0^{\,2}}(T')^2, \tag{5.15}$$

where the prime denotes a derivative with respect to the spatial coordinate. Note that, in the absence of t_0, Eq. (5.15) reduces to the entropy production equation for a classical thermoelastic body.

Finally, thermoelastic damping of the ORT body can be calculated in a similar way as in the case of the classical thermoelasticity using Eqs. (5.9) through (5.11). In the following section, we will apply the ORT theory to a specific case of thin beam vibrations.

5.3 Flexural vibrations of a Bernoulli-Euler beam

We consider a homogeneous isotropic elastic thin beam of thickness h with constant rectangular cross section (Fig. 5.1) subjected to a steady-state displacement boundary condition

$$u(x,t)=U(x)e^{i\omega t} \tag{5.16}$$

at the neutral axis, where $U(x)$ is a prescribed function and ω is the circular frequency in radians per second. We employ the classical Bernoulli-Euler assumptions: the x axis undergoes no extension, and the beam cross sections perpendicular to the neutral axis remain plane and perpendicular to it during deformation. Then, the strain-displacement relation becomes

$$\varepsilon_{xx}=-y\frac{\partial^2 u}{\partial x^2}=y\kappa_0 e^{i\omega t}, \tag{5.17}$$

where κ_0 is the beam curvature. It is worth mentioning that only the real part of Eq. (5.17) has a physical meaning and therefore should be considered.

For a typical MEMS material, the ratio $\frac{\Delta T}{T_0}$ is very small. For example, in the case of silicon ($\alpha = 2.5\cdot10^{-6}$ 1/K, $\rho = 2330$ kg/m^3, $c = 700$ J/kg·K) under the action of stress of 1 Mpa, $\frac{\Delta T}{T_0}$ is equal to $\approx 1.5\cdot10^{-6}$. The thermal stresses produced by this increase in temperature are negligibly small compared to the applied stress (Bishop & Kinra, 1997).

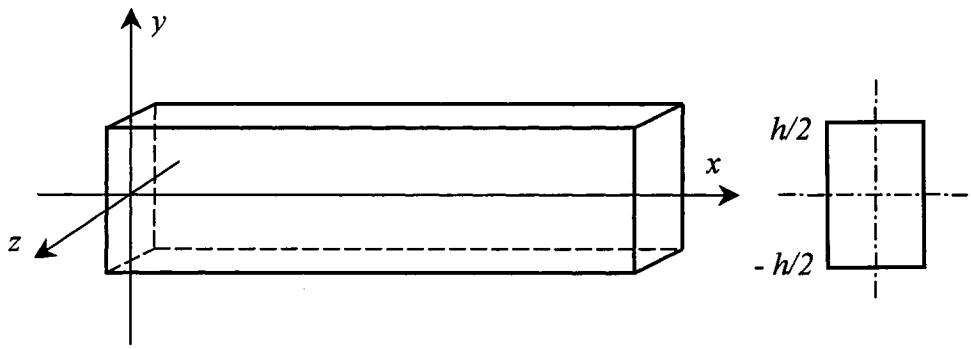

Figure 5.1. Coordinate system and geometry of the beam.

Therefore, the displacement field of a body can be assumed to be independent of the temperature, i.e., dilatation resulting from the thermoelastic effect can be ignored. Hence, we can write

$$\varepsilon_{kk} = -(1-2\nu)\varepsilon_{xx} = -(1-2\nu)\kappa_0 y e^{iwt}. \tag{5.18}$$

Noting that the thermal gradient across the thickness of the beam along the y direction is much larger than in any other direction, Eq. (5.13) reduces to

$$\frac{\partial^2 T}{\partial y^2} - \frac{\rho c}{k}\left(\frac{\partial T}{\partial t} + t_0 \frac{\partial^2 T}{\partial t^2}\right) = -\omega \frac{E\alpha T_0}{k}\kappa_0 y e^{i\omega t}(i - t_0\omega). \tag{5.19}$$

Assuming the conduction of heat in the beam to be much faster than the exchange of heat with the environment, i.e., the boundaries to be adiabatic, the boundary conditions can be written as follows

$$\frac{\partial T}{\partial y}\left(-\frac{h}{2}, t\right) = \frac{\partial T}{\partial y}\left(\frac{h}{2}, t\right) = 0. \tag{5.20}$$

Introducing a complex temperature field (Bishop & Kinra, 1997)

$$T = T_0(1+i) + V(y)e^{i\omega t}, \tag{5.21}$$

where T_0 is the absolute equilibrium temperature of the undisturbed beam, and $V(y)$ is the unknown spatial variation of the temperature, the coupled heat conduction equation (5.19) becomes

$$\frac{d^2 V^*}{dY^2} - \pi^2 \Omega V^*(i - \gamma\Omega) = -2\pi^2 \Omega Y(i - \gamma\Omega). \tag{5.22}$$

In Eq. (5.22), $Y = y/h$ is the nondimensional coordinate and $V^* = V/\Delta T$ is the normalized temperature, where ΔT is the change in temperature at the compressed upper surface of the beam under "adiabatic" conditions (Kinra & Milligan, 1992):

$$\Delta T = -\frac{\alpha}{\rho c}\sigma T_0 = \frac{\alpha}{\rho c}\frac{h}{2}ET_0\kappa_0, \tag{5.23}$$

and $\Omega = \omega\tau$ is the normalized frequency, where τ is the characteristic time of the beam in Zener's model of thermoelastic damping (Zener, 1948):

$$\tau = \frac{\rho c h^2}{\pi^2 k}. \tag{5.24}$$

Here $\gamma = t_0/\tau$ is the normalized relaxation time.

Equation (5.22) is a second-order non-homogeneous linear differential equation with constant coefficients. This equation can be solved using the method of undetermined coefficients to obtain

$$V^* = 2Y - \frac{2}{\Pi_1 + i\Pi_2}\frac{\sinh(Y\Pi_1)\cos(Y\Pi_2) + i\cosh(Y\Pi_1)\sin(Y\Pi_2)}{\cosh\left(\frac{\Pi_1}{2}\right)\cos\left(\frac{\Pi_2}{2}\right) + i\sinh\left(\frac{\Pi_1}{2}\right)\sin\left(\frac{\Pi_2}{2}\right)}, \tag{5.25}$$

where Π_1 and Π_2 are introduced for brevity and defined by

$$\Pi_1 = \pi\sqrt{\frac{\Omega}{2}\left(\sqrt{\gamma^2\Omega^2+1} - \gamma\Omega\right)}, \tag{5.26}$$

$$\Pi_2 = \pi\sqrt{\frac{\Omega}{2\left(\sqrt{\gamma^2\Omega^2+1} - \gamma\Omega\right)}}. \tag{5.27}$$

The classical counterpart of Eq. (5.25) can be reduced from it by setting γ equal to zero.

In order to obtain an expression for the net entropy production in the case of a non-zero temperature gradient, we should substitute the real part of temperature from Eq. (5.21) into the entropy production equation (5.15), and solve the corresponding differential equation. Let us first consider the second and the third term in parenthesis of Eq. (5.15). Substitution of the temperature from Eq. (5.25) gives the following relation for the second term

$$2t_0\frac{\dot{T}}{T_0} = \frac{2t_0\Delta T\omega}{T_0}\mathrm{Re}\left(iV^* e^{i\omega t}\right). \tag{5.28}$$

The normalized spatial variation of the temperature can be represented by two variables $V^* = A_R + iA_I$, where A_R is the real part and A_I is the imaginary part. Therefore,

$$2t_0\frac{\dot{T}}{T_0} = -2t_0\omega\frac{\Delta T}{T_0}\left(A_R\sin(\omega t) + A_I\cos(\omega t)\right). \tag{5.29}$$

The third term of Eq. (5.15) can be written in the following form

$$t_0\frac{\dot{T}'}{T'} = t_0\frac{\mathrm{Re}\left(i\omega\dfrac{\partial V^*}{\partial Y}e^{i\omega t}\right)}{\mathrm{Re}\left(\dfrac{\partial V^*}{\partial Y}e^{i\omega t}\right)}. \tag{5.30}$$

Separating $\dfrac{\partial V^*}{\partial Y}$ into its real (B_R) and imaginary (B_I) parts, we get

$$t_0\frac{\dot{T}'}{T'} = t_0\omega\frac{B_I\cos(\omega t) + B_R\sin(\omega t)}{B_I\sin(\omega t) - B_R\cos(\omega t)}. \tag{5.31}$$

As it is mentioned before, for the class of problems considered, the term $\dfrac{\Delta T}{T_0}$ is negligible (of the order of 10^{-6}). Therefore, the second term of Eq. (5.15) is much smaller than the third one and can be ignored without loss of accuracy. Eq. (5.15) simplifies to

$$\frac{\partial^2 s}{\partial t^2} + \frac{\partial s}{\partial t}\left(\frac{1}{t_0} - \omega\frac{B_I\cos(\omega t) + B_R\sin(\omega t)}{B_I\sin(\omega t) - B_R\cos(\omega t)}\right) = \frac{\Delta T^2 k}{t_0\rho h^2 T_0^{\,2}}\left(B_I\sin(\omega t) - B_R\cos(\omega t)\right)^2. \tag{5.32}$$

General solution of the above equation for the entropy production per unit time per unit mass is

$$\frac{\partial s}{\partial t} = \frac{\Delta T^2 k}{\rho h^2 T_0^2\left(1+\omega^2 t_0^2\right)}\left\{\left[B_I\sin(\omega t) - B_R\cos(\omega t)\right]^2 - \omega t_0\left[\frac{1}{2}\sin(2\omega t)\left(B_I^2 - B_R^2\right)\right.\right.$$

$$\left.\left. - B_I B_R\cos(2\omega t)\right]\right\} + C_1 e^{-\frac{t}{t_0}}\left[B_I\sin(\omega t) - B_R\cos(\omega t)\right], \tag{5.33}$$

where C_1 is an integration constant. For the function $\dot{s}$ to be periodic, we must set C_1 equal to zero.

Let us now examine the case when the gradient of the temperature is equal to zero. It corresponds to a condition

$$B_I\sin(\omega t) - B_R\cos(\omega t) = 0. \tag{5.34}$$

In this case the entropy production equation simply reduces to $\dot{s} = 0$.

The entropy production per unit mass per cycle period is given by (Kinra & Milligan, 1992):

$$\Delta s = \oint \frac{\partial s}{\partial t} dt . \tag{5.35}$$

Defining the period as $t = \frac{2\pi}{\omega}$ we get

$$\Delta s = \frac{\pi \Delta T^2 k}{\rho h^2 T_0^2 \omega \left(1 + \omega^2 t_0^2\right)} \left(B_I^2 + B_R^2\right). \tag{5.36}$$

Introducing this entropy production into Eq. (5.11), we can readily calculate the local specific damping capacity to be

$$\psi_L = \frac{\psi_0}{4\pi^2 \Omega Y^2 \left(1 + \gamma^2 \Omega^2\right)} \left(B_I^2 + B_R^2\right), \tag{5.37}$$

where ψ_0 is a characteristic Zener damping (Zener, 1948) defined by

$$\psi_0 = \frac{2\pi \alpha^2 E T_0}{\rho c} . \tag{5.38}$$

Then the averaged damping across the thickness of the beam is

$$\psi = \frac{3\psi_0}{\pi^2 \Omega \left(1 + \gamma^2 \Omega^2\right)} \int_{-1/2}^{1/2} \left(B_I^2 + B_R^2\right) dY . \tag{5.39}$$

5.4 Numerical results and discussion

The theoretical results obtained in the previous section are employed in this part to investigate the influence of the second sound effect on temperature distribution and damping capacity of thin beam resonators. Three of the most common NEMS materials with various γ values were chosen for the purpose of numerical evaluation and comparison. The set of material data used in the calculation is given in Table 5.1 (Shakelford & William, 2001; Broughton *et al.*, 1997; Pierson, 1993).

The corresponding classical and modified temperature curves for silicon beam vibration are presented in Figs. 5.2-5.5. It noteworthy that the classical temperature curves are identical to those obtained by Kinra and Milligan (1994). Silicon was chosen for the graphical representation as the most commonly used material in the MEMS/NEMS industry. Furthermore, the value of the normalized relaxation time for

silicon represents the most general case since it lies between the value for diamond (γ is about 33 times larger) and for quartz (γ is about 223 times smaller).

Figures 5.2 and 5.3 show the magnitude of the complex temperature as a function of Y and Ω respectively. Taking into account the symmetry of the complex temperature function V^* (it is an odd function of Y), we present results for the positive values of Y only. For both theories the temperature remains at the reference state at low frequencies. For higher values of Ω, the distinction between the classical and ORT theories is significant. It noteworthy that, within some range of frequency, temperature exceeds the adiabatic limit almost five times for the ORT theory (Fig. 5.3). For the case of the diamond, it can become up to 20 times higher than the adiabatic limit. With Ω increasing, the temperature variation across the beam thickness approaches the classical case (Fig. 5.3). Evidently, the nature of such a temperature distribution is defined by the difference in speed of propagation of mechanical and thermal waves. As in the classical case (Kinra and Milligan, 1994), at low frequencies, the system has enough time to relax and temperature distribution does not depend on Y; at higher frequencies the system has no time to relax and the temperature curve represents a line - an adiabatic limit. When the frequency of vibration is in the intermediate range, thermal waves have time to propagate for some finite distance, which, as a result, produce a wave-like temperature distribution across the thickness of the beam.

Considering real values of the complex temperature in Fig. 5.4, we observe that for specific ranges of frequency temperature disturbance has negative values, which is a quite unexpected result since it indicates cooling instead of heating in the compressed surface of the beam.

Figures 5.5 and 5.6 show the phase of a complex temperature as a function of Y and Ω. In order to avoid confusion due to overlapping, in Fig. 6 we have plotted curves for three values of Y only. As $\Omega \rightarrow 0$, the temperature outstrips the stress by $\pi/2$ and is independent of Y for both theories. The difference arises for higher values of frequency, where we notice strong dependence of the phase on Y, as well as a pronounced nonlinearity in phase variation across the beam thickness for the nonclassical theory, Fig. 5.6(b). Cases of $\Omega = 1$ and 100, nearly overlapping at zero level, are represented by thin lines in Fig. 5.5(b).

Figure 5.7 shows a comparison of the average damping across the beam thickness in the ORT theory with the damping obtained from the classical theory. It is evident that unlike the classical theory, which yields one single peak, the finite speed of thermal wave propagation results in the existence of many peaks with a decreasing amplitude as $\Omega \rightarrow \infty$. It is intriguing to note that the maximum value of damping is ~5 (Si) to ~33 (diamond) times higher than for the classical case, whereas in some regions of frequencies, ORT damping is much smaller than the predictions of the classical theory.

Attainable frequencies for the fundamental flexural modes of thin nano-beams of size 0.1×0.01×0.01 μm are in the range of 1.9 to 12 GHz (Roukes, 2000), which corresponds to $\Omega = 0.0044 \div 0.0279$ for quartz, $\Omega = 0.0002 \div 0.0013$ for silicon, and $\Omega = 0.000017 \div 0.00011$ for diamond. From examination of the graphical results it can be concluded that, at frequencies attainable at present, the second sound effect does not have any significant influence on the damping capacity of resonators and, therefore, a reasonable approximation can be obtained using the classical theory.

It should be also noted that since normalized relaxation time as well as fundamental resonant frequency of a beam is a function of beam's dimensions, it is impossible to obtain high values of γ and to increase the fundamental frequency of vibration simultaneously. Indeed, consider, for example, the first fundamental frequency of vibration of a cantilever beam

$$\omega = 1.015\sqrt{\frac{E}{\rho}}\frac{h}{l^2}. \tag{5.40}$$

Taking $l = 10h$, the normalized frequency becomes

$$\Omega = \omega\tau = 1.028 \cdot 10^{-3}\sqrt{\frac{E}{\rho}}\frac{\rho c}{k}h. \tag{5.41}$$

On the other hand, the normalized relaxation time can be expressed as a function of thickness h of the resonator as

$$\gamma = \frac{t_0}{\tau} = 3.289 \cdot \left(\frac{3k}{\upsilon\rho c}\right)^2 \frac{1}{h^2}. \tag{5.42}$$

Table 5.1. Material properties and normalized relaxation times for various MEMS/NEMS materials.

Material	Thermal conductivity, k (W/mK)	Acoustic velocity, υ (m/s)	Density, ρ (kg/m^3)	Heat capacity, C_v (J/kgK)	Second sound relaxation time, $t_0 \cdot 10^{12}$ (s)	Flexural time constant for h=10 nm, $\tau \cdot 10^{12}$ (s)	Normalized relaxation time, γ
Silicon (Si)	150	8430	2330	700	3.88	0.11	35.27
Silicon dioxide (quartz)	8	5900	2600	710	0.37	2.33	0.16
Diamond (CVD)	2000	17500	3520	520	10.7	0.0092	1163

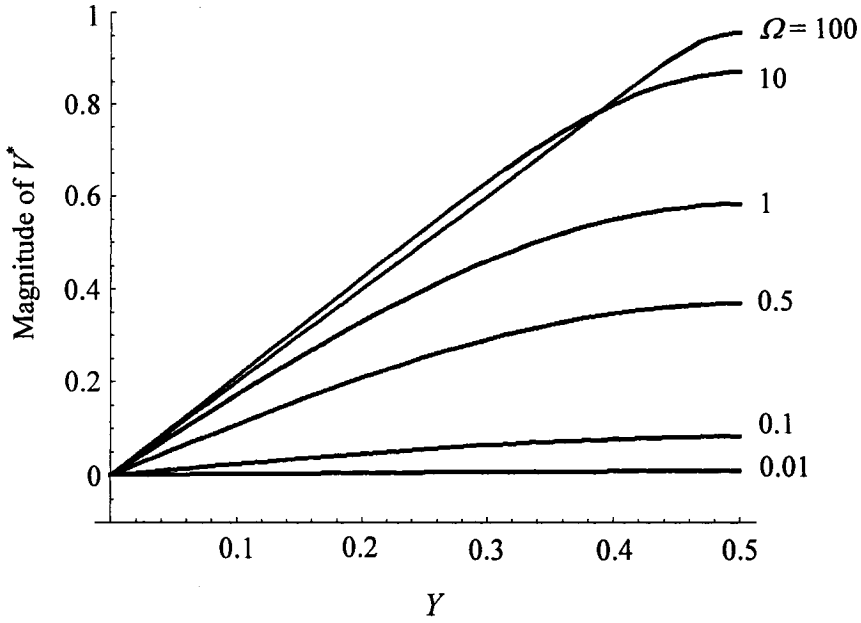

(a)

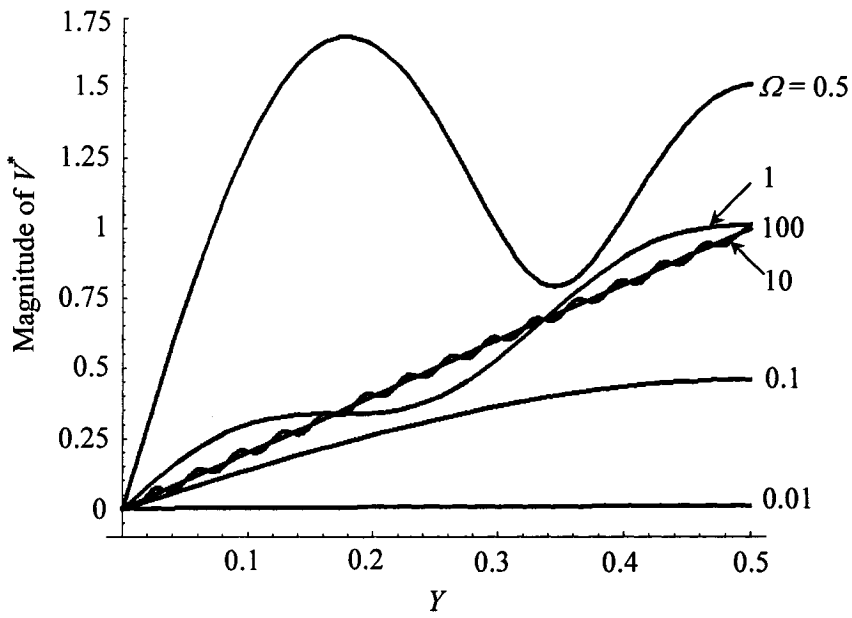

(b)

Figure 5.2. Variation of the magnitude of the temperature change across the thickness of the beam for (a) classical theory and (b) ORT theory (Si).

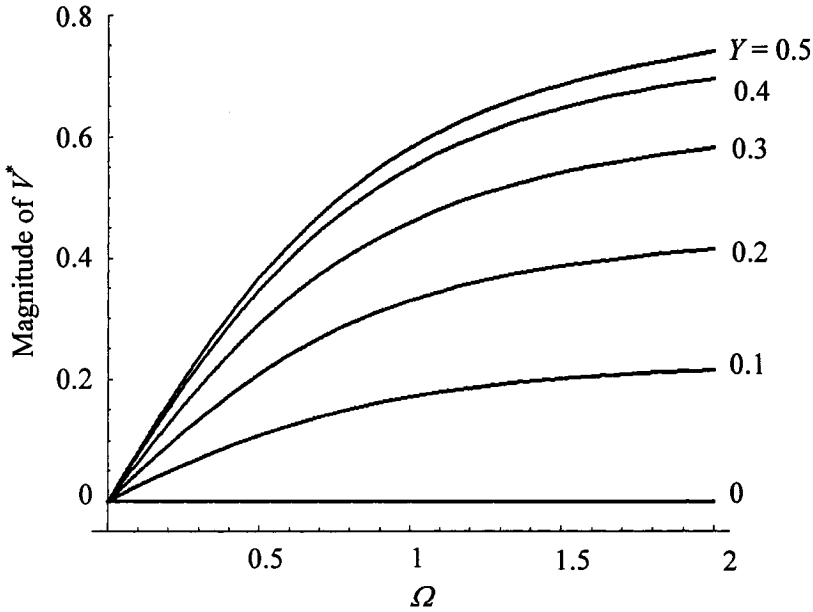

(a)

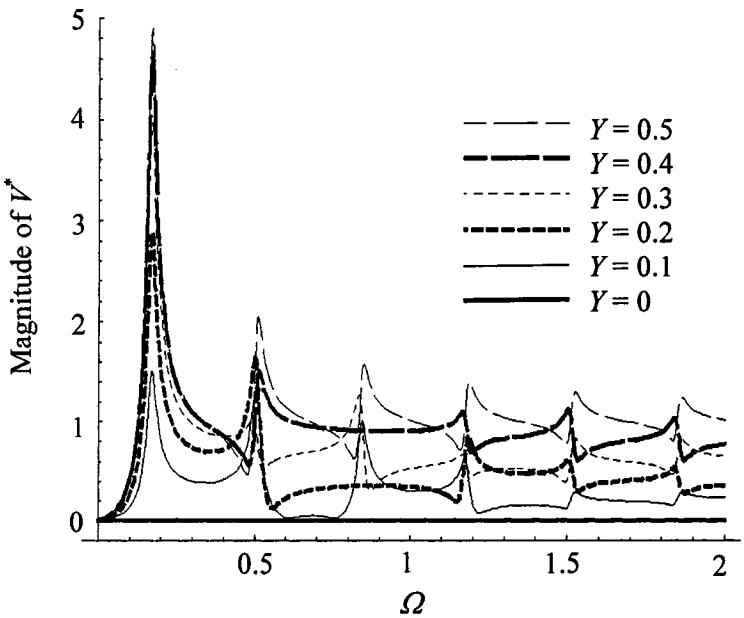

(b)

Figure 5.3. Variation of the magnitude of the temperature change with the normalized frequency for (a) classical theory and (b) ORT theory (Si).

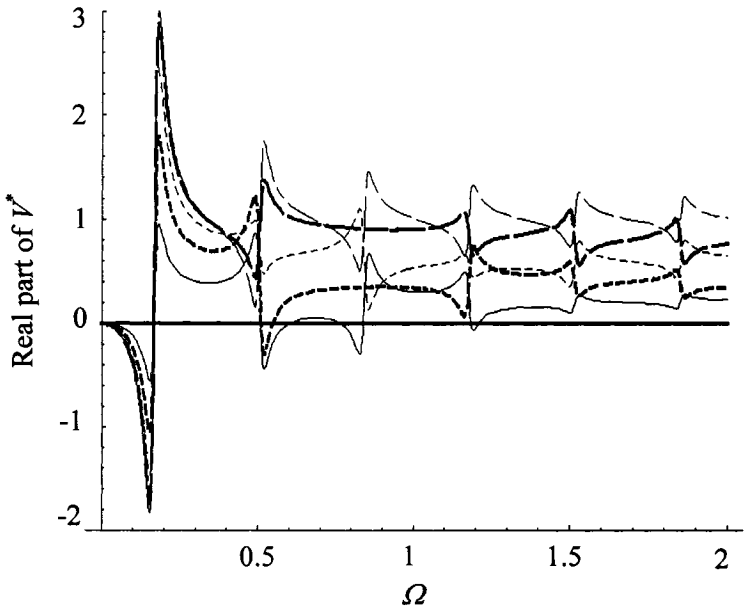

Figure 5.4. Dependence of the real part of the temperature variation on the normalized frequency for ORT theory (Si).

Combining Eqs. (5.41) and (5.42), we find that for any material the following relation holds

$$\gamma \approx \frac{31.31 \cdot 10^{-6}}{\Omega^2}, \tag{5.43}$$

which shows that γ and Ω^2 are inversely proportional.

5.5 Closure

In this chapter the generalized theory of heat conduction with one relaxation time is employed for the purpose of evaluation of thermoelastic damping of high frequency nanomechanical resonators. The resonator is modeled as a thin homogeneous thermoelastic Bernoulli-Euler beam. The approach of Kinra and Miligan (1994) is taken as the starting point and the difference in temperature distribution across the resonator thickness for a broad frequency range between classical and corresponding nonclassical theory was studied. Thermoelastic damping is presented graphically for three different materials most often used in MEMS/NEMS industry: silicon, quartz and diamond.

Numerical results reveal that, for relatively large values of vibration frequency, the finite speed of heat propagation gives rise to existence of many damping peaks contrary to the classical theory, which predicts just one maximum value of the damping curve. The results of this research show that the second sound effect may have impact on nanomechanical resonator behavior only at high frequencies of vibration and small length scales.

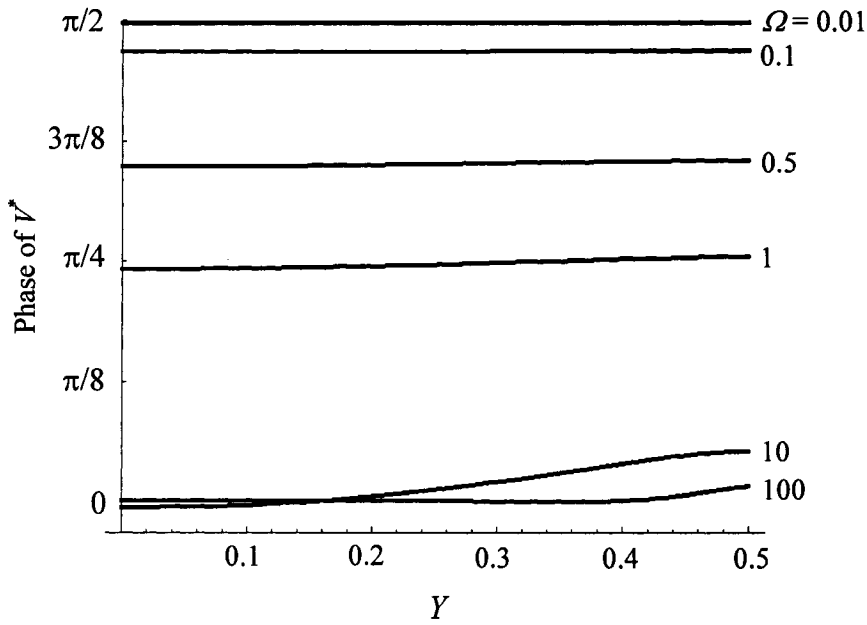

(a)

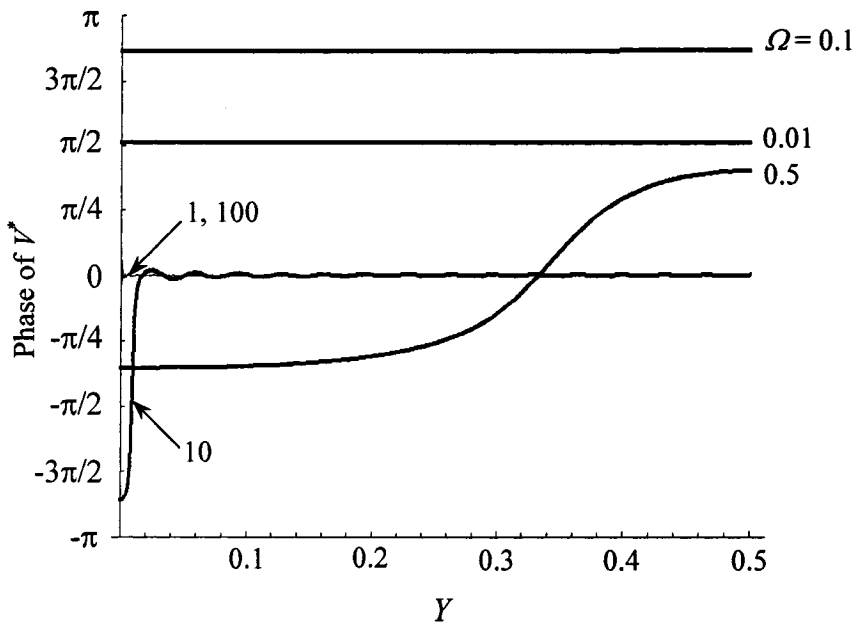

(b)

Figure 5.5. Variation of the phase of the temperature change across the thickness of the beam for (a) classical theory and (b) ORT theory (Si).

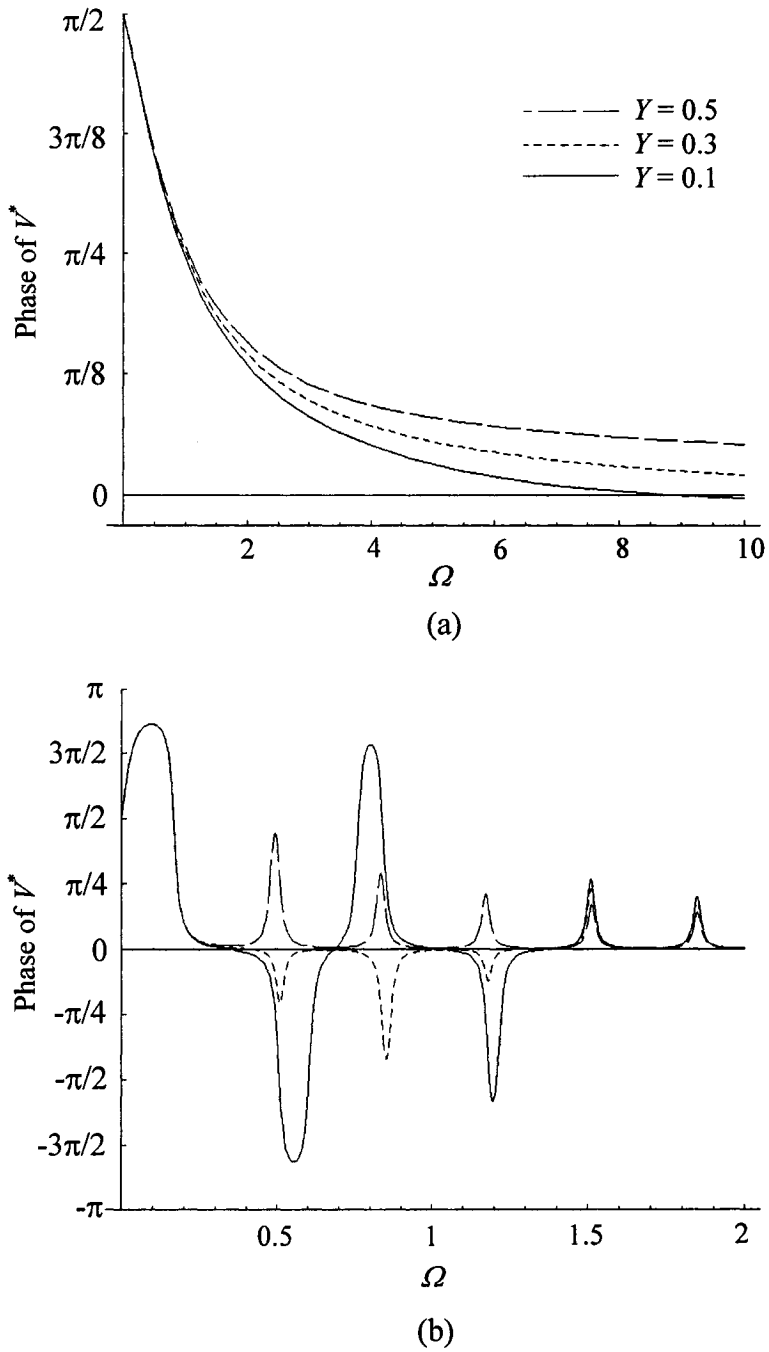

Figure 5.6. Variation of the phase of the temperature change with the normalized frequency for (a) classical theory and (b) ORT theory (Si).

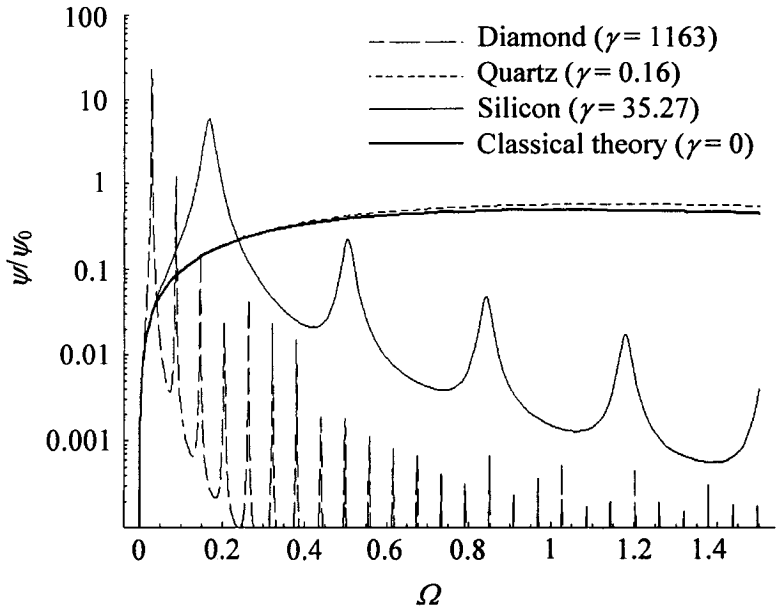

Figure 5.7. A comparison of a classical solution for thermoelastic damping with one relaxation time solution for different γ.

Chapter 6

Summary and future work

6.1 Summary

In this thesis, mesoscale asymptotic bounds on the effective response of random heterogeneous material in finite elasticity and thermoelasticity are derived and numerically investigated for different nonlinear composites. The presented approach makes it possible to study the behavior of nonlinear random composites without any assumption on periodicity of their microstructure. Scale-dependence of the constitutive response (i.e., elastic and thermoelastic material parameters) is studied, as is the effect of length scale on the thermoelastic damping of nanomechanical resonators.

The developed asymptotic homogenization theory allows establishing relationships between properties obtained on large and small set of samples and the hierarchy between them, thus, providing an estimation of the minimal RVE size. The homogenization strategy developed in this thesis may be summarized as follows:

1. The potential and complementary energy functionals for the physical problems considered are formulated. It is shown that the variational principles of Lee and Shield (1980) provide a simple and reliable estimate of the mesoscale bounds on the strain-energy density functions, commonly used in nonlinear elasticity. To account for the temperature effects, the variational principles are extended to nonlinear thermoelastostatics.

2. The conditions for which the minimum potential and complementary variational principles hold are considered.

3. Uniform kinematic and static boundary conditions, satisfying Hill average theorem, are formulated. It is shown that in nonlinear elasticity, the conjugate pair of the deformation gradient tensor and the first Piola-Kirchoff stress tensors satisfies the Hill condition.

4. The partitioning method with appropriate (either uniform kinematic or uniform static) boundary conditions is applied, and the hierarchy of bounds on the effective free-energy function of spatially homogeneous and ergodic random media is constructed.

Numerical verification of the developed homogenization procedure is done with the use of the Finite Element Method. The behavior of the microstructure and the minimum RVE size of different nonlinear composites subjected to isothermal and nonisothermal loadings are computed, providing a foundation for a general scale-dependant homogenization method in nonlinear elasticity and thermoelasticity. The effects of mismatch of composite components, deformation, deformation mode, and statistical properties of the microstructure on the minimal size of the RVE are also considered. The results are compared with those of linear theory of elasticity and thermoelasticity.

Finally, the effect of size and frequency of vibration on nanomechanical beam resonator behavior is studied. The size of the resonator, and, correspondingly, its frequency of vibration at which the effect of finite speed of heat conduction becomes significant, are investigated.

6.2 Future work

Following the investigations described in this thesis, there are a number of topics that can be further developed and researched:

1. Unstable materials

In the presented work, we studied one special type of nonlinear elastic materials described by a *convex* strain-energy function. The convexity condition is an important requirement to obtain a stable solution in computational mechanics, but it does not necessarily hold in a real world. One of the interesting extensions of the asymptotic homogenization framework is its application to more complex materials such as materials with instabilities, which are often encountered in nonlinear elasticity.

If the convexity condition on the strain-energy function fails, variational principles of Lee and Schield (1980) lead to *local* minimizer criteria, which are not sufficient to obtain bounds on the effective strain-energy function. Therefore, it is necessary to consider different variational principles, which would provide global minimizer criteria on both the upper and lower bounds. One of the variational principles that can be used in this case is the pure complementary variational principle in nonconvex elasticity discovered by Gao (1999).

2. Effect of heterogeneity shape, its distribution and volume fraction of inclusions

The primary goal of this thesis was to develop the homogenization framework, which would allow one to investigate the minimum size of the RVE for nonlinear materials. Many different parameters, such as the mismatch ratio, strain-energy function representation, deformation, and deformation mode have been studied. There are, however, other parameters, which can influence the size of the RVE and the rate of the bound convergence.

The material model presented in this study is a two-phase round disk composite. In many engineering applications the composite, however, can have more than two phases and more complicated geometries. Moreover, the volume fraction of inclusions in a typical composite ranges from 1 to 60%. The studies of inclusion distribution and its shape were reported for linear elastic and plastic materials, but have never been carried out in nonlinear elasticity. One reason is the required computational power to solve the nonlinear system of equations for a large number of specimens, which nevertheless can be overcome with the use of supercomputers. Consequently, further studies on mesoscale bounds in nonlinear elasticity can be pursued.

3. Three-dimentional model

It was shown by Bilger *et al.* (2005) that the trends for the macroscopic yield stress of voided materials are similar in two- and three-dimensional simulations. Note that the convergence of anti-plane elasticity is the slowest, while in-plane elasticity converges more quickly, and the three-dimensional elasticity demonstrates the fastest convergence (Ostoja-Starzewski, 1999). It would be interesting to study whether this type of trend is observed in nonlinear elasticity.

The difficulty associated with the three-dimensional nonlinear elasticity is severe distortion of the elements with increasing mismatch, and, as a result, poor convergence of the overall model. This makes it extremely complicated to study a large number of samples, unless small stretch values are considered, which, for example, was done by Löhnert and Wriggers (2003). Thus, the first step in this direction is the investigation of the neo-Hookean type composite subjected to small deformations.

4. Experimental investigation

It is difficult to experimentally apply the uniform static and kinematic boundary conditions. Mixed orthogonal boundary conditions, investigated in this thesis, propose a useful alternative to experimental study of the RVE problem. One of the challenges that should be addressed, however, is the rapid convergence of this bound toward the RVE, which would require a precise experimental setup that is able to deal with samples of different size.

5. Thermoelastic damping with fractional heat conduction

In this thesis, the classical theory of thermoelastic damping in nanoelectromechanical beam resonators was extended to account for a finite speed of heat transfer. The *one relaxation time theory* used in the presented work is the limiting case of heat conduction when it is described by a wave-like equation. Heat conduction in many elastic materials, however, can be represented by a time-fractional diffusion wave equation (Povstenko, 2005):

$$\rho c \frac{\partial^{\alpha} T}{\partial t^{\alpha}} = k \frac{\partial^2 T}{\partial y^2}, \tag{6.1}$$

where $0 < \alpha \leq 2$. The cases of $0 < \alpha \leq 1$, $\alpha = 1, 1 < \alpha \leq 2$, and $\alpha = 2$ correspond to "weak" heat transfer, classical Fourier's law, "strong" heat transfer, and heat transfer with one relaxation time, respectively.

The argument in favour of using "weak" or "strong" heat transfer is the occurrence of subdiffusive or superdiffusive transport in a variety of different materials, such as dielectrics, semiconductors, polymers, biological tissues, fractals, glasses, and porous and random media (see Povstenko, 2005, and references therein). It would be logical to assume that the distribution of stress and temperature in the body, and, therefore, thermoelastic damping would be affected dramatically by the value of the parameter α. This provides an interesting topic for future work: an analysis of thermoelastic damping in a material with "weak" or "strong" heat conduction.

Appendix A

The variational principles play a major role in the derivation of mesoscale bounds in finite elasticity and thermoelasticity. Because the complementary energy functional in nonlinear elasticity is generally unknown, the complementary variational principle should be formulated in a way that does not involve the inversion of constitutive relations. In this appendix we outline the derivation of such principles based on the original work of Lee & Shield (1980) in finite elastostatics. We present the thermoelastic case only, as isothermal elasticity can be obtained from it by setting $\Delta T = 0$.

Potential energy variational principle in finite thermoelasticity

Consider a functional

$$P\{U_i, \theta_0\} = \int_{V_0} \psi(U_{i,j}, \theta_0) dV - \int_{S_T} t_i^0 U_i dS, \tag{A.1}$$

where U_i is an admissible function such that $U_i = u_i^0$ on S_U. Assuming the displacement vector field to be the only fundamental unknown, u_i becomes the only independent variable subject to variation. Therefore, the first variation of functional (A.1) can be written as

$$\delta P = \int_{V_0} \frac{\partial \psi}{\partial U_{i,j}} \delta U_{i,j} dV - \int_{S_T} t_i^0 \delta U_i dS, \tag{A.2}$$

where δU_i vanishes on the part of the body where displacement is prescribed. After the application of the divergence theorem and assuming interface continuity of the displacement and traction field within the body, Eq. (A.2) becomes

$$\delta P = \int_{V_0} \left\{ \left(\frac{\partial \psi}{\partial U_{i,j}} \delta U_i \right)_{,j} - \left(\frac{\partial \psi}{\partial U_{i,j}} \right)_{,j} \delta U_i \right\} dV - \int_{S_T} t_i^0 \delta U_i dS$$

$$= \int_{S_0} \frac{\partial \psi}{\partial U_{i,j}} n_j \delta U_i dS - \int_{S_T} t_i^0 \delta U_i dS$$

$$= \int_{S_U} \frac{\partial \psi}{\partial U_{i,j}} n_j \delta U_i dS + \int_{S_T} t_i^0 \delta U_i dS - \int_{S_T} t_i^0 \delta U_i dS = 0 \tag{A.3}$$

provided that $\int_{V_0}\left(\frac{\partial\psi}{\partial U_{i,j}}\right)_{,j}\delta U_{i,j}dV=0$, which is possible only if $U_i=u_i$. We, therefore, have the following principle: the functional $P\{U_i,\theta_0\}$ is stationary for the actual solution u_i with respect to the admissible function U_i, which satisfies displacement boundary conditions $U_i=u_i^0$ on S_U.

In order to see when the functional (A.1) assumes a local minimum for the actual solution u_i, we consider the quantity ΔP defined by

$$\Delta P=P\{u_i+\delta u_i,u_{i,j}+\delta u_{i,j},\theta_0\}-P\{u_i,u_{i,j},\theta_0\}, \tag{A.4}$$

where $\delta u_i=U_i-u_i$. Expanding the first term of the right hand side of Eq. (A.4) in Taylor series we get

$$\Delta P=P+\frac{\partial P}{\partial u_i}\delta u_i+\frac{\partial P}{\partial u_{i,j}}\delta u_{i,j}+\frac{1}{2!}\frac{\partial^2 P}{\partial u_i\partial u_p}\delta u_i\delta u_p$$

$$+\frac{1}{2!}\frac{\partial^2 P}{\partial u_i\partial u_{p,q}}\delta u_i\delta u_{p,q}+\frac{1}{2!}\frac{\partial^2 P}{\partial u_{i,j}\partial u_{p,q}}\delta u_{i,j}\delta u_{p,q}+0(u^3)-P, \tag{A.5}$$

where $o(u^3)$ represents the terms of the third and higher orders in u_i. Now, noting that $\frac{\partial P}{\partial u_i}\delta u_i+\frac{\partial P}{\partial u_{i,j}}\delta u_{i,j}=0$, $\frac{\partial^2 P}{\partial u_i\partial u_p}=0$, and $\frac{\partial^2 P}{\partial u_i\partial u_{p,q}}=0$, we get

$$\Delta P=\frac{1}{2}\frac{\partial^2 P}{\partial u_{i,j}\partial u_{p,q}}\delta u_{i,j}\delta u_{p,q} \tag{A.6}$$

and, thus, the functional P assumes a local minimum for the actual solution u_i if

$$\int_{V_0}\frac{\partial^2\psi}{\partial u_{i,j}\partial u_{p,q}}\delta u_{i,j}\delta u_{p,q}dV>0 \tag{A.7}$$

Complementary energy variational principle in finite thermoelasticity

The complementary energy functional can be written as:

$$Q\{U_{ij},\theta_0\}=\int_{V_0}\left\{\frac{\partial\psi(U_{ij},\theta_0)}{\partial U_{ij}}U_{ij}(U_{ij},\theta_0)-\psi(U_{ij},\theta_0)\right\}dV-\int_{S_U}\frac{\partial\psi(U_{ij},\theta_0)}{\partial U_{ij}}n_j u_i^0 dS \tag{A.8}$$

where U_{ij} is an admissible deformation gradient tensor field satisfying

$$\frac{\partial}{\partial X_j}\left(\frac{\partial\psi(U_{ij},\theta_0)}{\partial U_{ij}}\right)=0 \text{ in } V_0 \text{ and } \frac{\partial\psi(U_{ij},\theta_0)}{\partial U_{ij}}n_j=t_i^0 \text{ on } S_T. \tag{A.9}$$

As is well known, in the constrained minimization problems, the admissible functions and their admissible variations should not only satisfy boundary conditions, but they should also satisfy constrained conditions. In our case, Eq. $(A.9)_1$ is the constrained condition to be satisfied. Introducing the Lagrange multipliers μ_i, we form a new functional

$$\tilde{Q}\{U_{ij},\theta_0\}=Q\{U_{ij},\theta_0\}+\int_{V_0}\mu_i\frac{\partial}{\partial X_j}\left(\frac{\partial\psi}{\partial U_{ij}}\right)dV \tag{A.10}$$

defined for functions U_{ij}, which satisfy Eq. $(A.9)_2$. The variation of the functional $\tilde{Q}$ with respect to variations in U_{ij} is

$$\delta\tilde{Q}=\int_{V_0}\left\{\frac{\partial^2\psi}{\partial U_{ij}\partial U_{pq}}\delta U_{pq}U_{ij}+\mu_i\frac{\partial}{\partial X_j}\left(\frac{\partial^2\psi}{\partial U_{ij}\partial U_{pq}}\delta U_{pq}\right)\right\}dV$$

$$-\int_{S_U}\frac{\partial^2\psi}{\partial U_{ij}\partial U_{pq}}\delta U_{pq}n_ju_i^0dS\,. \tag{A.11}$$

Application of the Green-Gauss theorem and the fact that the variations δU_{ij} satisfy $\frac{\partial^2\psi}{\partial U_{ij}\partial U_{pq}}\delta U_{pq}n_j=0$ on S_T give

$$\delta\tilde{Q}=\int_{V_0}(U_{ij}-\mu_{i,j})\frac{\partial^2\psi}{\partial U_{ij}\partial U_{pq}}\delta U_{pq}dV+\int_{S_U}(\mu_i-u_i^0)\frac{\partial^2\psi}{\partial U_{ij}\partial U_{pq}}\delta U_{pq}n_jdS\,, \tag{A.12}$$

which is equal to zero, if $\mu_{i,j}=U_{ij}$ in V_0, and $\mu_i=u_i^0$ on S_U. But, for those variations of U_{ij} satisfying Eqs. (A.9), $\delta\tilde{Q}=\delta Q$ and consequently $\delta Q=0$. Thus, the functional $Q\{U_{ij},\theta_0\}$ is stationary for $U_{ij}=u_{i,j}+\delta_{ij}$, where u_i is the actual solution of equilibrium equations and boundary conditions with respect to the admissible function U_{ij}, which satisfies Eqs. (A.9).

In order to see when the functional (A.8) assumes a local minimum for the actual solution u_i, we consider a quantity ΔQ defined by

$$\Delta Q = Q\{u_{i,j} + \delta u_{ij}, \theta_0\} - Q\{u_{i,j}, \theta_0\}. \tag{A.13}$$

Expanding the first term of the right hand side of Eq. (A.13) in Taylor series and noting that

$$\frac{1}{\partial X_j}\left(\frac{\partial^2 \psi}{\partial u_{i,j}\partial u_{p,q}}\delta u_{pq} + \frac{1}{2}\frac{\partial^3 \psi}{\partial u_{i,j}\partial u_{p,q}\partial u_{r,s}}\delta u_{pq}\delta u_{rs}\right) = 0 \text{ in } V_0, \tag{A.14}$$

$$\left(\frac{\partial^2 \psi}{\partial u_{i,j}\partial u_{p,q}}\delta u_{pq} + \frac{1}{2}\frac{\partial^3 \psi}{\partial u_{i,j}\partial u_{p,q}\partial u_{r,s}}\delta u_{pq}\delta u_{rs}\right) n_j = 0 \text{ on } S_T \tag{A.15}$$

we get

$$\Delta Q = \frac{1}{2}\int_{V_0} \frac{\partial^2 \psi}{\partial u_{i,j}\partial u_{p,q}}\delta u_{ij}\delta u_{pq} dV + 0(u^3). \tag{A.16}$$

and, thus, the functional Q assumes a local minimum for $U_{ij} = u_{i,j} + \delta_{ij}$, where u_i is the solution of the equilibrium equations and the boundary conditions, if

$$\int_{V_0} \frac{\partial^2 \psi}{\partial u_{i,j}\partial u_{p,q}}\delta u_{ij}\delta u_{pq} dV > 0. \tag{A.17}$$

Appendix B

For the completeness of the presentation, here, we outline proofs of the averaging theorems presented in section 2.4 of the thesis.

Average deformation gradient theorem

The average theorem for the deformation gradient takes the form:

$$\overline{F}_{ij} = F^0_{ij}, \tag{B.1}$$

where F^0_{ij} is the prescribed deformation gradient acting on the boundary S_0 in the reference configuration.

Proof: Volume average of the deformation gradient is defined as

$$\overline{F}_{ij} \equiv \frac{1}{V_0}\int_{V_0} F_{ij}\, dV = \frac{1}{V_0}\int_{V_0} x_{i,j}\, dV . \tag{B.2}$$

Applying the Green-Gauss theorem and assuming no jumps in the displacement field we get

$$V_0 \overline{F}_{ij} = \int_{S_1} x_i^{(1)} n_j dS + \int_{S_2} x_i^{(2)} n_j dS = \int_{S_0} x_i\, n_j dS . \tag{B.3}$$

Since under uniform displacement boundary conditions, $x_i = x_i^0$ on the boundary, we obtain

$$\overline{F}_{ij} = \frac{1}{V_0}\int_{S_0} x_i^0 n_j dS = \frac{1}{V_0}\int_{V_0} x^0_{i,j} dV = \frac{1}{V_0}\int_{V_0} F^0_{ij} dV = F^0_{ij} . \tag{B.4}$$

Average stress theorem

For the first Piola-Kirchoff stress tensor the average theorem takes the form:

$$\overline{P}_{ij} = P^0_{ij}, \tag{B.5}$$

where $t^0_i = P^0_{ij} n_j$ is a prescribed traction field acting on the boundary S_0 in the reference configuration.

Proof: The average of the internal stresses over the reference volume V_0 is defined as

$$\overline{P}_{ij} \equiv \frac{1}{V_0}\int_{V_0} P_{ij}\, dV \tag{B.6}$$

Right hand side integral can be rewritten as

$$\int_{V_0} P_{ij}\, dV = \int_{V_0} P_{kj}\delta_{ik}\, dV = \int_{V_0} P_{kj} X_{i,k}\, dV\,. \tag{B.7}$$

Applying the Green-Gauss theorem, and noting that from the balance of linear momentum in the absence of body forces $P_{kj,k} = 0$, we get

$$\int_{V_0} P_{ij}\, dV = \int_{S_1} P_{kj}^{(1)} X_i n_k\, dS + \int_{S_2} P_{kj}^{(2)} X_i n_k\, dS\,, \tag{B.8}$$

where S_1 is the boundary of the matrix, and S_2 is the boundary of the inclusions (Figure B.1). Assuming no jumps in traction $t_i^{(1)} = -t_i^{(2)}$, we have

$$\int_{S_1} P_{kj}^{(1)} X_i n_k\, dS + \int_{S_2} P_{kj}^{(2)} X_i n_k\, dS = \int_{S_0} P_{kj} X_i n_k\, dS\,, \tag{B.9}$$

where S_0 is the outer boundary of the body in the reference configuration. Since under uniform traction boundary conditions $P_{kj} = P_{kj}^0$ on the boundary

$$\int_{S_0} P_{kj} X_i n_k\, dS = P_{kj}^0 \int_{S_0} X_i n_k\, dS = P_{kj}^0 \int_{S_0} \delta_{ik}\, dS = P_{ij}^0 V_0\,, \tag{B.10}$$

Finally, we get

$$\overline{P}_{ij} = \frac{1}{V_0}\int_{V_0} P_{ij}\, dV = \frac{1}{V_0} P_{ij}^0 V_0 = P_{ij}^0\,, \tag{B.11}$$

which is the required result. In an analogous way, it can be shown that, for the Cauchy stress tensor, one has

$$\overline{\sigma}_{ij} = \sigma_{ij}^0\,. \tag{B.12}$$

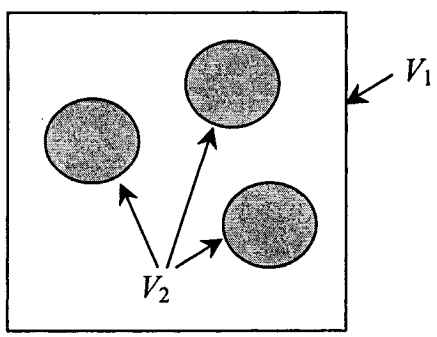

Figure B.1. Material microstructure of a two-phase composite.

Hill condition for finite deformations

In finite elasticity, the Hill condition can be expressed in terms of different conjugate pairs (Nemat-Nasser, 1999), however only the product of the deformation gradient tensor and the first Piola-Kirchoff stress tensor will lead to the canonical boundary conditions (2.26)-(2.28):

$$\overline{P_{ij}F_{ij}} - \overline{P}_{ij}\overline{F}_{ij} = \frac{1}{V_0}\int_{S_0}\left(t_i - \overline{P}_{ij}n_j\right)\left(u_i - (\overline{F}_{ij} - \delta_{ij})X_j\right)dV = 0. \qquad \text{(B.17)}$$

In order to derive Eq. (B.17) consider an identity

$$\overline{P_{ij}F_{ij}} - \overline{P}_{ij}\overline{F}_{ij} = \frac{1}{V_0}\int_{V_0}\left(P_{ij} - \overline{P}_{ij}\right)\left(F_{ij} - \overline{F}_{ij}\right)dV. \qquad \text{(B.18)}$$

Noting that $F_{ij} = u_{i,j} - \delta_{ij}$, and applying the divergence theorem the right hand side of Eq. (B.18) becomes

$$\frac{1}{V_0}\int_{V_0}\left[\left(P_{ij} - \overline{P}_{ij}\right)\left(u_i - \overline{u}_i\right)\right]_{,j}dV - \frac{1}{V_0}\int_{V_0}\left(P_{ij} - \overline{P}_{ij}\right)_{,j}\left(u_i - \overline{u}_i\right)dV$$

$$= \frac{1}{V_0}\int_{S_0}\left(P_{ij}n_j - \overline{P}_{ij}n_j\right)\left(u_i - \overline{u}_i\right)dS = \frac{1}{V_0}\int_{S_0}\left(t_i - \overline{P}_{ij}n_j\right)\left(u_i - \left(\overline{F}_{ij} - \delta_{ij}\right)X_j\right)dS, \qquad \text{(B.19)}$$

which is identical to Eq. (B.17). Here, we used the assumption of the divergence-free stress field in the body $P_{ij,j} = 0$.

It is important to note that the derivation of the averaging theorems does not involve any assumption regarding the constitutive response of the body, and, therefore, can be equally applied to both the isothermal and non-isothermal elasticity, and even to inelasticity.

References

Balch, D.K., Fitzgerald, T.J., Michaud, V.J., Mortensen, A., Shen, Y.-L., Suresh, S., 1996. Thermal expansion of metals reinforced with ceramic particles and microcellular foams. *Metal. Mat. Trans. A* **27**, 3700-3717.

Ball, J. M., 1977. Convexity conditions and existence theorems in nonlinear elasticity, *Arch. Ration. Mech. Anal.* **63**, 337–403.

Bejan, A., 1988. *Advanced Engineering Thermodynamics*, Wiley, New York.

Bilger, N., Auslender, F., Bornet, M., Michel, J.-C., Moulinec, H., Suquet, P., Zaoui, A., 2005. Effect of a nonuniform distribution of voids on the plastic response of voided materials: a computational and statistical analysis. *Int. J. Solids Struct.* **42**, 517-538.

Bishop, J.E., Kinra, V.K., 1992. Some improvements in the flexural damping measurement technique, *M3D: Mechanics and Mechanisms of Material Damping*, ASTM No. 1169, 457-470.

Bishop, J.E., Kinra, V.K., 1997. Elastothermodynamic damping in laminated composites, *Int. J. Solids Struct.* **34**, 1075-1092.

Boyce, M.E., Argon, A.S., Parks, D.M., 1987. Mechanical properties of compliant composite particles effective in toughening glassy polymers. *Polymer* **28**, 1680-1694.

Brain network laboratory. Texas A&M University, Texas. http://research.cs.tamu.edu/bnl/galleryData.html. Cited 3Apr 2006 (2006)

Broughton, G.Q., Meli, C.M., Vashishta, P., Kalia, R.K., 1997. Direct atomistic simulation of quartz crystal oscillators: Bulk properties and nanoscale devices, *Phys. Rev. B* **56**, 611-618.

Castañeda, P.P., 1989. The overall constitutive behavior of nonlinearly elastic composites, *Proc. R. Soc. Lond. A* **422**, 147-171.

Castañeda, P.P., Telega, J.J and Gambin B., 2004. *Nonlinear Homogenization and its Applications to Composites, Polycrystals and Smart Materials*, Kluwer, 349 pp.

Castañeda, P.P., 1991. The effective mechanical properties of nonlinear isotropic composites. *J. Mech. Phys. Solids* **39**, 45-71.

Chadwick, P., Creasy, C.F.M., 1984. Modified entropic elasticity of rubberlike materials, *J. Mech. Phys. Solids* **32**, 337-357.

Chandrasekharaiah, D.S., 1986. Thermoelasticity with second sound: A review, *Appl. Mech. Rev.* **39**, 355-376.

Chester, M., 1963. Second sound in solids, *Phys. Rev.* **131**, 2013-2015.

Ciarlet, P.G., 1988. *Mathematical Elasticity, Vol. I Three-Dimensional Elasticity,* North–Holland, Amsterdam.

Costanzo, F., Gray, G.L., Andia, P.C., 2005. On the definition of effective stress and deformation gradient for use in MD: Hill's macro-homogeneity and the virial theorem, *Int. J. Eng. Sci.* **43**, 533-555.

Crowley, E.F., van Schoor, M.C., 1987. Material damping in aluminum and metal matrix composites, *J. Compos. Mat.* **21**, 553-568.

de Veubeke, B.F., 1972. A new variational principle for finite elastic displacement, *Int. J. Eng. Sci.* **10**, 745-763.

Drugan, W.J., 2000. Micromechanics-based variational estimates for a higher-order nonlocal constitutive equation and optimal choice of effective moduli for elastic composites. *J. Mech. Phys. Solids* **48**, 1359-1387.

Drugan, W.J., Willis J.R., 1996. A micromechanics-based nonlocal constitutive equation and estimates of representative volume element size for elastic composites. *J. Mech. Phys. Solids* **44**, 497-524.

Du, X., 2006. Scaling laws in permeability and thermoelasticity of random media. PhD thesis, McGill University.

Du, X., Ostoja-Starzewski, M., 2005. Mesoscale bounds on effective thermal expansion of random composites, *6th Intl. Cong. Therm. Stresses*, Vienna, Austria, 755-758.

Du, X., Ostoja-Starzewski, M., 2006. On scaling from statistical to representative volume element in thermoelasticity of random materials. *Networks and Heterogeneous Media*, **1**, 259-274.

Forest, S., Barbe, F., Cailletaud, G., 2000. Cosserat modelling of size effects in the mechanical behavior of polycrystals and multi-phase materials. *Int. J. Solids Struct.* **37**, 7105–7126.

Francis, P.H., 1972. Thermo-mechanical effects in elastic wave propagation: a survey, *J. Sound Vib.* **21**, 181-192.

Gao, D.Y., 1999. General analytic solution and complementary variational principles for large deformation nonsmooth mechanics, *Meccanica.* **34**, 169-198.

Gatos, K.G., Thomann, R., Karger-Kocsis, J.K., 2004. Characteristics of ethylene propylene diene monomer rubber/organoclay nanocomposites resulting from different processing conditions and formulations. *Polym. Int.* **53**, 1191–1197.

Guido, D., 2004. *The Finite Element Method for Three-dimensional Thermomechanical Applications*, John Willey & Sons, Munich.

Gusev, A.A., 1997. Representative volume element size for elastic composites: a numerical study. *J. Mech. Phys. Solids* **45**, 1449-1459.

Hashin, Z., Shtrikman S., 1963. A variational approach to the theory of the elastic behaviour of multiphase materials. *J. Mech. Phys. Solids* **11**, 127-140.

Hazanov, S., 1998. Hill condition and overall properties of composites. *Arch. Appl. Mech.* **68**, 385-394.

Hazanov, S., 1999. On apparent properties of nonlinear heterogeneous bodies smaller than the representative volume. *Acta Mech.* **134**, 123-134.

Hazanov, S. and Amieur, M., 1995. On overall properties of elastic heterogeneous bodies smaller than the representative volume. *Int. J. Engng. Sci.* **33**, 1289-1301.

Hazanov, S., Huet, C., 1994. Order relationships for boundary conditions effect in heterogeneous bodies smaller than the representative volume. *J. Mech. Phys. Solids* **42**, 1995-2011.

Hill, R., 1963. Elastic properties of reinforced solids: some theoretical principles, *J. Mech. Phys. Solids* **11**, 357-372.

Hill, R., 1972. On constitutive macro-variables for heterogeneous solids at finite strain, *Proc. R. Soc. Lond. A.* **326**, 131-147.

Hohe, J., Becker, W., 2005. A probabilistic approach to the numerical homogenization of irregular solid foams in the finite strain regime. *Int. J. Solids Struct.* **42**, 3549-3569.

Holzapfel, G.A., 2000. *Nonlinear Solid Mechanics. A Continuum Approach for Engineering*, John Wiley & Sons.

Holzapfel, G.A., Gasser, T.C., Ogden, R.W., 2000. A new constitutive framework for arterial wall mechanics and a comparative study of material models, *J. Elast.* **61**, 1-48.

Holzapfel, G.A., Simo, J.C., 1996. Entropy elasticity of isotropic rubber-like solids at finite strains. *Comput. Methods Appl. Mech. Engrg.* **132**, 17-44.

Huet, C., 1990 Application of variational concepts to size effects in elastic heterogeneous bodies, *J. Mech. Phys. Solids* **38**, 813-841.

Huet, C., 1999 Coupled size and boundary condition effects in viscoelastic heterogeneous and composite bodies, *Mech. Mater.* **31**, 787-829.

Ignaczak, J., 1989. Generalized thermoelasticity and its applications, in R.B. Hetnarski, Ed., *Thermal Stresses III*, 279-354, Elsevier, New York.

Jiang, M., Ostoja-Starzewski, M., Jasiuk, I., 2001. Scale-dependent bounds on effective elastoplastic response of random composites, *J. Mech. Phys. Solids* **49**(3), 655-673.

Jones, J.P., 1966. Thermoelastic vibrations of a beam, *J. Acous. Soc. Am.* **39**, 542-548.

Kanit, T., Forest, S., Galliet I., Mounoury V., Jeulin, D., 2003. Determination of the size of the representative volume element for random composites: statistical and numerical approach. *Int. J. Solids Structures* **40**, 3647-3679.

Kerner, E. H.,1956. The elastic and thermoelastic properties of composite media. *Proc. Phys. Soc. B* **69**, 808-813.

Khisaeva, Z.F., Ostoja-Starzewski, M. Scale effects in infinitesimal and finite thermoelasticity of random composites. *Journal of Thermal* Stresses, 2007 (in press).

Khisaeva, Z.F., Ostoja-Starzewski, M., 2006. On the size of RVE in finite elasticity of random composites. *J. Elasticity* **85**, 153-173.

Khisaeva, Z.F., Ostoja-Starzewski, M., 2006. Mesoscale bounds in finite elasticity and thermoelasticity of random composites. *Proc. R. Soc. Lond. A* **462**, 1167-1180.

Khisaeva, Z.F., Ostoja-Starzewski, M., 2006. Thermoelastic damping in nanomechanical resonators with finite wave speeds, *J. Therm. Stresses*, **29**, 201-216.

Kinra, V.K., Milligan, K.B., 1992. Irreversible heat transfer as a source of thermoelastic damping, *M3D: Mechanics and Mechanisms of Material Damping*, ASTM No. 1169, 94-123.

Kinra, V.K., Milligan, K.B., 1994. A second law analysis of thermoelastic damping, *ASME J. Appl. Mech.* **61**, 71-76.

Koiter, W. T., 1976. On the complementary energy theorem in non-linear elasticity. *Trends in Applications of Pure Mathematics*, pp. 207–232.

Kouznetsova, V., Geers, M.G.D., Brekelmans, W.A.M., 2004. Size of a representative volume element in a second-order computational homogenization framework. *Int. J. Mult. Comp. Eng.* **2**, 575-598.

Lachihab, A., Sab K., 2005. Aggregate composites: a contact based modeling. *Comp. Mat. Sci.* **33**, 467-490.

Lee, S.J., Shield, R.T., 1980. Variational principles in finite elastostatics, *ZAMP* **31**, 437-453.

Levin, V.M., 1967. On the Coefficients of Thermal Expansion in Heterogeneous Materials. *Mech. Solids* **2**, 58–61.

Levinson, M., 1965. Complementary energy theorem in finite elasticity. *ASME J. Appl. Mech.* **32**, 826-828.

Lifshitz, R., Roukes, M.L., 2000. Thermoelastic damping in micro- and nanomechanical systems, *Phys. Rev. B* **61**, 5600-5609.

Li, W., Ostoja-Starzewski, M., 2006 Yield of random elasto-plastic materials. *J. Mech. Mat. Struct.* (in press).

Liu, C., 2005. On the minimum size of representative volume element: an experimental investigation. *Exper. Mech.* **45**, 238-243.

Lopez-Pamies, O., Castañeda, P.P., 2006. On the overall behavior, microstructure evolution, and macroscopic stability in reinforced rubbers at large deformations: I-Theory. *J. Mech. Phys. Solids* **54**, 807-830.

Lopez-Pamies, O., Castañeda, P.P., 2006. On the overall behavior, microstructure evolution, and macroscopic stability in reinforced rubbers at large deformations: II-Application to cylindrical fibers. *J. Mech. Phys. Solids* **54**, 831-863.

Löhnert, S., 2004. Computational homogenization of microheterogeneous materials at finite strains including damage. Dissertation, Hannover University.

Löhnert, S., Wriggers, P., 2003. Homogenisation of microheterogeneous materials considering interfacial delamination at finite strains, *Tech. Mechanik* **23**, 167-177.

Lord, H.W., Shulman, Y., 1967. Generalized dynamical theory of thermoelasticity, *J. Mech. Phys. Solids* **15**, 299-309.

Martin, P., Maquet, C., Legras, R., Bailly, C., Leemans, L., van Gurp, M., van Duin, M., 2004. Particle-in-particle morphology in reactively compatibilized poly(butylene terephthalate)/epoxide-containing rubber blends. *Polymer* **45**, 3277–3284.

McGee, S., McCullough, R.L., 1981. Combining rules for predicting the thermoelastic properties of particulate filled polymers, polyblends, and foams. *Polymer Composites* **2**, 149–161.

Meille, S., Garboczi, E., 2001. Linear elastic properties of 2-d and 3-d models of porous materials made from elongated objects. *Mod. Sim. Mater. Sci. Engng.* **9**, 1–20.

Mesarovic, S.D., Padbidri, J., 2005. Minimal kinematic boundary conditions for simulations of disordered microstructures. *Phil. Mag.* **85**, 65-78.

Michel, J.C., Moulinec, H., Suquet, P., 1999. Effective properties of composite materials with periodic microstructure: a computational approach. *Comput. Methods Appl. Mech. Eng.* **172**, 109-143.

Michel, J.C., Suquet, P., 2004. Computational analysis of nonlinear composite structures using the nonuniform transformation field analysis. *Comput. Methods Appl. Mech. Engrg.* **193**, 5477–5502.

Moulinec, H., Suquet, P., 1998. A numerical method for computing the overall response of nonlinear composites with complex microstructure. *Comput. Methods Appl. Mech. Eng.* **157**, 69-94.

Moulinec, H., Suquet, P., 2003. Intraphase strain heterogeneity in nonlinear composites: a computational approach. *Eur. J. Mech. A/Solids* **22**, 751-770.

Nemat-Nasser, S., 1999. Averaging theorems in finite deformation plasticity, *Mech. Mat.* **31**, 493-523.

Nemat-Nasser, S., Hori, M., 1999. *Micromechanics: Overall Properties of Heterogeneous Materials*, Elsevier.

Nowacki, W., 1986. *Thermoelasticity*, Oxford, New York.

Ogden, R.W., 1972. Large deformation isotropic elasticity: on the correlation of theory and experiment for compressible rubberlike solids, *Proc. R. Soc. Lond. A* **328**, 567-583.

Ogden, R.W., 1978. Extremum principles in nonlinear elasticity and their application to composites - I, *Int. J. Solids Structures* **14**, 265-282.

Ogden, R.W., 1984. *Non-Linear Elastic Deformations*, Halsted Press.

Ogden, R.W., 1992. On the thermoelastic modeling of rubberlike solids, *J. Therm. Stresses* **15**, 533-557.

Ogden, R.W., Saccomandi, G., Sgura, I., 2004. Fitting hyperelastic models to experimental data. *Comp. Mech.* **34**, 484-501.

Ostoja-Starzewski, M., 1998. Random field models of heterogeneous materials. *Int. J. Solids Struct.* **35**, 2429-2455.

Ostoja-Starzewski, M., 1999. Microstructural disorder, mesoscale finite elements, and macroscopic response. *Proc. R. Soc. Lond. A* **455**, 3189-3199.

Ostoja-Starzewski, M., 2001. Mechanics of random materials: stochastics, scale effects, and computation. In *Mechanics of Random and Multiscale Microstructures* (D. Jeulin and M. Ostoja-Starzewski, eds.), *CISM Courses and Lectures*, **430**, 93-161. Springer, Wien-New York.

Ostoja-Starzewski, M., 2005. Scale effects in plasticity of random media: Status and challenges, *Int. J. Plast.* **21**, 1119-1160.

Ostoja-Starzewski, M., 2006. Material spatial randomness: From statistical to representative volume element. *Prob. Eng. Mech.* **21**, 112-132.

Ostoja-Starzewski, M., Castro, J., 2003. Random formation, inelastic response, and scale effects in paper, *Phil. Trans. R. Soc. Lond. A* **361** (1806), 965-986.

Ostoja-Starzewski, M., Du, X., Khisaeva, Z.F., Li, W., 2007. On the size of representative volume element in elastic, plastic, thermoelastic and permeable random microstructures. *Materials Science Forum*, **539-543**, pp. 201-206.

Ostoja-Starzewski, M., Wang, C., 1989. Linear elasticity of planar Delaunay networks: Random field characterization of effective moduli. *Acta Mech.* **80**, 61-80.

Ostoja-Starzewski, M., Schulte, J., 1996. Bounding of effective thermal conductivities by essential and natural boundary conditions. *Phys. Rev. B* **54**, 278-284.

Paul, D.R. and Bucknall, C.B., 2000. *Polymer blends*, V.1-2, Wiley&Sons.

Pierson, H.O., 1993. *Handbook of Carbon, Graphite, Diamond and Fullerenes - Properties, Processing and Applications*, chap. 13, Noyes Publications, Park Ridge.

Povirk, G.L., 1994. Incorporation of microstructural information into models of two-phase materials. *Acta Metall. Mater.* **43**, 3199–3206.

Ren, Z.-Y., Zheng Q.-S., 2004. Effects of grain sizes, shapes, and distribution on minimum sizes of representative volume elements of cubic polycristals. *Mech. Mat.* **36**, 1217-1229.

Rivlin, R.S., 1948. Large elastic deformations of isotropic materials. I. Fundamental concepts. *Phil. Trans. Roy. Soc. A* **240**, 459-490.

Roberts, A., Garboczi, E., 2000. Elastic properties of model porous ceramics. *J. Am. Ceram. Soc.* **83** (12), 3041–3048.

Roberts, A., Garboczi, E., 2001. Elastic moduli of model random three-dimensional closed-cell cellular solids. *Acta Mater.* **49**, 189–197.

Rosen, B.W., 1970. Thermoelastic energy functions and minimum energy principles for composite materials. *Int.J.Engng.Sci.* **8**, 5–18.

Rosen, BW, Hashin, Z., 1970. Effective thermal expansion coefficients and specific heats of composite materials. *Int. J. Engng. Sci.* **8**, 157--173.

Roukes, M.L., 2000. Nanoelectromechanical systems, *Technical Digest of the 2000 Solid-State Sensor and Actuator Workshop*, 1-10.

Sab, K., 1992. On the homogenization and simulation of random materials, *Eur. J. Mech. A/Solids* **11**, 585-607.

Sab, K., Nedjar, B., 2005. Periodization of random media and representative volume element size for linear composites. *Comptes Rendus Mécanique* **333**, 187-195

Sanchez-Palencia, E., Zaoui, A., 1987. Homogenization techniques for composite media. Lecture Notes in Physics No. 272, Springer-Verlag, Berlin.

Schapery, R.A., 1968. Thermal expansion coefficients of composite materials based on energy principle. *J. Comp. Mat.* **2**, 380-404.

Schneider, M., Pith, T., Lambla, M., 1997. Toughening of polystyrene by natural rubber-based composite particles. *J. Mat. Sci.* **32**, 6331 – 6342.

Segurado, J., Llorca, J., 2002. A numerical approximation to the elastic properties of sphere-reinforced composites. *J. Mech. Phys. Solids* **50**, 2107-2121.

Shakelford, J.F., William, A. (ed.), 2001. *Materials Science and Engineering Handbook*, Boca Raton, CRC Press.

Selvadurai, A.P.S., 2006. Deflections of a rubber membrane. *J. Mech. Phys. Solids* **54**, 1093-1119.

Srikar, V.T. and Senturia, S.D., 2002. Thermoelastic damping in fine-grained polysilicon flexural beam resonators, *J. Microelectromech. Syst.* **11**, 499-504.

Steigmann, D.J., 2003. On isotropic, frame-invariant, polyconvex strain-energy functions, *Quarterly J. Mech. Appl. Math.* **56**, 483–491.

Suquet, P., 1992. On bounds for the overall potential of power law materials containing voids with an arbitrary shape. *Mech. Research Comm.* **19**, 51-58.

Suquet, P., 1997. *Continuum micromechanics.* CISM Courses and Lectures No. 377, Springer-Verlag, Berlin.

Talbot, D.R.S., Willis, J.R., 1985. Variational principles for inhomogeneous nonlinear media. IMA *J. Appl. Math.* **35**, 39–54.

Tanov, R., Tabiei, A., 2001. Computationally efficient micromechanical models for woven fabric composite elastic moduli, J. Appl. Mech. 68, 553-560.

Theocaris, P.S., Varias, A.G., 1985. Thermal expansion properties of particulates based on the concept of mesophase. *J. Appl. Polym. Sci.* **30**, 2979–2995.

Terada, K., Ito, T., Kikuchi, N., 1998. Characterization of the mechanical behaviors of solid-fluid mixture bythe homogenization method. *Comput. Methods Appl. Engng.* **153**, 223–257.

Torquato, S., 2002. *Random Heterogeneous Materials. Microstructure and Macroscopic Properties,* Springer-Velag, New York.

Van Der Wal, C.W., Bree, H.W., Schwarzl, F.R., Mechanical properties of highly filled elastomers. II. Relationship between filler characteristics, thermal expansion, and bulk moduli. *J. Appl. Polimer Sci.* **9**, 2143-2166.

Willis, J., 1981. Variational and related methods for the overall properties of composites, *Adv. Appl. Mech.* **21**, 1–78.

Willis, J. R., 1989. The structure of overall constitutive relations for a class of nonlinear composites. *J. Appl. Math.* **43**, 231-242.

Willis, J. R., 1991. On methods for bounding the overall properties of nonlinear composites. *J. Mech. Phys. Solids* **39**, 73-86.

Wong, S.C., Mai, Y.W., 1999. Effect of rubber functionality on microstructures and fracture toughness of impact-modified nylon 6,6/polypropylene blends: 1. Structure–property relationships. *Polymer* **40**, 1553–1566.

Yasumura, K.Y., Stowe, T.D., Chow, E.M., Pfafman, T., Kenny, T.W., Stipe B.C., Rugar, D., 2000. Quality factors in micron- and submicron-thick cantilevers, *J. Microelectromech. Syst.* **9**, 117-125.

Yourgrau, W., 1966. *Treatise on Irreversible and Statistical Thermophysics: an Introduction to Nonclassical Thermodynamics*, New York, MacMillan.

Yu S., Hing, P., Hu, X., 2000. Thermal expansion behavior of polysterene-aluminium nitride composites. *J. Phys. D* **33**, 1606-1610.

Zener, C., 1948. *Elasticity and Anelasticity of Metals*, Chicago, IL: University of Chicago Press.

Zeman, J., Sejnoha, M., 2001. Numerical evaluation of effective elastic properties of graphite fiber tow impregnated bypoly mer matrix. *J. Mech. Phys. Solids* **49**, 69–90.

Zohdi, T.I., Wriggers, P., 2000 On the sensitivity of homogenized material responses at infinitesimal and finite strains. *Comm. Numer. Meth. Eng.* **16**, 657-670.

Zohdi, T.I., Wriggers, P., 2001. Aspects of the computational testing of the mechanical properties of microheterogeneous material samples. *Int. J. Numer. Meth. Eng.* **50**, 2573-2599.

Zubov, L.M., 1971. Variational principles of the nonlinear theory of elasticity, *J. Appl. Math. Phys. (ZAMP)* **35**, 369-373.